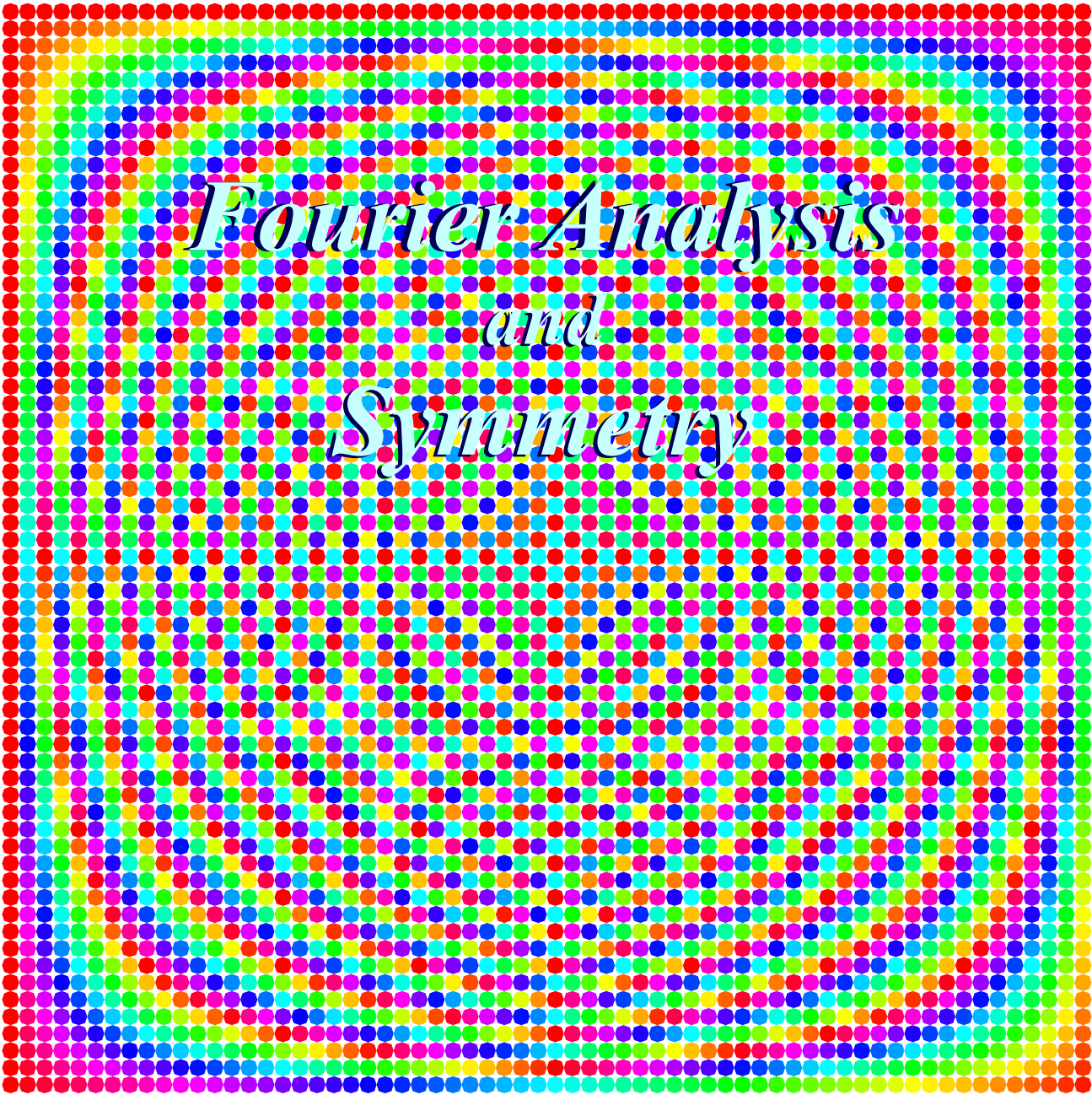


# *Quantum Theory for the Computer Age Unit 3*



## *Fourier Analysis and Symmetry*

## Unit 3 Fourier Analysis and Symmetry

Unit 2 discussed quantum  $e^{i(\mathbf{k}\cdot\mathbf{r}-\omega t)}$ -wave propagation in space and time and introduced wavevector and frequency  $(c\mathbf{k},\omega)$ -space while deriving the basic Einstein relativistic transformations and Planck-deBroglie quantum relations. But, what are  $e^{i(\mathbf{k}\cdot\mathbf{r}-\omega t)}$ -waves? One answer comes from understanding relations between space-time  $(\mathbf{x},ct)$  and  $(c\mathbf{k},\omega)$ -space known as Fourier transformations. Unit 3 begins with discussions of Fourier  $\langle \mathbb{X} | \mathbb{Y} \rangle$  transformation matrices and shows their connection to translational symmetry. This with Planck's axiom gives the quantum equation of motion known as Schrodinger's time equation, the evolution operator, and its generator, the quantum Hamiltonian operator, the *sine qua non* of Schrodinger theory. Unit 3 continues with a detailed description of quantum beats and revivals using symmetry analysis. The final chapter describes 2-state and spin-1/2 systems while introducing U(2) symmetry analysis.

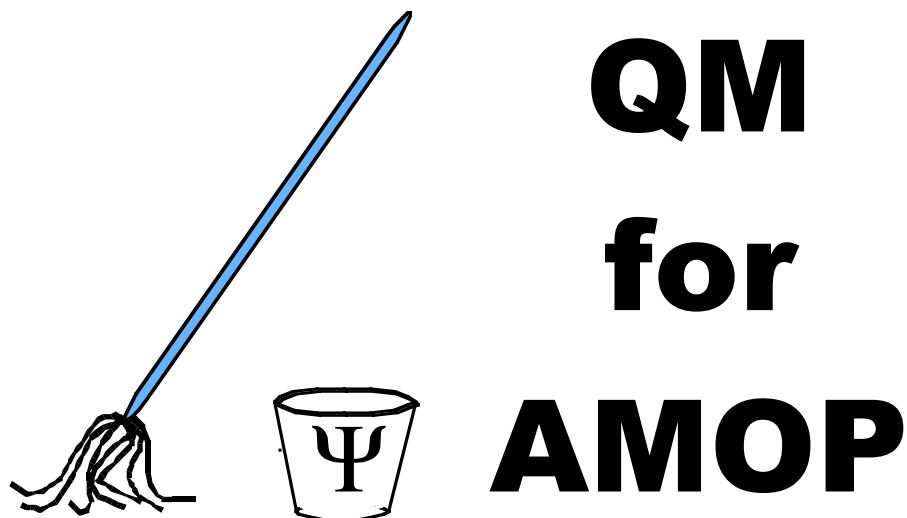
**W. G. Harter**  
**Department of Physics**  
**University of Arkansas**  
**Fayetteville**

*Hardware and Software by*

**HARTER-Soft**

*Elegant Educational Tools Since 2001*

# Unit 3 Fourier Analysis and Symmetry



## Chapter 7 Fourier Transformation Matrices

**W. G. Harter**

**CHAPTER 7. FOURIER TRANSFORMATION MATRICES ..... 1**

**7.1 Continuous but bounded x. Discrete but unbounded k .....1**

- (a) Orthonormality axiom-3 .....2
- (b) Completeness axiom-4 .....3
- (c) Fourier series representation of a state .....3
- (d) Bohr dispersion relation and energies .....3
- (e) Sine and cosine Fourier series worth remembering .....4

**7.2 Continuous and unbounded x. Continuous and unbounded k .....7**

- (a) Fourier integral transforms .....7
- (b) Fourier coefficients: Their many names .....8
- (c) Time: Fourier transforms worth remembering .....9

**7.3 Discrete and bounded x. Discrete and bounded k .....13**

- (a) N-nary counting for N-state systems .....15
- (b) Discrete orthonormality and completeness .....15
- (c) Discrete Fourier transformation matrices .....16
- (d) Introducing aliases and Brillouin zones .....17

**Problems for Chapter 7 .....20**

**CHAPTER 8. FOURIER SYMMETRY ANALYSIS ..... 3**

**8.1. Introducing Cyclic Symmetry: A C6 example .....3**

- (a) Cyclic symmetry CN: A 6-quantum-dot analyzer .....3
- (b) CN Symmetry groups and representations .....5
- (c) So what’s a group representation? .....6

**8.2 CN Spectral Decomposition: Solving a C6 transfer matrix .....7**

- (a) Spectral decomposition of symmetry operators  $r_p$  .....7
- (b) Writing transfer operator T in terms of symmetry operators  $r_p$  .....9
- (c) Spectral decomposition of transfer operator T .....10
  - What do the  $k_m$ - eigensolutions mean? .....11
- (d) OK, where did those  $e^{ikx}$  wavefunctions come from? .....12

**8.3 Related Symmetry Analysis Examples .....13**

- (a) Dihedral symmetry D2 .....14
  - D2 group structure .....14
  - D2 spectral decomposition: The old “1=1•1 trick” again .....15
  - Spectral decomposition of D2 transfer matrices .....15
- (b) Outer product structure: Double qubit registers .....16
  - Big-endian versus Little-endian .....16
  - C6 is product C3× C2 (but C4 is NOT C2× C2) .....17
  - Symmetry Catalog .....17

**Problems for Chapter 8 .....18**

**CHAPTER 9. TIME EVOLUTION AND FOURIER DYNAMICS ..... 1**

**9.1 Time Evolution Operator.....1**  
 (a) Planck's oscillation hypothesis .....1

**9.2 Schrodinger Time Equations .....3**  
 (a) Schrodinger's time equations. Hamiltonian time generators.....3  
 (b) Schrodinger's matrix equations .....4  
 (c) Writing Hamiltonian H in terms of symmetry operators rp .....5

**9.3 Schrodinger Eigen-Equations.....6**  
 (a) Solving Schrodinger's eigen-equations for C6 system.....8  
 (b) Energy spectrum and tunneling rates .....8  
 (c) Brillouin's boundary .....10  
     Effective mass: Another quantum view of inertia.....12  
 (d) Bohr wavepacket dynamics: Uncertainty and revival .....16  
     Semi-classical Theory: Farey Sums and Quantum Speed Limits .....16

**9.4 Homo-cyclic Cn Revivals .....20**  
 (a) Two-state C2 systems: Beats .....20  
 (b) Cn group structure: n=3, 4,...6 Eigenstates .....22  
 (c) Cn dynamics: n=3, 4,...6 Fractional Revivals .....24  
     Bohr vs. Bloch dispersion .....29

**Problems for Chapter 9.....31**

**REVIEW TOPICS & FORMULAS FOR UNIT 3 .....34**

Expressing arbitrary wavefunctions or states in terms of spectral components or plane waves is known as Fourier analysis. Fourier transformation matrices relate space and time (coordinate) bases to wavevector and frequency (Energy-momentum) bases of plane waves. Fourier analysis comes in different flavors depending on whether various bases are discretely numbered or continuous. Chapter 7 compares the continuous coordinate bases of Bohr rotor states to the fully continuous plane wave states of an unbounded continuum. Then a discrete “quantum-dot” system is introduced in which both coordinates and wavevectors are discrete. The later is the basis for the introduction of Fourier symmetry analysis in the following Chapter 8 and time evolution in Chapter 9. Discrete symmetry in space and time helps to clarify quantum beats and “revivals” which all quantum systems will exhibit to some degree.

## Unit 3 Fourier Analysis and Symmetry

### Chapter 7. Fourier Transformation Matrices

We have noted that a quantum experiment cannot move at all unless two or more frequency components can interfere with each other. A single (mono-chromatic) wave  $\Psi = \psi e^{-i\omega t}$  is not enough to make anything happen. Such a  $\Psi$ -system is a stationary state and appears to be dead. What we can observe is determined by the absolute square  $\Psi^*\Psi$ , which kills the single oscillating phase.

Similarly, a wave  $\Psi = \psi e^{ikx}$  with a single momentum component appears to be a uniform cloud of random counts in space. To obtain any structure in the quantum world, that is, atoms, molecules, solids, people, and so forth, we need *many* momentum components in our matter waves.

The mathematics used to deal with multiple frequency or momentum components is called *Fourier analysis* after Jean Baptiste Fourier, a French artillery officer turned mathematician. This section will review the fundamentals of Fourier theory relevant to quantum theory using the Dirac notation. Fourier analysis has several flavors depending on whether its coordinates and parameters, that is space-time and wavevector-frequency are discrete or continuous and whether  $x$  or  $k$  are bounded or unbounded. We consider several distinct cases in turn. Each has different forms for its completeness and orthonormality axioms-3 to 4.

#### 7.1 Continuous but bounded $x$ . Discrete but unbounded $k$

One of the most famous and widely used wavefunction systems in quantum theory are the one-dimensional (1-D) *Bohr orbitals*  $\psi_k(x) = \langle x | k \rangle$ . Examples are sketched in Fig. 7.1.1.

$$\psi_{k_m}(x) = \langle x | k_m \rangle = \frac{e^{ik_m x}}{\sqrt{\text{norm.}}} = \psi_{k_m}(x+L) \quad (7.1.1)$$

These can be thought of as a set of waves on a ring of circumference  $L$ . The basic waves have just the right wavevectors  $k_m$  to put integral numbers of whole wavelengths along  $L$  and thereby repeat the wave again after each complete  $L$ -revolution. Such requirements are known as *periodic boundary conditions*.

$$\psi_{k_m}(x) = \psi_{k_m}(x+L) = \frac{e^{ik_m x}}{\sqrt{\text{norm.}}} = \frac{e^{ik_m(x+L)}}{\sqrt{\text{norm.}}} = \psi_{k_m}(x) e^{ik_m L} \quad (7.1.2)$$

The boundary conditions lead to wavevector *quantization conditions*.

$$e^{ik_m L} = 1, \text{ or: } k_m = \frac{2\pi}{L} m, \text{ where: } m = 0, \pm 1, \pm 2, \pm 3, \dots, \pm \infty \quad (7.1.3)$$

The allowed wavevectors, while still infinite in number, are forced to be *discrete*.

This is a very common feature of quantum theory for which it owes its name *quantum*, but it happens to classical waves, too. A bounded continuum leads to an unbounded but discrete set of allowed waves. For another example, cavity modes in the Hall of Mirrors in Sec. 6.3 (d) acquire discrete frequencies as soon as the doors are shut. If an indiscrete type of wave is put in a cage, then it is forced to be discrete. (Perhaps, this is just another sad anthropomorphic metaphor.)

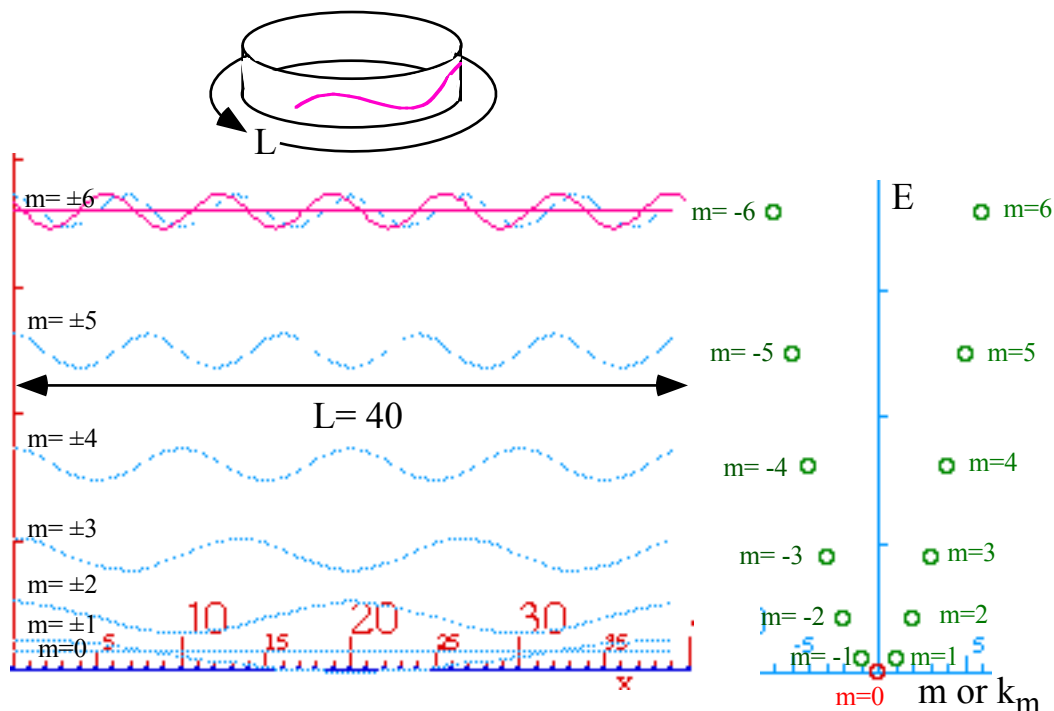


Fig. 7.1.1 Sketches of Bohr orbitals confined to 1-D  $L$ -interval and quantum energies (for  $m=0$  to 6).

The resulting amplitudes must satisfy Axioms 1-4. In particular, the orthonormality axiom-3 requires  $\langle k_1 | k_1 \rangle = 1$  but  $\langle k_1 | k_2 \rangle = 0$ , and so forth, or that the following Kronecker delta representation.

$$\langle k_m | k_n \rangle = \delta_{m n} \tag{7.1.4a}$$

Completeness axiom-4 requires that  $|k_n\rangle \langle k_n|$  sum up to a unit operator or an  $x$ -Dirac-delta expression.

$$\sum |k_n\rangle \langle k_n| = \mathbf{1}, \text{ or: } \sum \langle x | k_n \rangle \langle k_n | x' \rangle = \langle x | x' \rangle = \delta(x-x'). \tag{7.1.4b}$$

**(a) Orthonormality axiom-3**

Using the integral form (2.1.2) of the completeness relation sum we get the following.

$$\delta_{mn} = \langle k_m | k_n \rangle = \int_{-L/2}^{L/2} dx \langle k_m | x \rangle \langle x | k_n \rangle = \int_{-L/2}^{L/2} dx \frac{e^{-ik_m x}}{\sqrt{norm.}} \frac{e^{ik_n x}}{\sqrt{norm.}} \tag{7.1.5}$$

The conjugation axiom-2 was used to write

$$\langle k_m | x \rangle = \langle x | k_m \rangle^* = \frac{e^{-ik_m x}}{\sqrt{norm.}} \tag{7.1.6}$$

After integrating, this determines the *normalization constant*  $norm.$  as follows.

$$\begin{aligned} \delta_{mn} &= \int_{-L/2}^{L/2} dx \frac{e^{-ik_m x}}{\sqrt{norm.}} \frac{e^{ik_n x}}{\sqrt{norm.}} = \int_{-L/2}^{L/2} dx \frac{e^{-i(k_m - k_n)x}}{norm.} = \frac{e^{-i(k_m - k_n)L/2} - e^{-i(k_m - k_n)(-L/2)}}{-i(k_m - k_n)norm.} \\ &= \frac{e^{-i(k_m - k_n)L/2} - e^{i(k_m - k_n)L/2}}{-i(k_m - k_n)norm.} = \frac{2 \sin[(k_m - k_n)L/2]}{(k_m - k_n)norm.} \end{aligned} \tag{7.1.8}$$

Using the quantization conditions (7.1.3) gives the desired  $norm.$  value and satisfies axiom-3.

$$\delta_{mn} = \frac{2 \sin \pi(m-n)}{\frac{2\pi}{L}(m-n) \text{norm.}} = \begin{cases} 0 & \text{if: } m \neq n \\ \frac{L}{\text{norm.}} & \text{if: } m = n \end{cases}, \text{ or: } \text{norm.} = L. \quad (7.1.9)$$

Normalized wave amplitudes are therefore

$$\psi_{k_m}(x) = \langle x | k_m \rangle = \frac{e^{ik_m x}}{\sqrt{L}}. \quad (7.1.10)$$

### (b) Completeness axiom-4

Completeness axiom-4 has a Dirac-delta form in the mixed discrete-continuous wave space.

$$\delta(x-x') = \sum_{m=-\infty}^{m=+\infty} \langle x | k_m \rangle \langle k_m | x' \rangle \quad (7.1.11)$$

We test it with amplitudes (7.1.10) using orthonormality (7.1.4) and conjugation (7.1.5).

$$\int_{-L/2}^{L/2} dx \delta(x-x') = \int_{-L/2}^{L/2} dx \sum_{n=-\infty}^{n=+\infty} \frac{e^{ik_n x}}{\sqrt{L}} \frac{e^{-ik_n x'}}{\sqrt{L}} = \sum_{n=-\infty}^{n=+\infty} \frac{e^{-ik_n x'}}{\sqrt{L}} \int_{-L/2}^{L/2} dx \frac{e^{ik_n x}}{\sqrt{L}} \quad (7.1.12)$$

The last integral is a representation of a Kronecker delta  $\delta_{0,n}$ . Recall that  $k_0 = 0$  and use (7.1.4).

$$\begin{aligned} \int_{-L/2}^{L/2} dx \frac{e^{ik_n x}}{\sqrt{L}} &= \sqrt{L} \int_{-L/2}^{L/2} dx \frac{e^{-ik_0 x}}{\sqrt{L}} \frac{e^{ik_n x}}{\sqrt{L}} = \sqrt{L} \langle k_0 | k_n \rangle = \sqrt{L} \delta_{0,n} \\ \int_{-L/2}^{L/2} dx e^{ik_n x} &= L \delta_{0,n}. \end{aligned} \quad (7.1.13)$$

Then (7.1.12) is consistent with (7.1.11) and (7.1.10) and the definition of Dirac's delta.

$$\int_{-L/2}^{L/2} dx \delta(x-x') = \int_{-L/2}^{L/2} dx \sum_{n=-\infty}^{n=+\infty} \frac{e^{ik_n x}}{\sqrt{L}} \frac{e^{-ik_n x'}}{\sqrt{L}} = \sum_{n=-\infty}^{n=+\infty} e^{-ik_n x'} \delta_{0,n} = e^{-ik_0 x'} = 1 \quad (7.1.14)$$

### (c) Fourier series representation of a state

With completeness one can quickly derive a representation of arbitrary state  $|\Psi\rangle$  if you know its complex wavefunction  $\Psi(x) = \langle x | \Psi \rangle$ . Formally, you just operate on  $|\Psi\rangle$  with the unit  $\mathbf{1} = \sum |k_m\rangle \langle k_m|$ .

$$\begin{aligned} \langle x | \Psi \rangle &= \sum_{m=-\infty}^{m=+\infty} \langle x | k_m \rangle \langle k_m | \Psi \rangle = \sum_{m=-\infty}^{m=+\infty} \frac{e^{ik_m x}}{\sqrt{L}} \langle k_m | \Psi \rangle \\ &= \sum_{m=-\infty}^{m=+\infty} e^{ik_m x} \Psi_m \end{aligned} \quad (7.1.15a)$$

where the Fourier coefficient  $\Psi_m$  is given by the following integral (Use  $x$ -completeness  $\mathbf{1} = \int dx |x\rangle \langle x|$ .)

$$\begin{aligned} \Psi_m &= \frac{\langle k_m | \Psi \rangle}{\sqrt{L}} = \frac{1}{\sqrt{L}} \int_{-L/2}^{L/2} dx \langle k_m | x \rangle \langle x | \Psi \rangle = \frac{1}{\sqrt{L}} \int_{-L/2}^{L/2} dx \frac{e^{-ik_m x}}{\sqrt{L}} \langle x | \Psi \rangle \\ &= \frac{1}{L} \int_{-L/2}^{L/2} dx e^{-ik_m x} \Psi(x) \end{aligned} \quad (7.1.15b)$$

The only requirement is that the function be *periodic* in  $L$ , that is,  $\Psi(x) = \Psi(x+L)$ .

### (d) Bohr dispersion relation and energies

In Fig. 7.1.1 the waves with higher  $k_m$  have higher energy  $E_m$  and are drawn higher according to the  $E$ -values given by the *Bohr dispersion function* first drawn in Fig. 5.6.3.

$$E_m = \hbar\omega_m = \frac{(\hbar k_m)^2}{2M}, \text{ where: } p_m = \hbar k_m = \hbar \frac{2\pi}{L} m. \quad (7.1.16)$$

This is just a non-relativistic approximation for energy that neglects the rest energy  $Mc^2$  and higher order terms in (5.2.5b). It is kinetic energy only, that is  $KE = 1/2Mu^2 = p^2/2M$  with the momentum  $p=p_m$  and wavevector  $k=k_m$  quantized by conditions (7.1.3). The dispersion function is then a simple parabola of discrete values as shown on the right hand side of Fig. 7.1.1. Note that each energy value  $E_m$ , except  $E_0$ , has two orthogonal wavefunctions  $\psi_{\pm k_m}$  or states  $|\pm k_m\rangle$  corresponding to pairs of oppositely moving wavevectors  $\pm k_m$  on either side of the dispersion parabola. The  $|\pm k_m\rangle$  are called *degenerate states* because they share a single energy  $E_m$ . Such degenerate pairs are each an example of a U(2) two-state system. As long as the degeneracy remains, any unitary linear combination of the two states is also an eigenstate with the same frequency and energy  $E=h\nu$ .

### (e) Sine and cosine Fourier series worth remembering

A function defined by Fourier series (7.1.15) repeats after its fundamental wavelength  $L=2\pi/k_1$  or period  $T=2\pi/\omega_1$ . So do the real and imaginary parts that are series of sine or cosine functions of  $m^{\text{th}}$  spatial overtone argument  $k_mx$  or  $m^{\text{th}}$  overtone frequency argument  $\omega_mt$ . Moving wave terms use both:  $(k_mx - \omega_mt)$ .

Let us consider wave functions with *zero-DC-bias* or zero ( $k=0$ )-Fourier component:  $0=\Psi_0=\int\Psi$ . The integrals and derivatives of unbiased functions may also be unbiased. An example of a series of unbiased functions starts with the *alternating Dirac delta function adel(x)* shown at the top of Fig. 7.1.2. Its integrals and derivatives are useful series worth remembering because they are easy to compute and visualize. Compare this function to the simple delta pulse train (5.3.2) shown in Fig. 5.3.2.

The first integral of *adel(x)* is a *square wave function box(x)* shown next in line in Fig. 7.1.2. Below it is a *saw-tooth wave saw(x)* and then a *parabolic amplitude wave paw(x)*. Each wave has an overall scale factor attached so plots that are not delta-like end up with comparable amplitudes.

Wave *paw(x)* looks like a sine wave but isn't quite. The derivative of a genuine sine wave is a cosine wave that looks just like a sine wave but is moved back by  $\pi/2$ . The derivative of *paw(x)* is *saw(x)*, which is moved back, but it looks nothing like good old *paw(x)*! Subsequent derivatives only accentuate the differences between *sin(x)* and *paw(x)*. Differentiation amplifies little blips or bends (It differentiates!) while integration does the opposite by smoothing out sharp corners or other differences.

There are at least two famous physics topics that make use of functions that are derivatives or integrals of each other. Classical mechanics in one dimension is one such topic where the functions of *acceleration a(t)*, *velocity v(t)*, and *position x(t)*, are each the integral of one above or the derivative of the one below. Classical electrostatics is another topic in which the *charge-density ρ(x)*, *electric field E(x)*, and *potential Φ(x)*, are so related. (Various conventions may put  $\pm$  signs and scale factors onto these relations.)

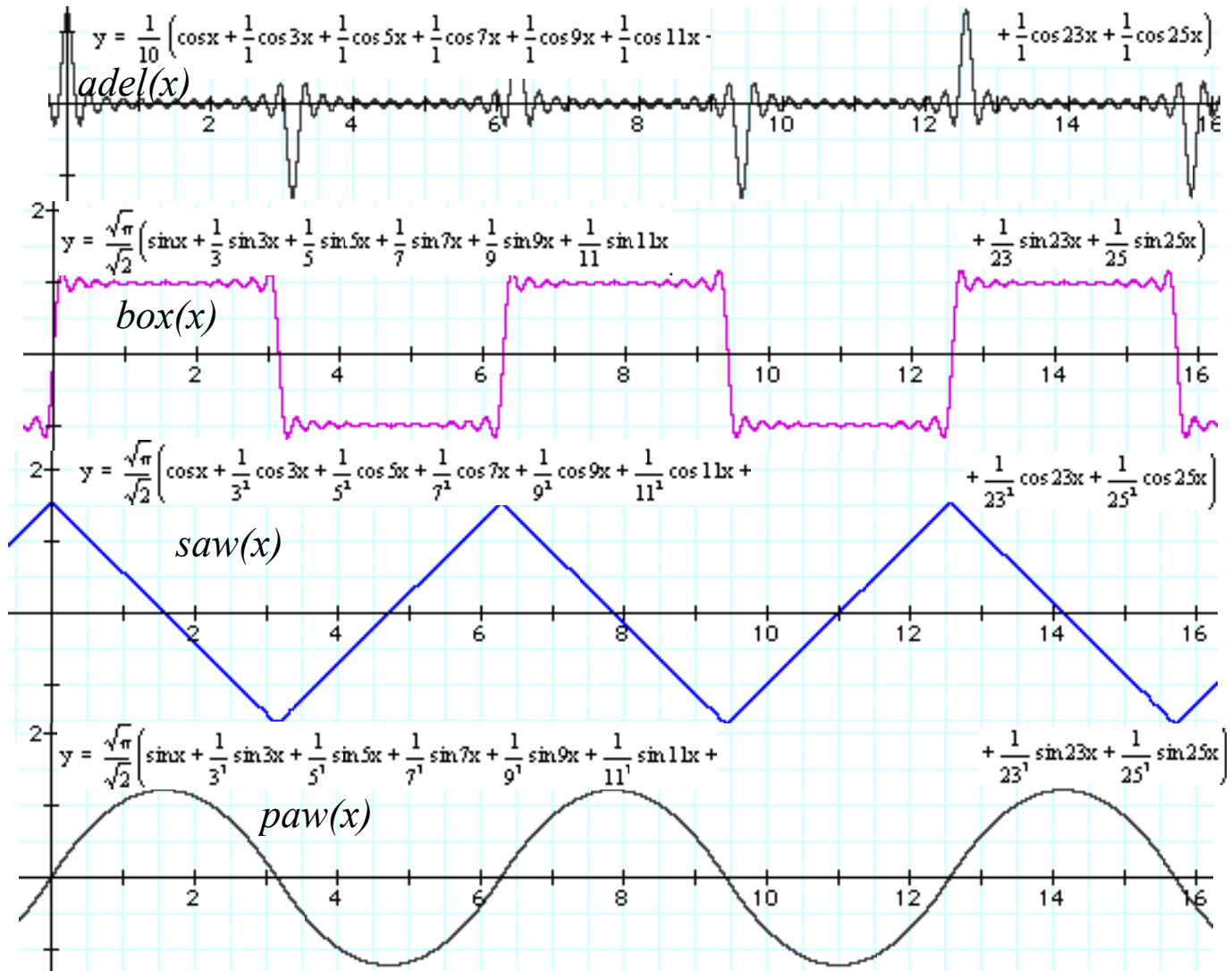
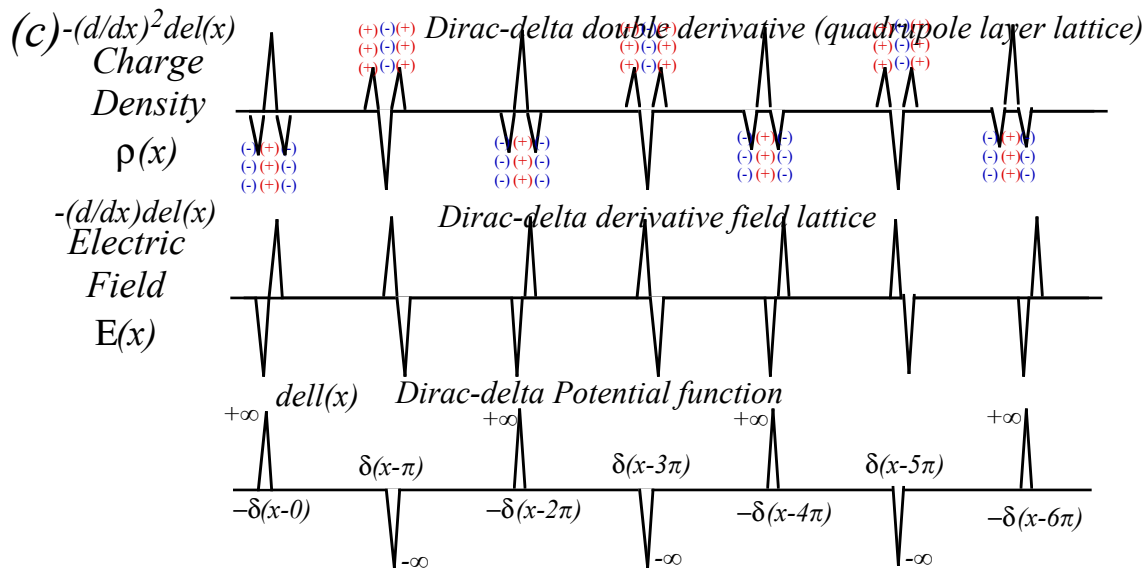
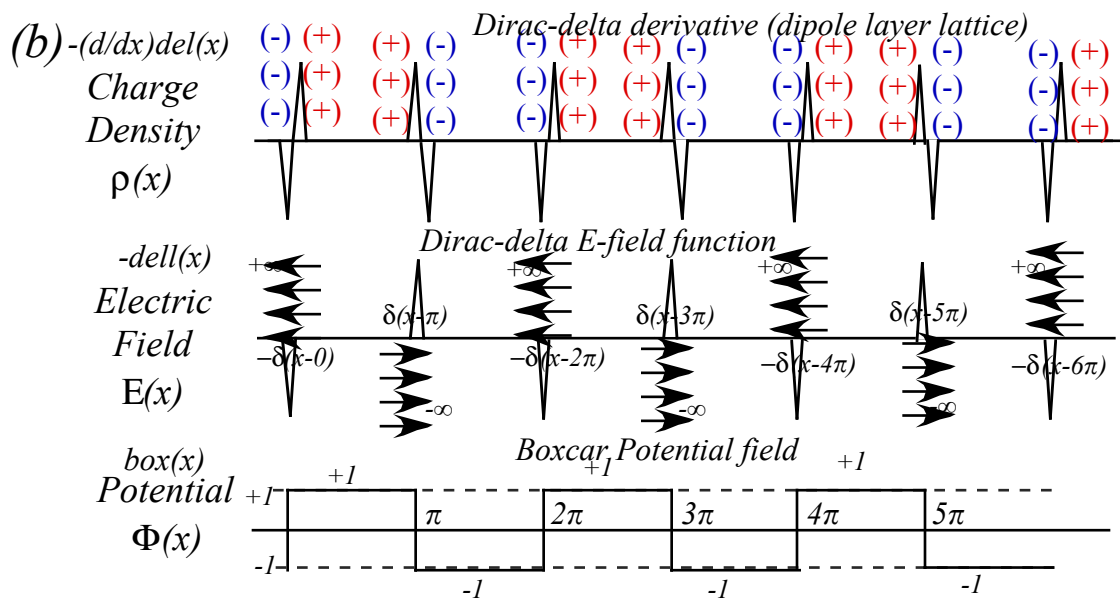
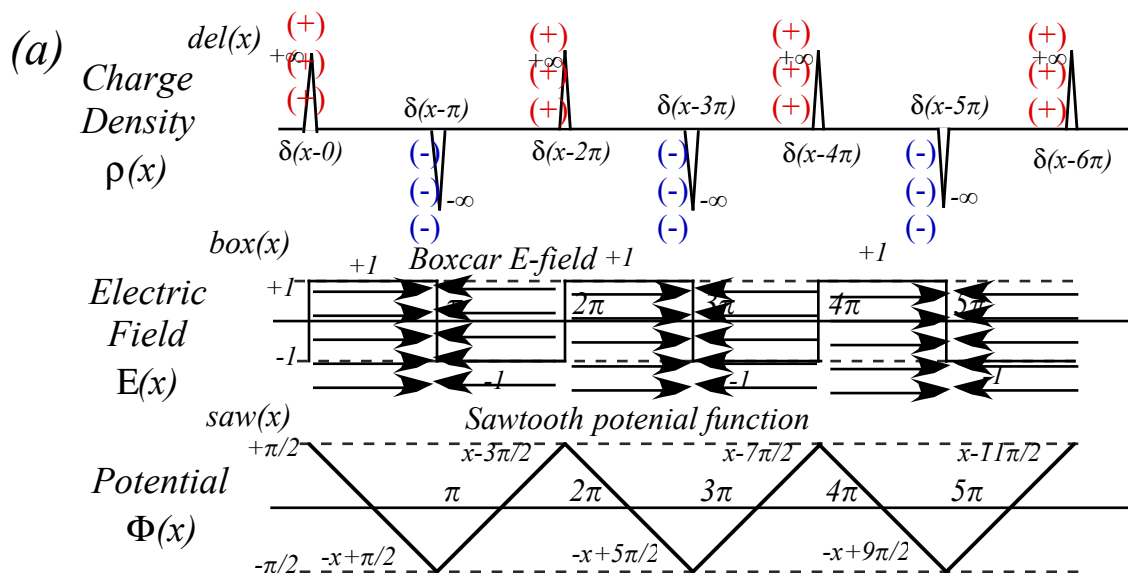


Fig. 7.1.2 Fourier series sharing simple integral or derivative relations to each other.

Some more or less extreme examples of charge and field distributions are sketched in Fig. 7.1.3 on the following page. The first set in Fig. 7.1.3(a) is due to alternating charge layers. The field is that of a series of alternating parallel-plate capacitors. By taking a derivative of the alternating charge layers we make the dipole layer distribution shown in the top of the middle Fig. 7.1.3(b). The final example in Fig. 7.1.3(c) actually has a Dirac-delta potential lattice, one of many favorite models for nano science these days. We shall be modeling periodic potentials, too. The preceding gives you some feeling how difficult it may be to actually *produce* some of these exotic potentials! Seldom is theory so easy and the lab so hard.

Also it is worth considering these as time-pulse series. As we will explain later, you may taper the Fourier series amplitudes gradually to zero and thereby replace the sharp and wrinkled deltas and squares by smoother Gaussian or Lorentzian features that are useful spectroscopic models. Of course, you may taper them right back to single term series of one sine or one cosine wave each!

Following page: Fig. 7.1.3 Exotic 1-D electric charge and field distributions.



## 7.2 Continuous and unbounded $x$ . Continuous and unbounded $k$

In the preceding cases all wavevectors are restricted by the quantization condition (7.1.3).

$$k_m = \frac{2\pi}{L} m, \text{ where: } m = 0, \pm 1, \pm 2, \pm 3, \dots, \pm \infty \quad (7.1.3)_{\text{repeated}}$$

If you let the "cage" become infinitely large ( $L \rightarrow \infty$ ) then the wavevector set becomes finer and finer and approaches a *continuum*. The trick is to replace each sum over index  $m$  by an integral over a continuous  $k$ -value. If it is done right the wave functions will take a continuous form in *both*  $x$  and  $k$ .

$$\psi_k(x) = \langle x | k \rangle = \frac{e^{ikx}}{\sqrt{\text{norm.}}} , \quad (7.2.1a)$$

We need to verify  $k$ -orthonormality relations based on wavevector Dirac-delta  $\delta(k', k)$ -functions.

$$\langle k' | k \rangle = \delta(k' - k) = \int_{-\infty}^{\infty} dx \langle k' | x \rangle \langle x | k \rangle = \int_{-\infty}^{\infty} dx \psi_{k'}(x)^* \psi_k(x) , \quad (7.2.1b)$$

We also need the usual  $x$ -completeness relations based on spatial Dirac-delta  $\delta(x', x)$ -functions.

$$\langle x' | x \rangle = \delta(x' - x) = \int_{-\infty}^{\infty} dk \langle x' | k \rangle \langle k | x \rangle = \int_{-\infty}^{\infty} dk \psi_k(x')^* \psi_k(x) \quad (7.2.1c)$$

It seems that orthonormality and completeness relations are two sides of the same coin. Orthonormality (7.2.1b) for the  $k$ -states  $\{|k\rangle \dots |k'\rangle \dots\}$  expresses completeness for the  $x$ -states  $|x\rangle$ , and completeness (7.2.1c) of the  $k$ -states  $|k\rangle$  expresses orthonormality for the  $x$ -states  $\{|x\rangle \dots |x'\rangle \dots\}$ .

The Dirac notation is extremely efficient but can be confusing. There is a world of difference between the states  $\{|k\rangle \dots |k'\rangle \dots\}$  of perfectly monochromatic plane waves and the Dirac position states  $\{|x\rangle \dots |x'\rangle \dots\}$  of perfectly localized particles. Recall that we said that an  $|x\rangle$  state was physically unrealizable; crushing a particle into a single position- $x$  would cost infinite energy. Technically, a  $|k\rangle$  state is unrealizable, too, since it requires an infinite amount of real estate; we have to let its cage dimension  $L$  be infinite, but that seems easier than the extreme solitary confinement needed to make an  $|x\rangle$  state. If space is cheaper than energy, then  $|k\rangle$  is easier to approach than  $|x\rangle$ . Lasers easily make approximate  $|k\rangle$ 's by being stable and coherent, but producing approximate  $|x\rangle$ 's for extremely short pulses requires more difficult engineering.

Use caution to not abuse this notation, though it is easily done. It should be obvious why the following rendition of (7.2.1a) is a dreadful mistake.

$$\langle k | k \rangle = \frac{e^{i k k}}{\sqrt{\text{norm.}}} = \frac{e^{i k^2}}{\sqrt{\text{norm.}}} \quad (\text{Dirac abuse. Very BAD mistake!})$$

Letters  $x$  and  $k$  denote very different bases which must not to be confused.

### (a) Fourier integral transforms

To achieve the limit of infinite real estate ( $L \rightarrow \infty$ ) we replace sums over  $k_m = \frac{2\pi}{L} m$  such as

$$S = \sum_{m=-\infty}^{m=+\infty} \Phi_{k_m} = \sum_{m=-\infty}^{m=+\infty} \Delta m \Phi_{k_m}, \text{ where: } \Delta m = 1 . \quad (7.2.2)$$

Integrals over  $k$  with differential  $\Delta k_m = \frac{2\pi}{L} \Delta m = \frac{2\pi}{L} \rightarrow dk$  or:  $\frac{\Delta m}{\Delta k_m} = \frac{L}{2\pi}$  are used as follows.

$$S = \sum_{m=-\infty}^{m=+\infty} \Delta m \Phi_{k_m} = \sum_{m=-\infty}^{m=+\infty} \frac{\Delta m}{\Delta k_m} \Delta k_m \Phi_{k_m} \text{ becomes } \rightarrow \frac{L}{2\pi} \int_{-\infty}^{+\infty} dk \Phi(k) \quad (7.2.3)$$

This, by itself, blows up as we let  $(L \rightarrow \infty)$ , but so do the normalization denominators  $\sqrt{norm.} = \sqrt{L}$ , and they cancel. Finally, the Fourier series (7.1.15a) becomes a finite integral.

$$\langle x | \Psi \rangle = \sum_{m=-\infty}^{m=+\infty} \frac{e^{ik_m x}}{\sqrt{L}} \langle k_m | \Psi \rangle \text{ becomes } \rightarrow \frac{L}{2\pi} \int_{-\infty}^{+\infty} dk \frac{e^{ikx}}{\sqrt{L}} \langle k_m | \Psi \rangle = \int_{-\infty}^{+\infty} dk \frac{e^{ikx}}{\sqrt{2\pi}} \frac{\sqrt{L}}{\sqrt{2\pi}} \langle k_m | \Psi \rangle$$

The trick is to renormalize the  $k$ -bases so  $\frac{\sqrt{L}}{\sqrt{2\pi}} \langle k_m |$  becomes  $\langle k |$  letting the  $L$ 's cancel.

$$\langle x | \Psi \rangle = \int_{-\infty}^{+\infty} dk \frac{e^{ikx}}{\sqrt{2\pi}} \langle k | \Psi \rangle = \int_{-\infty}^{+\infty} dk \langle x | k \rangle \langle k | \Psi \rangle, \quad (7.2.4a)$$

The newly “normalized” plane wave function  $\psi_k(x) = \langle x | k \rangle$  is defined as follows.

$$\langle x | k \rangle = \frac{e^{ikx}}{\sqrt{2\pi}} \quad (7.2.4b)$$

This  $\langle x | k \rangle$  is the *kernel* of a *Fourier integral transform*. An inverse follows by converting (7.1.15b).

$$\frac{\langle k_m | \Psi \rangle}{\sqrt{L}} = \frac{1}{L} \int_{-L/2}^{L/2} dx e^{-ik_m x} \langle x | \Psi \rangle \text{ becomes } \rightarrow \langle k | \Psi \rangle = \frac{\sqrt{L}}{\sqrt{2\pi}} \frac{\sqrt{L}}{L} \int_{-\infty}^{+\infty} dx e^{-ikx} \langle x | \Psi \rangle,$$

$$\langle k | \Psi \rangle = \int_{-\infty}^{+\infty} dx \frac{e^{-ikx}}{\sqrt{2\pi}} \langle x | \Psi \rangle = \int_{-\infty}^{+\infty} dx \langle k | x \rangle \langle x | \Psi \rangle, \quad (7.2.4c)$$

Here the *inverse kernel*  $\langle k | x \rangle$  is simply the conjugate of  $\langle x | k \rangle$  as required by conjugation axiom-2.

$$\langle k | x \rangle = \frac{e^{-ikx}}{\sqrt{2\pi}} = \langle x | k \rangle^* . \quad (7.2.4d)$$

**(b) Fourier coefficients: Their many names**

The efficiency of the Dirac notation (provided it isn't abused!) should be clear by now. The simple bra-ket  $\langle x | k \rangle$  stands for so many different mathematical and physical objects. Let's list some.

- (1)  $\langle x | k \rangle$  is a *scalar product* of bra  $\langle x |$  and ket  $| k \rangle$
- (2)  $\langle x | k \rangle$  is an *x-wavefunction* for a state  $| k \rangle$  of definite momentum  $p = \hbar k$ .
- (3)  $\langle k | x \rangle = \langle x | k \rangle^*$  is a *k-wavefunction* for a state  $| x \rangle$  of definite position  $x$ .
- (4)  $\langle x | k \rangle$  is a unitary *transformation matrix* from position states to momentum states.
- (5)  $\langle x | k \rangle$  is the *kernel* of a Fourier transform between position states and momentum states.

As beautiful and compact as it is, the continuum functional Fourier analysis is merely an infinite and unbounded abstraction that lets us use calculus to derive formulas in special cases. Its validity as a limiting case for experimental and numerical analysis should always be questioned. Laboratory and computer experiments, on the other hand, invariably deal with finite and bounded spaces, and it these that we turn to in the next section. We finish this section by relating square-wave Fourier transforms to square-wave Fourier series of the preceding section to help clarify discrete-vs.-continuum relations.

### (c) Time: Fourier transforms worth remembering

Fourier time-frequency (time-per-time) transforms resemble space- $k$ -vector (space-per-space) transforms (7.2.4). But, a negative sign is put in the exponent so the time phasor turns clockwise.

$$\langle t | \Psi \rangle = \int_{-\infty}^{+\infty} d\omega \frac{e^{-i\omega t}}{\sqrt{2\pi}} \langle \omega | \Psi \rangle = \int_{-\infty}^{+\infty} d\omega \langle x | \omega \rangle \langle \omega | \Psi \rangle \quad (7.2.5a) \quad \langle t | \omega \rangle = \frac{e^{-i\omega t}}{\sqrt{2\pi}} \quad (7.2.5b)$$

$$\langle \omega | \Psi \rangle = \int_{-\infty}^{+\infty} dt \frac{e^{i\omega t}}{\sqrt{2\pi}} \langle t | \Psi \rangle = \int_{-\infty}^{+\infty} dt \langle \omega | t \rangle \langle t | \Psi \rangle \quad (7.2.5c) \quad \langle \omega | t \rangle = \frac{e^{i\omega t}}{\sqrt{2\pi}} = \langle t | \omega \rangle^*$$

Consider, for example, a single square bump of amplitude  $B$  and duration  $T/2$ . Its Fourier transform (7.2.5c) is an *elementary diffraction function*  $\sin \omega/\omega$  that is plotted in Fig. 7.2.1.

$$\langle \omega | \Psi \rangle = \int_{-T/4}^{+T/4} dt \frac{e^{i\omega t}}{\sqrt{2\pi}} B = B \frac{e^{i\omega T/4} - e^{-i\omega T/4}}{i\omega\sqrt{2\pi}} = \frac{2B \sin(\omega T/4)}{\omega\sqrt{2\pi}} \quad (7.2.6)$$

It is the first approximation to an optical diffraction function for a single square aperture.

The Fourier amplitude due to multiple square humps is a combination of finer and finer elementary diffraction patterns. Three half-humps give the following frequency function plotted in Fig. 7.2.2(a).

$$\begin{aligned} \langle \omega | \Psi \rangle &= \frac{1}{\sqrt{2\pi}} \left[ A \int_{-3T/4}^{-T/4} dt e^{i\omega t} + B \int_{-T/4}^{+T/4} dt e^{i\omega t} + A \int_{+T/4}^{+3T/4} dt e^{i\omega t} \right] \\ &= A \frac{e^{-i\omega T/4} - e^{i3\omega T/4}}{i\omega\sqrt{2\pi}} + B \frac{e^{i\omega T/4} - e^{-i\omega T/4}}{i\omega\sqrt{2\pi}} + A \frac{e^{i3\omega T/4} - e^{i\omega T/4}}{i\omega\sqrt{2\pi}} \quad (7.2.7) \\ &= \frac{2(B-A)\sin(\omega T/4)}{\omega\sqrt{2\pi}} + \frac{2A\sin(3\omega T/4)}{\omega\sqrt{2\pi}} \end{aligned}$$

The frequency functions in Fig. 7.2.3 are the result of a lot more bumps. Each one consists of a series of spikes corresponding to the Fourier series amplitudes  $1, 1/3, 1/5, 1/7, \dots$  for the fundamental  $\omega=2\pi/T$  and odd-overtones  $3\omega, 5\omega, 7\omega, \dots$ , respectively, for the *box(x)* function in Fig. 7.1.2. This is an even box function in Fig. 7.2.3 so the series amplitudes alternate sign as  $1, -1/3, 1/5, -1/7, \dots$  as shown. The very last example is an unbiased function with no DC ( $\omega=0$ )-Fourier component.

The "ringing" between the peaks is generally considered to be a nuisance. One way to get rid of ringing is to turn on the square wave more gradually. Fig. 7.2.4 shows the Fourier transform of a wave that has been turned on and off by a Gaussian ( $\exp(-x/a)^2$ ). This *windowing* kills the ringing. The width of each frequency peak varies inversely with the width  $a$  of the Gaussian window.

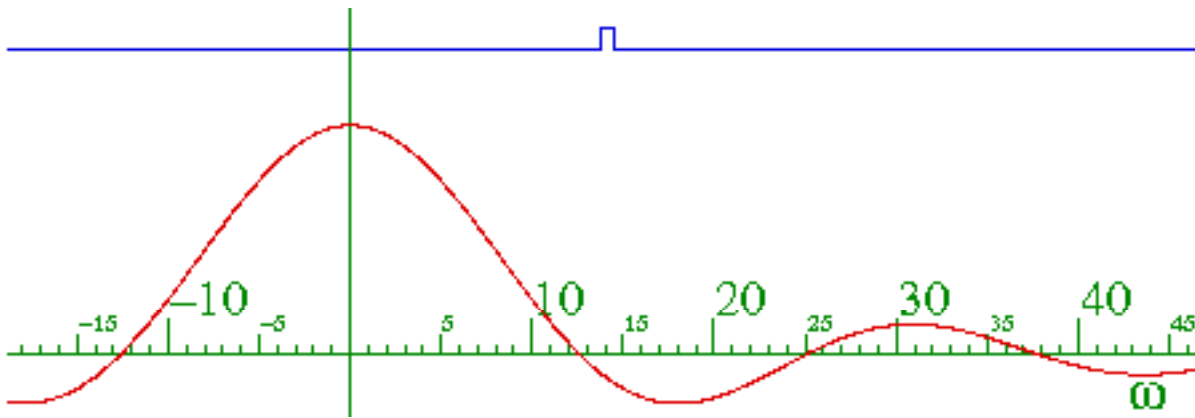


Fig.7.2.1 Elementary diffraction function: Fourier transform of single half square wave.

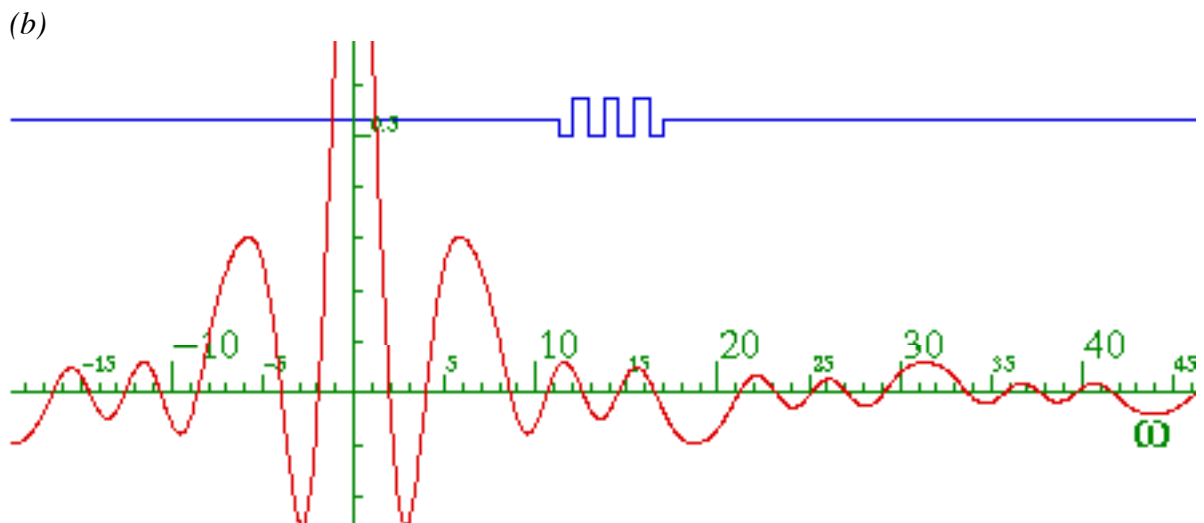
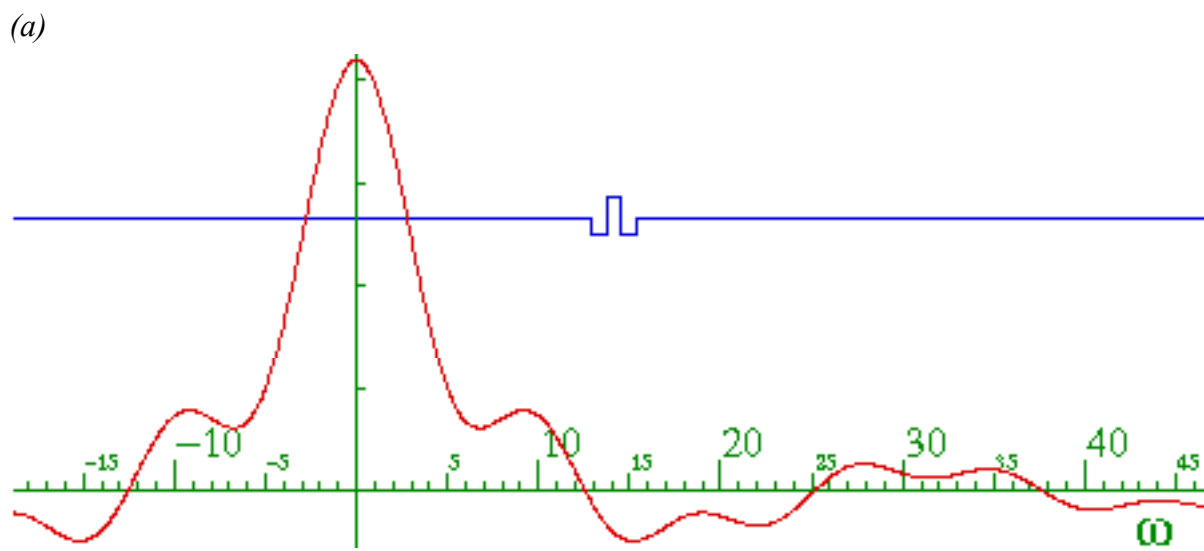
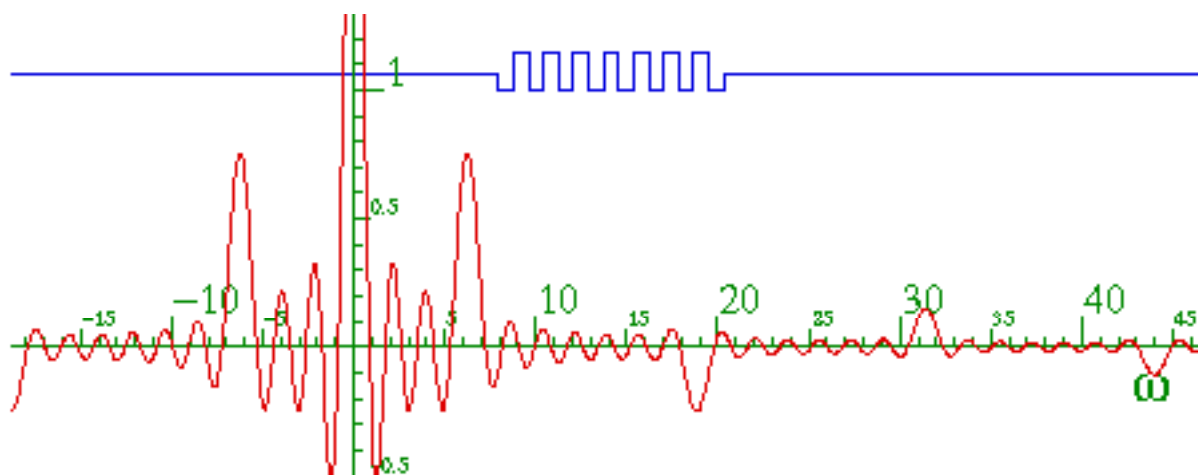
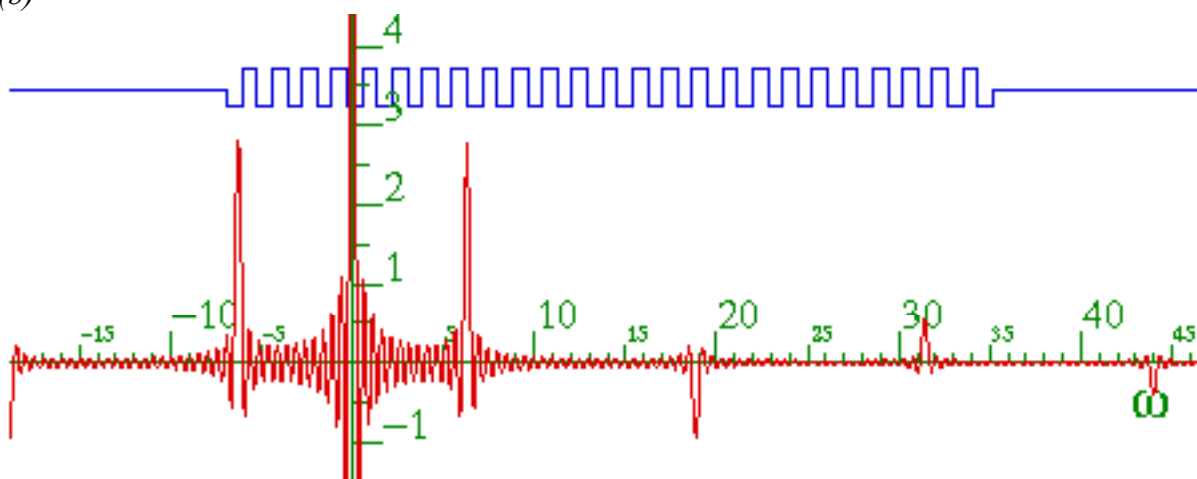


Fig. 7.2.2 Fourier transform of (a) three half- square waves. (b) seven half-square waves.

(a)



(b)



(c)

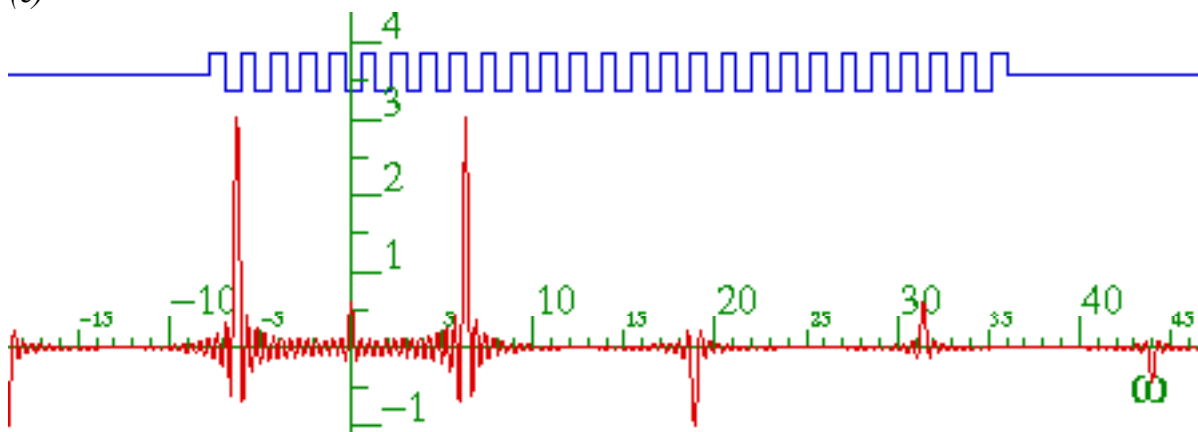


Fig. 7.2.3 Fourier transforms of square half-bumps (a) fifteen (b) forty-nine (c) fifty one .

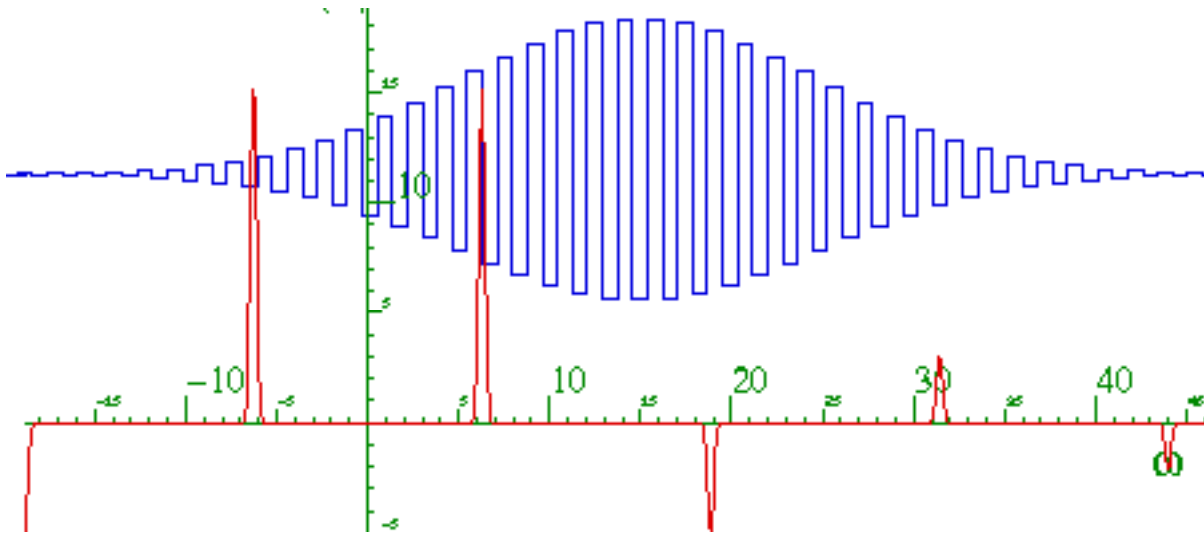


Fig. 7.2.4 Fourier transform of windowed square waves.

The idea of the Fourier integral, as opposed to Fourier series, is that any function, periodic or otherwise can be approximated by sines and cosines from a frequency *continuum*. Fourier series require that the function be periodic and repeat itself perfectly after some fixed period of time. The Fourier integral is supposed to be an enduring and time-invariant frequency map that provides the predestination of a time function forever and ever!

One should be suspicious of something that requires an infinite continuum of perfect frequency oscillators to be behind the scenes running your life. Pure sines and cosines are forever functions but we, like our world, certainly are not so enduring. Consider Fourier integrals as a cute limit-taking tool but not ultimately realistic.

Consider the fictitious function of time shown in Fig. 2.6.6. It is only periodic for awhile, but like most of us, cannot maintain the pace forever and finally gets in trouble with the hereafter.

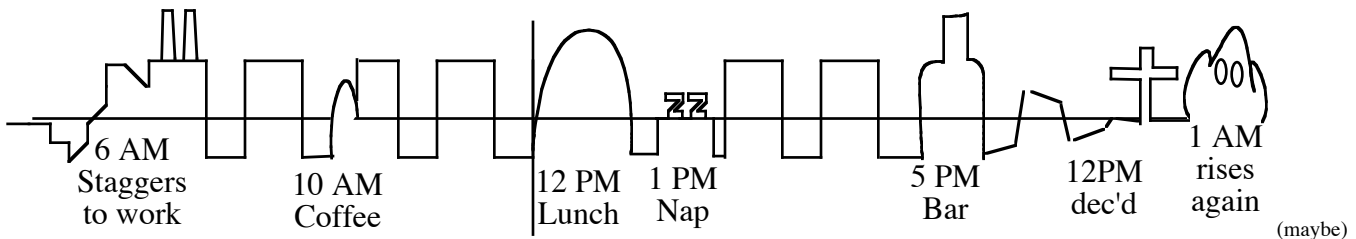


Fig. 7.2.5 A day in the life of a real function.

Now we go on to a practical Fourier analysis that is both finite and discrete.

### 7.3 Discrete and bounded $x$ . Discrete and bounded $k$

This is the most restrictive case, but also, due to practical considerations mentioned previously, the one that actually gets used the most these days. However, in spite of its practical value it is not always treated as carefully as the more “mathematically sophisticated” continuum case (b). It should be!

We begin by supposing that space itself is periodic as in case (a) but further is divided into  $N$  discrete pieces or points. So the only  $x$ -values allowed are the following  $N$  values

$$\{ x_0=0, x_1=a, x_2=2a, x_3=3a, \dots, x_{N-1}=(N-1)a, x_N=0 \} \tag{7.3.1a}$$

and there are only  $N$  position states are the following. The last  $|N\rangle$  state is the same as the first  $|0\rangle$  state.

$$\{ |0\rangle, |1\rangle, |2\rangle, |3\rangle, \dots, |N-1\rangle, |N\rangle=|0\rangle \} \tag{7.3.1b}$$

Fig. 7.3.1 shows ways to visualize this as  $N$  beads on a ring of length  $L = Na$  that wraps around so that the  $N$ -th bead is the same as the zero-th. (Zero-based numbering is the modern computing standard.) Otherwise, we invoke the so-called *periodic* or *Born-VonKarman* boundary conditions and imagine our 1-D world repeats like a computer game outside its boundaries. As shown in Fig. 7.3.1, there is a distance  $a$  between the lattice of beads. It is called the *lattice spacing*  $a$ .

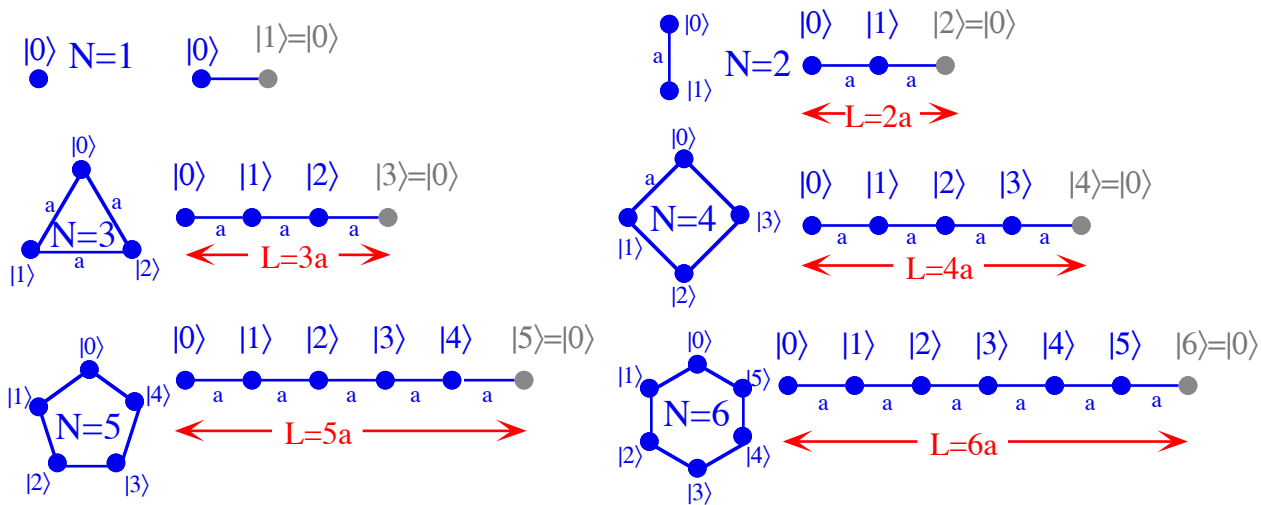


Fig. 7.3.1 Finite coordinate spaces for  $N$ -cyclic ( $C_N$ ) discrete systems ( $N = 1, 2, \dots, 6\dots$ )

These *ideal quantum dots* will be among our first examples of 2-state, 3-state, ..., and 6-state systems. By studying them carefully, it will be possible to learn important principles which will greatly help later study of molecules and solids which have  $N$ -states with large- $N$  but the same basic theory. Also, the quantum dots might have hidden inventions that could make you wealthy!

The basic wavefunctions that live on the discrete dots or beads are a subset of the continuum wavefunctions  $e^{ikmx}$  of (2.6.1), as though  $N$  equally spaced points of (2.6.1) were extracted and plotted over each lattice point  $x_p$  where

$$x_p = p a = p L/N \quad ( p = 0, 1, 2, 3, \dots, N-1 ) \tag{7.3.2}$$

The basic wavefunctions are given explicitly below.

$$\psi_{k_m}(x_p) = \langle x_p | k_m \rangle = \frac{e^{ik_m x_p}}{\sqrt{N}} = \psi_{k_m}(x_p + L) \tag{7.3.3}$$

The only change from (7.1.1) is the use of a discrete coordinate  $x_p$  defined in (7.3.2) above. Also, the normalization constant has been set to the dimension  $N$  since all  $N$  exponentials  $e^{ik_m x}$  contribute unit magnitude ( $|e^{ik_m x}|^2 = 1$ ) in the normalization sum.

$$\langle k_m | k_m \rangle = \sum_{p=0}^{N-1} \langle k_m | x_p \rangle \langle x_p | k_m \rangle = \sum_{p=0}^{N-1} \frac{e^{-ik_m x_p}}{\sqrt{N}} \frac{e^{ik_m x_p}}{\sqrt{N}} = N \frac{1}{\sqrt{N}} \frac{1}{\sqrt{N}} = 1 \tag{7.3.4}$$

The quantization conditions due to periodicity requirement (7.3.3) over "cage" length  $L=Na$  are similar to (7.1.3) but now expressed in terms of the discrete number  $N$  and spacing  $a$  of lattice points.

$$e^{ik_m L} = 1, \text{ or: } k_m = \frac{2\pi}{L} m = \frac{2\pi}{Na} m \tag{7.3.5a}$$

Wave amplitude at lattice point  $p$  is a power- $p$  of ( $e^{i2\pi/N}$ ), the  $N$ -th root of unity (normalized, of course)

$$\psi_{k_m}(x_p) = \langle x_p | k_m \rangle = \frac{e^{ik_m x_p}}{\sqrt{N}} = \frac{1}{\sqrt{N}} \left( e^{i2\pi/N} \right)^{mp} \tag{7.3.5b}$$

All  $N$  roots, together, form  $N$ -polygons in the complex plane as shown in Fig. 7.3.2. The allowed wave amplitudes in Fig. 7.3.2 resemble the "ring" coordinate positions in Fig. 7.3.1. The complex  $z_{m,p} = \exp(ik_m x_p)$  are the  $N$ -th roots of unity ( $z^N = 1$ ) introduced in a complex arithmetic review (App 1.A).

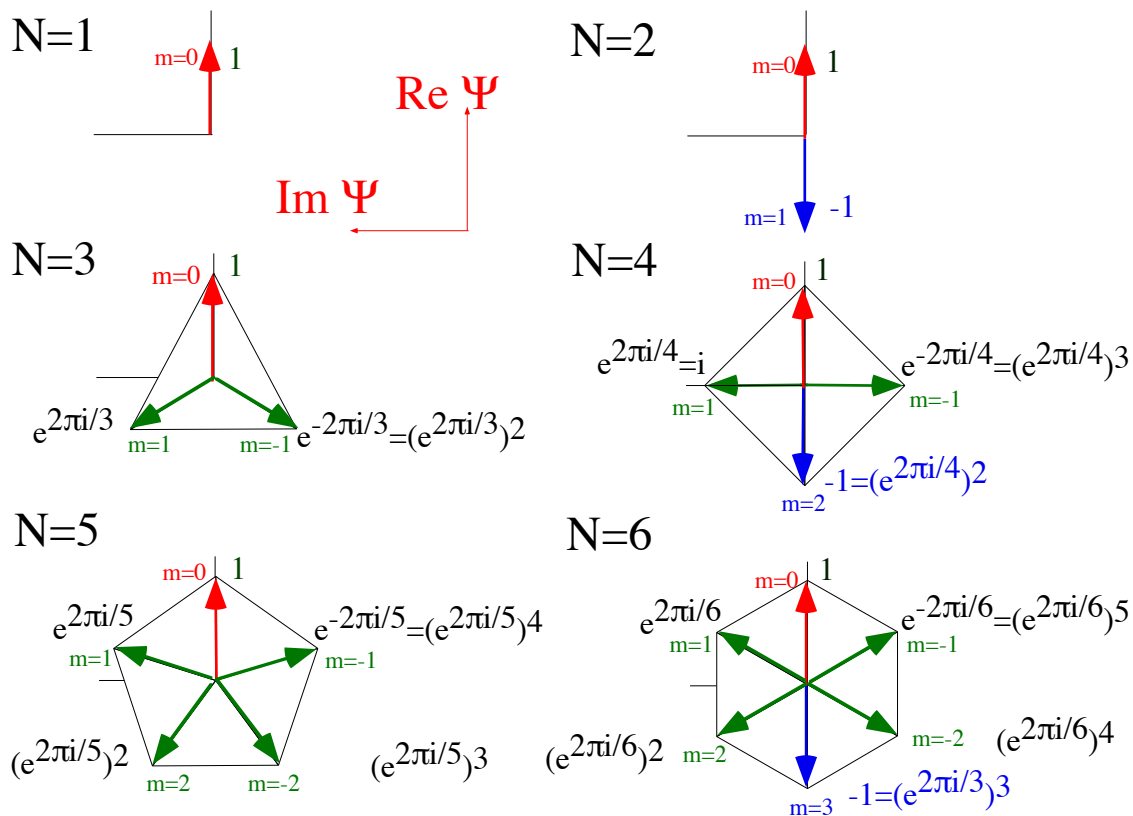


Fig. 7.3.2 Discrete wave amplitudes allowed for  $N$ -cyclic ( $C_N$ ) systems ( $N = 1, 2, \dots, 6, \dots$ )

### (a) N-nary counting for N-state systems

Fig. 7.3.2 shows different counting schemes for *odd-N* and *even-N*. In the unbounded cases the  $k$ -values go from  $-\infty$  to  $+\infty$ . Here, letting  $m$  count from  $-N$  to  $+N$  over-counts and gives  $2N+1$  states when we know there are only  $N$ . We could let  $m$  count from  $0$  to  $N-1$ , just like the lattice points. Or, we let  $m$  count from  $-(N-1)/2$  to  $+(N-1)/2$ , (*odd-N*) and from  $-(N-2)/2$  to  $+(N)/2$  (*even-N*) as shown below.

It helps to think of  $N$ -state cyclic system as an *N-nary* computer element. Ever since 1950, we have become accustomed to binary ( $N=2$ ) data storage in 2-bit registers. Inevitably, someone will discover how to make  $N$ -state registers. Until then, we imagine them. For an  $N$ -state register the quantum counting index  $m$  is defined only by an *integer modulo-N* or  $(m)_N$ .

$$(m)_N = m \text{ modulo } N \quad (7.3.6)$$

For example, for  $N=6$  in Fig. 7.3.2, all the following values of the quantum index  $m$  in a given line below have the same value modulo-6.

$$\begin{aligned} \dots &= (-9)_6 = (-3)_6 = \underline{(3)}_6 = (9)_6 = (15)_6 = \dots = 3 \text{ mod } 6 \\ \dots &= (-8)_6 = \underline{(-2)}_6 = (4)_6 = (10)_6 = \dots = -2 \text{ mod } 6 \\ \dots &= (-7)_6 = \underline{(-1)}_6 = (5)_6 = (11)_6 = \dots = -1 \text{ mod } 6 \\ \dots &= (-6)_6 = \underline{(0)}_6 = (6)_6 = (12)_6 = \dots = 0 \text{ mod } 6 \\ \dots &= (-5)_6 = \underline{(1)}_6 = (7)_6 = (13)_6 = \dots = 1 \text{ mod } 6 \\ \dots &= (-4)_6 = \underline{(2)}_6 = (8)_6 = (14)_6 = \dots = 2 \text{ mod } 6 \\ \dots &= (-3)_6 = \underline{(3)}_6 = (9)_6 = (15)_6 = \dots = 3 \text{ mod } 6 \\ \dots &= (-8)_6 = \underline{(-2)}_6 = (4)_6 = (10)_6 = \dots = -2 \text{ mod } 6 \end{aligned} \quad (7.3.7)$$

How do we choose a  $k_m$  number label? We choose the underlined ones with the smallest  $|m|$  and pick the positive one if two are equal. This choice  $\{m=-2, -1, 0, 1, 2, 3\}$  of  $N=6$   $m$ -values is used in Fig. 7.3.2.

### (b) Discrete orthonormality and completeness

Orthonormality relations for wave states reduce to finite geometric sums.

$$\langle k_m' | k_m \rangle = \sum_{p=0}^{N-1} \frac{e^{-ik_m' x_p}}{\sqrt{N}} \frac{e^{ik_m x_p}}{\sqrt{N}} = \frac{1}{N} \sum_{p=0}^{N-1} e^{i(k_m - k_m') x_p}, \text{ where: } x_p = p a \quad (7.3.8a)$$

Substituting (7.3.2) and (7.3.5) gives

$$\langle k_m' | k_m \rangle = \sum_{p=0}^{N-1} z^p = \frac{1+z+z^2+\dots+z^{N-1}}{N}, \text{ where: } z = e^{i(k_m - k_m') a} = e^{i2\pi(m-m')/N}$$

The geometric sum yields a result that satisfies  $k_m$ -orthonormality axiom-3.

$$\langle k_m' | k_m \rangle = \frac{1}{N} \frac{1-z^N}{1-z} = \frac{1}{N} \frac{1-e^{i2\pi(m-m')}}{1-e^{i2\pi(m-m')/N}} = \delta_{mm'} \quad (7.3.8b)$$

The  $k_m$ -completeness axiom-4 (or  $x_p$ - orthonormality) is satisfied for these wave states, as well.

$$\langle x_p' | x_p \rangle = \sum_{m=0}^{N-1} \langle x_p' | k_m \rangle \langle k_m | x_p \rangle = \sum_{m=0}^{N-1} \frac{e^{ik_m x_p'}}{\sqrt{N}} \frac{e^{-ik_m x_p}}{\sqrt{N}} = \frac{1}{N} \sum_{m=0}^{N-1} e^{i(x_p' - x_p) k_m} = \delta_{pp'} \quad (7.3.9)$$

**(c) Discrete Fourier transformation matrices**

Below are shown Fourier transformation matrices and discrete  $x_p$ -wavefunctions (7.3.5b)

$$\langle k_m | x_p \rangle = \Psi_{k_m}(x_p)^* = e^{-ik_m x_p} / \sqrt{N} \tag{7.3.10a}$$

They are drawn as complex phasor amplitudes for the cyclic  $N$ -state systems ( $C_N$ ) for  $N= 1, 2, 3, 4, 5, \text{ and } 6$ .

Also drawn over the phasors is the Re-part of the "Bohr's ghost" continuum  $x$ -wavefunctions

$$\langle k_m | x \rangle = \Psi_{k_m}(x)^* = e^{-ik_m x} / \sqrt{L} \tag{7.3.10b}$$

Recall (7.1.10) or Fig. 7.1.1. "Bohr's ghosts" match the discrete waves (7.3.10a) with phasor clocks.

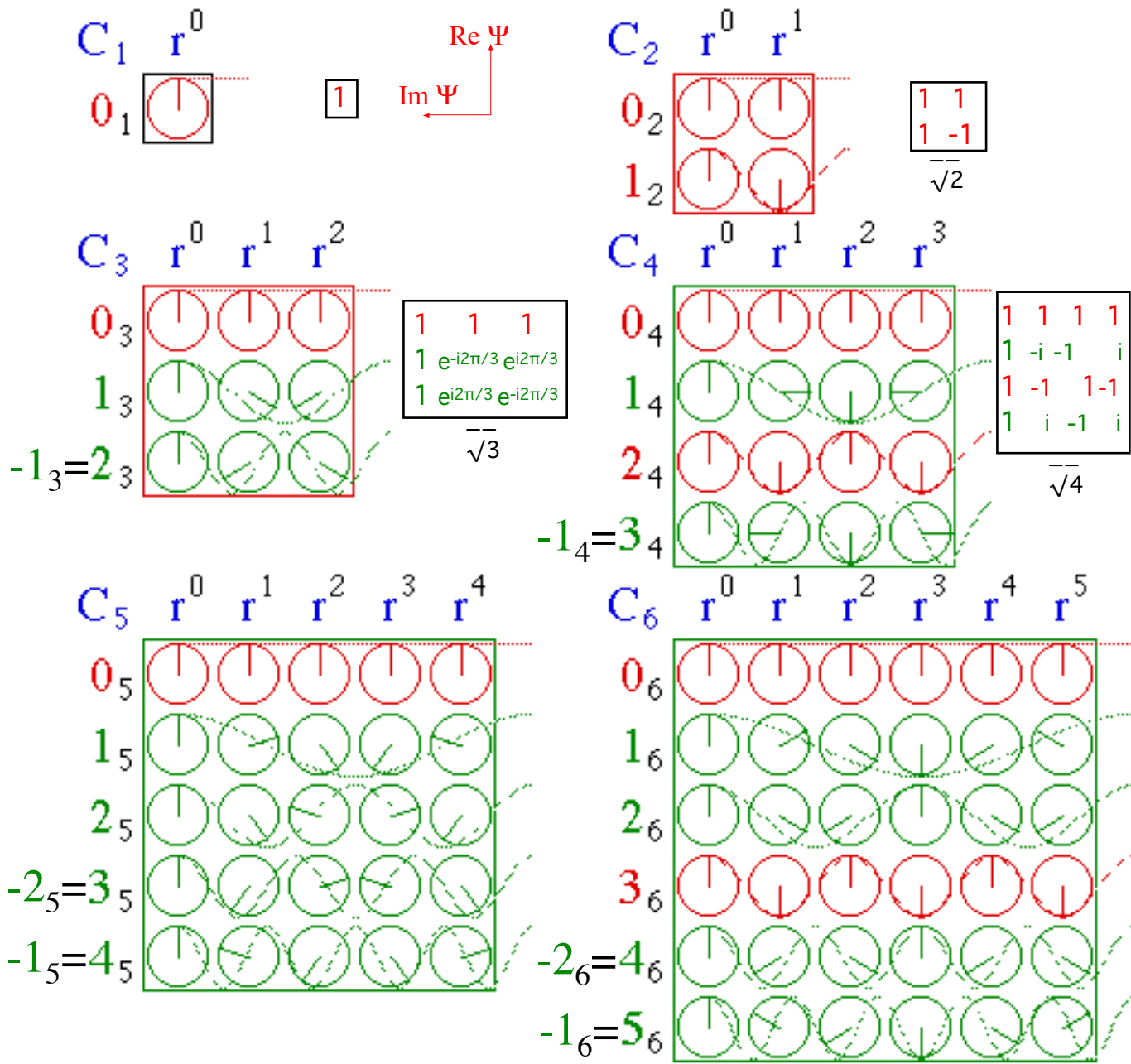


Fig.

7.3.3 Discrete Fourier transformation matrices for  $N$ -cyclic ( $C_N$ ) systems ( $N = 1, 2, \dots, 6\dots$ )

### (d) Introducing aliases and Brillouin zones

It is important to see the relation between the continuum waves and their "course-grained" images thatves with integral wave-numbers of  $m \bmod N$  whole wavelengths within each  $\langle k_m |$ -row of phasors. We might as well call them "row-waves" or "bra-waves." Note also, that the same wave shape exists in the columns or kets  $|x_p\rangle$ . Each "ket-wave"  $|x_p\rangle$  represents a  $\delta$ -position state or "pulse" localized at point  $x_p$ . The inverse Fourier transformation  $\langle k_m |x_p\rangle$  relates  $|x_p\rangle$  to a bra-wave  $\langle k_m |$ . As required by conjugation axiom-2, namely,  $\langle k_m |x_p\rangle = \langle x_p |k_m\rangle^*$ , the relation is the same as between  $|k_m\rangle$  and  $\langle x_p |$ , except for conjugation.

For low wave number like, say  $(m_N)=(1)_6$  or  $(2)_6$ , it is easy to see the "Bohr's-ghost wave" mirrored in the phasors as in the second and third row of the  $C_6$  matrix in Fig. 7.3.1. Note however, that these phasors are set so the phase of the one to the right is clockwise (that is it appears ahead) of the one to the left. This means, if the phasors turned clockwise, that the one to the right is feeding energy into the one to its left, so the wave would be moving right-to-left with wave momentum minus  $(1)_6$  or minus  $(2)_6$ , respectively. But, they're conjugated bras so their clocks go backwards and so the labels are OK, after all.

For high wave number like, say  $(m_N)=(4)_6$  or  $(5)_6$ , it is not so easy to see the "Bohr's-ghost wave" mirrored in the phasors as in the fifth and sixth row of the  $C_6$  matrix in Fig. 7.3.1. But, you can see *alias* waves of negative wave momentum  $(m_N)=(-2)_6$  or  $(-1)_6$ , respectively, that is oppositely moving waves of low wavenumber. Recall that  $(4 \bmod 6)$  equals  $(-2 \bmod 6)$  and  $(5 \bmod 6)$  equals  $(-1 \bmod 6)$ .

Right in the middle row of the *even-N* matrix is a wave that isn't going in either direction. In the  $C_6$  matrix it is the  $(3)_6$  wave. Since  $(3 \bmod 6)$  equals  $(-3 \bmod 6)$  this is a good old push-me-pull-you standing wave with all real amplitudes of  $(1, -1, 1, -1, 1, -1)$ . This can only happen for even- $N$  and is known as a *first Brillouin zone boundary* wave in solid-state physics.

All cases have a zero-momentum wave  $(0_N)$  at the top of the transformation matrix. This is called the *Brillouin zone center* wave in solid-state physics. Indeed, it is centered at the bottom of the dispersion plot in Fig. 2.6.1. Its phasor settings are the same as that of a higher  $(N_N)$ , or  $(2N_N)$ , or  $(3N_N)$ , ...etc. wave. However, this  $N$ -state system does not count higher than  $N-1$  without recycling.

Consider, for example, a  $k_{-11}$  wave of wavevector  $(-11)_{12}$  (with minus-eleven-kinks-modulo-12) as plotted in Fig. 7.3.4 (a). Since  $(-11)\text{-mod-}12$  equals  $(+1)\text{-mod-}12$  (that is,  $(-11)_{12}=(+1)_{12}$ ) it follows that the wave shown has the same effect as a  $(+1)_{12}$  wave. Indeed, the twelve masses in Fig. 7.3.4(a) line up on a single-kink ( $k=1$ )-wave moving positively, while the ( $k=-11$ )-wave moves negatively. (See *WaveIt* movie.) This is an example of aliasing. In a  $C_{12}$  lattice,  $(k=-11)$  is an alias for  $(k=+1)$ .

Fig. 7.3.4(b) shows the  $k$ -space with a typical frequency dispersion function plotted above it. The difference between any two alias wavevectors such as  $(k=+1)$  and  $(k=-11)$  is a *reciprocal lattice vector*  $k_{12}$  or  $(12)_{12}=(0)_{12}$ . The reciprocal lattice vector  $k_{12}$  also spans the first Brillouin-zone from  $(-6)_{12}$  to  $(+6)_{12}$  as shown at the bottom of the figure. An important idea here is that a wavevector  $k$ -space must have the same  $N$ -fold periodic symmetry as the coordinate  $x$ -space. Moving across row of a  $\langle k_m |x_p\rangle$  matrix gives the same variation as moving up the corresponding column since  $\langle k_m |x_p\rangle$  is unitary. Both are  $N$ -fold periodic!

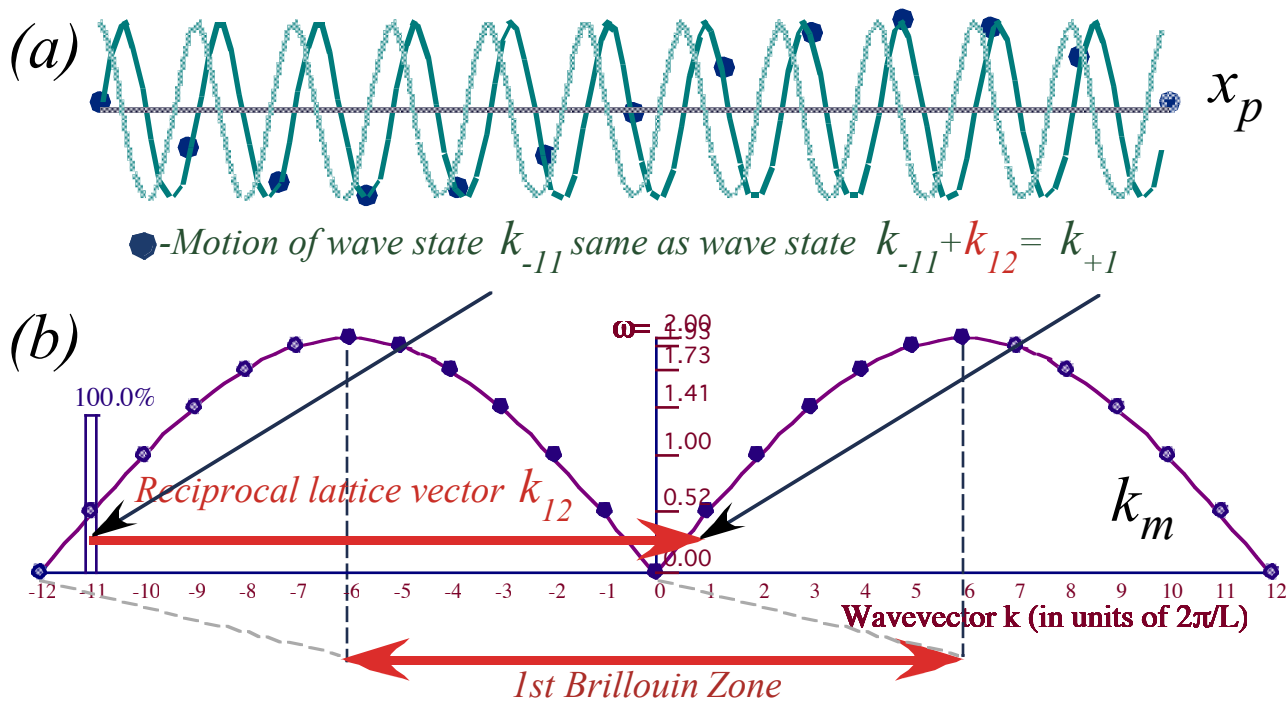


Fig. 7.3.4 (a) (-11)-wave has the same effect as its alias (+1)-wave. (b) Difference is zone vector  $k_{12}$ .

To appreciate the symmetry of a Fourier transform matrix, it may help to examine some larger ones. For example, Fig. 7.3.5 shows the Fourier matrix for  $N=24$ . Phase of each amplitude  $\langle k_m | x_p \rangle$  is color coded so it can be more easily spotted. Symmetry patterns should now be more evident. Remember, that these patterns repeat forever in all directions right and left or up and down in a great checkerboard quilt!

This beginning discussion of discrete wave analysis should make it clear that there is considerable physical and mathematical complexity hiding in these "simple" Fourier structures. Indeed, this is a key to understanding fundamental quantum symmetry properties and techniques which are generally labeled by a mathematical misnomer as "group theory." We shall explore some more of this shortly.

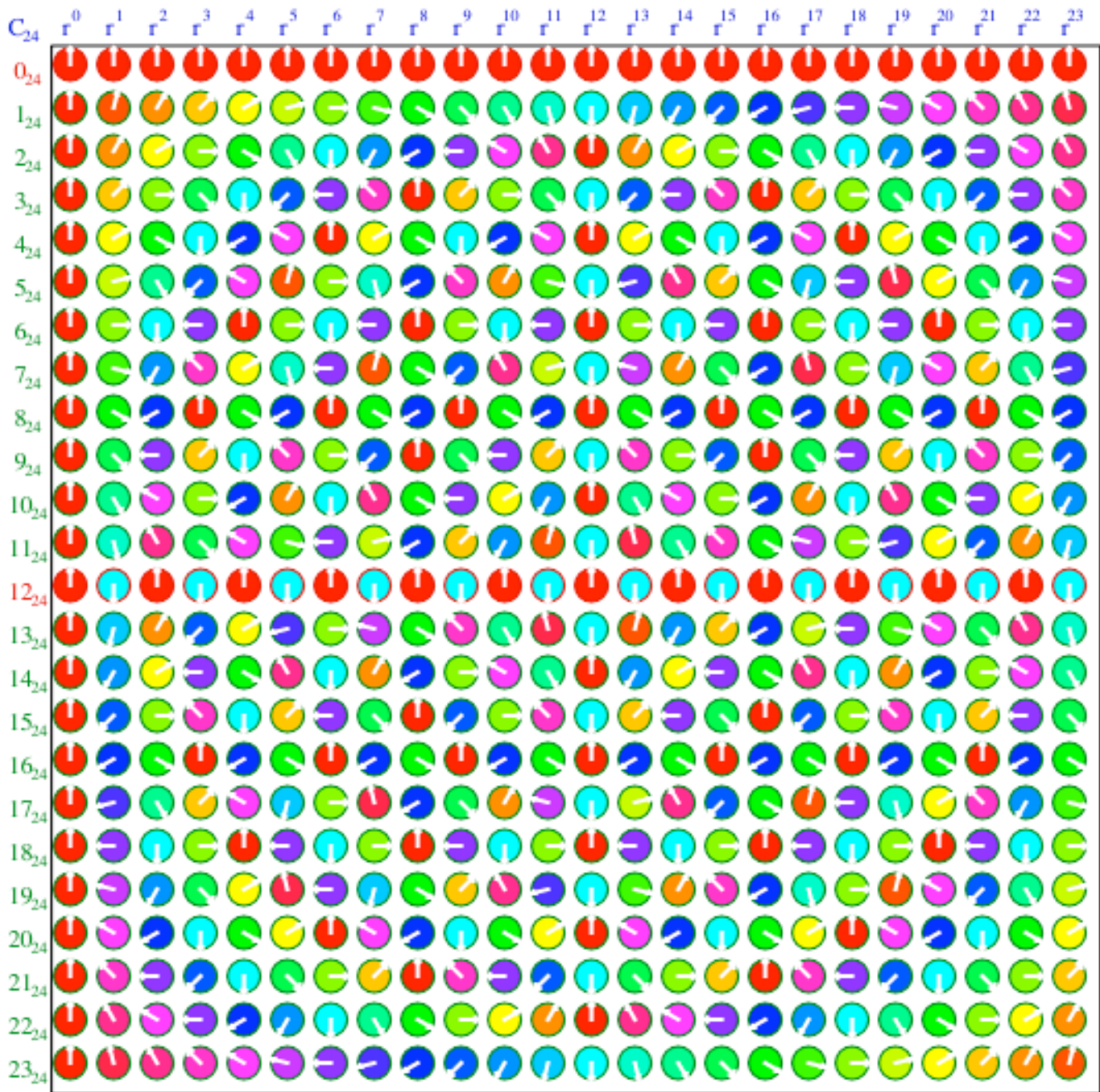


Fig. 7.3.5 Phase color coded Fourier transformation matrix for  $N=24$ .

## Problems for Chapter 7

### Bohring problems

**7.1.1.** For a Bohr ring of fixed circumference  $L = 1nm$  consider the following wavefunction  $\Psi(x) = \langle x | \Psi \rangle$  distributions around the ring at  $t=0$ , and deduce the amplitudes  $\langle m | \Psi \rangle$  of each of the eigenstates  $|m\rangle$  for  $m=0, \pm 1, \pm 2, \dots$ . Let the eigenfrequencies be  $\nu_m = (0, 1, 4, \dots, m^2, \dots)MHz$ .

(a)  $\Psi(x) = \text{const.}$  .

(b)  $\Psi(x) = \text{const.}(1 + \cos 2\pi x/L)$  .

(c)  $\Psi(x) = \text{const.}$  for  $-L/4 < x < L/4$  and  $\Psi(x) = 0$  elsewhere.

For each case evaluate *const.* assuming one particle occupies the ring.

(d) For each case (a) to (c) answer: "Is it a stationary state?" If not, calculate, plot, and discuss the wavefunctions of each case at time  $t = 1\mu\text{sec}$ , and at  $0.5\mu\text{sec}$  .

### Continuously boring problems

**7.2.1.** For an infinite line ( $-\infty < x < \infty$ ) consider the following wavefunction  $\Psi(x) = \langle x | \Psi \rangle$  distributions along the line. Calculate, plot, and discuss the amplitude functions  $\langle k | \Psi \rangle$  of each of the eigenstates  $|k\rangle$  for ( $-\infty < k < \infty$ ). Let the eates  $|k\rangle$  for ( $-\infty < k < \infty$ ). Let the eigenfrequencies be  $\nu_k = (kL/2\pi)^2 MHz$ . (Let unit length be  $L = 1nm$ .)

(a)  $\Psi(x) = \text{const.}$  .

(b)  $\Psi(x) = \text{const.}(1 + \cos 2\pi x/L)$  . .

(c)  $\Psi(x) = \text{const.}$  for  $-L/4 < x < L/4$  and  $\Psi(x) = 0$  elsewhere.

Evalu per unit length ( $L = 1nm$ ).

(d) For each case (a) to (c) answer: "Is it a stationary state?" If not, calculate, plot, and discuss the wavefunctions of each case at time  $t = 1\mu\text{sec}$ , and at  $0.5\mu\text{sec}$  .

### Continuously discrete or discretely continuous?

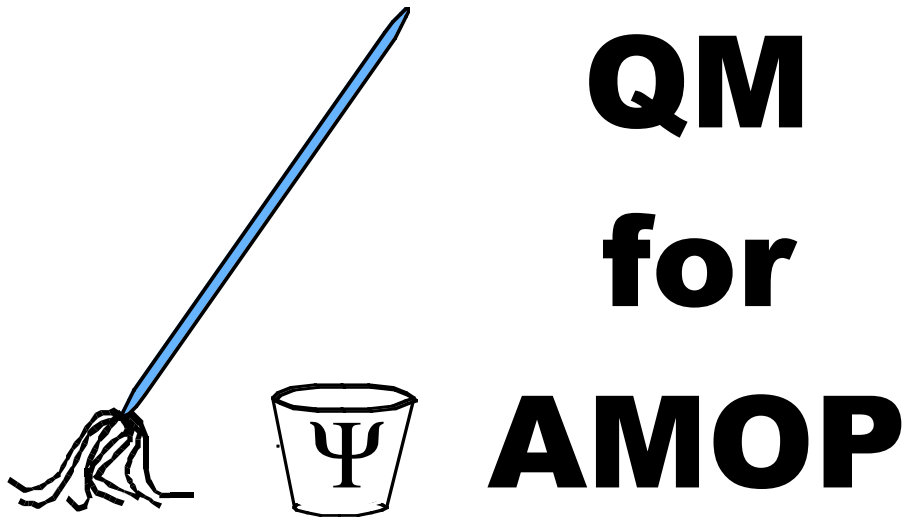
**7.3.1.** Ch.7 contains discussion of 1D Fourier wave systems with (a) Continuous  $x$  and discrete  $k$ , (b) Continuous  $x$  and continuous  $k$ , and (c) Discrete  $x$  and discrete  $k$ . Using physical models of each to discuss how physically relizeable these are. Is there a 4th possibility? Discuss.

### Aliases on the move

**7.3.2.** Consider the two aliases (-1) and (+1) in Fig. 7.3.4. Discuss whether a dispersion function  $\omega(k)$  should repeat periodically. Should the period be the zone vector  $k_{12}$ ? For computation use  $\omega(k) = |\sin(\pi k/12)|$  as plotted where  $k=0, \pm 1, \pm 2, \pm 3, \dots$  in units of  $2\pi/L$ . Use  $V_{\text{phase}} = \omega/k$  and  $V_{\text{group}} = d\omega/dk$  .

(a) Is the phase velocity the same for the two alias states (-1) and (+1)? Compute and discuss why or why not.

(a) Is the group velocity the same for the two alias states (-1) and (+1)? Compute and discuss why or why not.



**Chapter 8**  
**Fourier Symmetry Analysis**

**W. G. Harter**

**CHAPTER 8. FOURIER SYMMETRY ANALYSIS .....3**

**8.1. Introducing Cyclic Symmetry: A  $C_6$  example.....3**

(a) Cyclic symmetry  $C_N$ : A 6-quantum-dot analyzer.....3

(b)  $C_N$  Symmetry groups and representations .....5

(c) So what’s a group representation? .....6

**8.2  $C_N$  Spectral Decomposition: Solving a  $C_6$  transfer matrix.....7**

(a) Spectral decomposition of symmetry operators  $r^p$ .....7

(b) Writing transfer operator  $T$  in terms of symmetry operators  $r^p$  .....9

(c) Spectral decomposition of transfer operator  $T$  .....10

    An eigenvalue formula for all possible  $C_6$  symmetric  $T$ -matrices.....10

    What do the  $k_m$ - eigensolutions mean?.....11

(d) OK, where did those  $e^{ikx}$  wavefunctions come from?.....12

**8.3 Related Symmetry Analysis Examples .....13**

(a) Dihedral symmetry  $D_2$  .....14

$D_2$  group structure.....14

$D_2$  spectral decomposition: The old “1=1•1 trick” again .....15

    Spectral decomposition of  $D_2$  transfer matrices .....15

(b) Outer product structure: Double qubit registers .....16

$D_2$  is product  $C_2 \times C_2$ .....16

    Big-endian versus Little-endian .....17

$C_6$  is product  $C_3 \times C_2$  (but  $C_4$  is NOT  $C_2 \times C_2$ ) .....17

    Symmetry Catalog .....17

**Problems for Chapter 8. ....18**

Fourier analysis is most useful when there is a symmetry  $G$  in which all the coordinate points are indistinguishable. For an unbounded  $x$ -continuum,  $G$  is an infinite translational symmetry group labeled  $T$ . For a bounded  $x_p$ -ring of “quantum dots” the symmetry  $G$  is an  $N$ -cyclic rotation group labeled  $C_N$ . In Chapter 8 a fictitious hexagonal beam analyzer with  $C_6$  symmetry is considered. The transfer matrix eigensolutions of such a device are found using a modern form of Fourier analysis known as group representation theory or symmetry analysis, one of the most powerful tools in quantum theory. The symmetry of the bounded Bohr  $x$ -ring continuum is also discussed.

## Chapter 8. Fourier Symmetry Analysis

From where do the wavefunctions like  $\Psi = e^{i(kx - \omega t)}$  come? One answer to this involves the concept of *symmetry analysis* and *group representation theory*. These sound like big names for what is still regarded as a pretty scary mathematical subject. However, the basic ideas of this powerful tool are actually quite simple as we hope to show now. Most of the needed algebraic work has been done in Ch. 3 regarding spectral decomposition. The physical ideas of Fourier analysis and Bohr ring waves are in Ch. 7. Symmetry group representation theory is really just a beautiful generalization of *Fourier analysis* that gives eigensolutions of “difficult” operators using simple properties of commuting symmetry operators.

### 8.1. Introducing Cyclic Symmetry: A $C_6$ example

A ring of quantum dots was introduced in Section 7.3 as a model for finite Fourier analysis. The Fourier transformation matrix was discussed with examples for  $N=1, 2, 3, 4, 5,$  and  $6$ . The idea of cyclic symmetry  $C_N$  was broached as a property of the matrices in Fig. 7.3.3 and Fig. 7.3.5. Here that idea is put on a more solid footing.

#### (a) Cyclic symmetry $C_N$ : A 6-quantum-dot analyzer

Suppose someone invents some beam analyzer that takes an  $N$ -state beam and sorts it into  $N$  beams arrayed around a circular device as imagined in Fig. 8.1.1 for  $N=6$ . Let each beam path entering the device contain particles in one of  $N$  states  $\{|0\rangle, |1\rangle, |2\rangle, \dots, |N-1\rangle\}$  after which the device does things which causes the beams to interfere or be otherwise modified before recombining and counting.

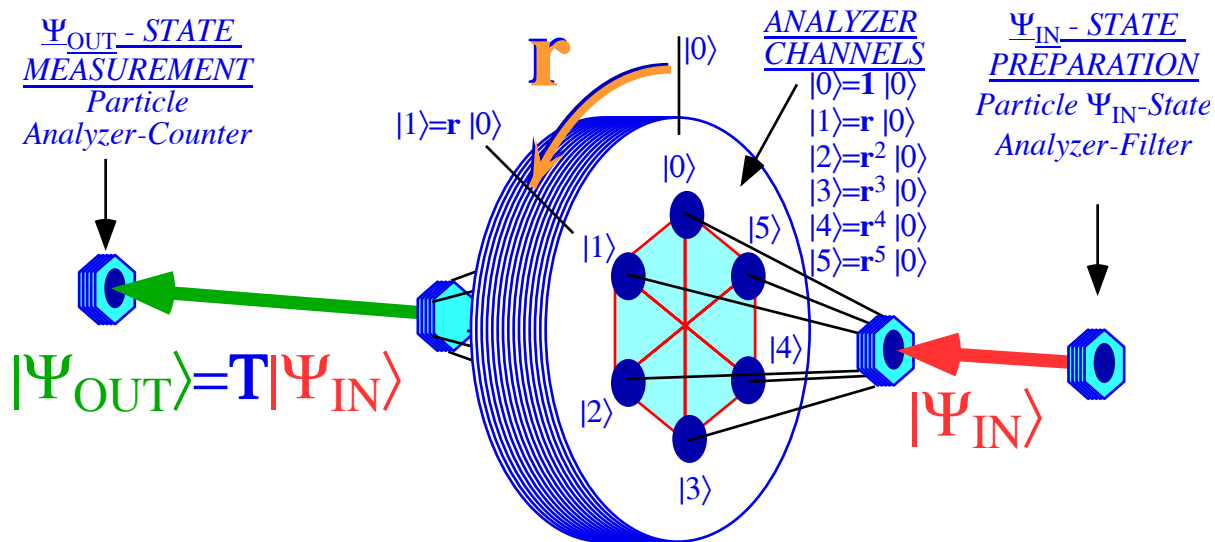


Fig. 8.1.1 Generic  $N$ -state ( $C_N$ ) beam analyzer experiment with ( $N = 6$ ) channels

We are intentionally being vague about the nature of the states. (After all, this device hasn't even been invented yet!) Let us just say they are some kind of hyper-polarization states. (Put a prefix like 'hyper' on something ordinary and people stop asking questions.) The point is that by just knowing the symmetry of a device it is possible to work out a lot of the quantum mechanics without knowing so much of the underlying

details. It is a lot like the photon polarization and electron spin problems discussed in Chapter 1. Electron and photon “spin” are physically quite different but use much of the same mathematical theory.

By *symmetry*, we mean any operators  $\mathbf{r}, \mathbf{r}^2, \dots$  that do not alter the analyzer experiment no matter how many times you apply them. In particular, suppose a  $60^\circ$  rotational operator  $\mathbf{r}$  indicated in Fig. 8.1.1. could be done some night by the lab janitor, so when the physicists show up the next morning all their experiments work the same as the day before.

However, it is important to state what we mean the janitor's  $\mathbf{r}$ -operation to do. He could just rotate the whole lab building by  $60^\circ$ . That, indeed, is a symmetry, but not one we will discuss until later. Besides, a rotation like that happens every four hours as the Earth turns; no janitor needed! This is called the *symmetry of isotropy of space*. It is a *continuous* or *Lie symmetry* for which  $60^\circ$  has no special significance.

Instead, what we have in mind for the janitor to do is rotate just the analyzer in the center of Fig. 8.1.1 by  $60^\circ$  as indicated in the figure. Well, that analyzer looks pretty heavy, so, instead we'll ask that the janitor just rotate the little input source and the little output counter both by minus  $60^\circ$ , which is operation  $\mathbf{r}^{-1} = \mathbf{r}^5$ . This does the same as a whole-Earth/lab rotation by  $-60^\circ$  (which no one detects) followed by a positive  $60^\circ$  rotation of the big analyzer to "upright" leaving input and output devices behind at  $-60^\circ$ .

It is important to understand that all transformations are *relative transformations*; something gets moved or mapped relative to something else. You've probably heard it quoted, "Everything's relative!" Well, that's often garbage, but here it isn't. Rotations, Lorentz transformations, and our analyzer operators  $\mathbf{T}$  (Recall Fig. 1.6.1), and  $\mathbf{r}$  in Fig. 8.1.1 are all mappings of one vector or thing relative to another.

By the way, our helpful suggestion to the janitor won't help much if the input and output devices are big analyzers, too. It was noted in Chapter 1 that filters and counters are analyzers set in certain ways. But, the analyzer in Fig. 8.1.1 is a more powerful one than heretofore discussed. (And, isn't better always bigger?) So let's assume that the janitor can easily do  $\mathbf{r}^{-1} = \mathbf{r}^5$  to the smaller input and output devices whose in and out states are written as follows in Dirac notation,

$$|\Psi_{\text{OUT}(\mathbf{r}^{-1})}\rangle = \mathbf{r}^{-1}|\Psi_{\text{OUT}}\rangle, \quad |\Psi_{\text{IN}(\mathbf{r}^{-1})}\rangle = \mathbf{r}^{-1}|\Psi_{\text{IN}}\rangle. \quad (8.1.1)$$

Symmetry of the transformation operator  $\mathbf{T}$  means it does exactly the same relative thing to any state  $|\Psi_{\text{IN}}\rangle$  as it does to the janitor-rotated state  $|\Psi_{\text{IN}(\mathbf{r}^{-1})}\rangle$ , that is

$$|\Psi_{\text{OUT}}\rangle = \mathbf{T}|\Psi_{\text{IN}}\rangle \quad \text{implies:} \quad |\Psi_{\text{OUT}(\mathbf{r}^{-1})}\rangle = \mathbf{T}|\Psi_{\text{IN}(\mathbf{r}^{-1})}\rangle \quad (8.1.2a)$$

or

$$\mathbf{r}^{-1}|\Psi_{\text{OUT}}\rangle = \mathbf{T}\mathbf{r}^{-1}|\Psi_{\text{IN}}\rangle \quad (8.1.2b)$$

$$|\Psi_{\text{OUT}}\rangle = \mathbf{r}\mathbf{T}\mathbf{r}^{-1}|\Psi_{\text{IN}}\rangle \quad (8.1.2c)$$

If this is true for all input states  $|\Psi_{\text{IN}}\rangle$  then it follows that effect of analyzer operator  $\mathbf{T}$  in (8.1.2a) and in (8.1.2c) are indistinguishable, or  $\mathbf{T}$  is *invariant* to  $\mathbf{r}$

$$\mathbf{T} = \mathbf{r}\mathbf{T}\mathbf{r}^{-1} \quad \text{or:} \quad \mathbf{r}^{-1}\mathbf{T}\mathbf{r} = \mathbf{T} \quad (8.1.2d)$$

or, that  $\mathbf{r}$  *commutes* with  $\mathbf{T}$ ; the latter being the most common way to say that  $\mathbf{T}$  *has r-symmetry*.

$$\mathbf{T}\mathbf{r} = \mathbf{r}\mathbf{T} \quad (8.1.2e)$$

All the above parts of equation (8.1.2) are really the same requirement for *r-symmetry of T*.

Note: This is not the same as just multiplying both sides of  $|\Psi_{OUT}\rangle = \mathbf{T} |\Psi_{IN}\rangle$  by  $\mathbf{r}$  or  $\mathbf{r}^{-1}$  which just gives a whole-Earth/lab rotation, that is, operate with  $\mathbf{r}^{-1}$  and insert the identity ( $\mathbf{r} \mathbf{r}^{-1} = \mathbf{1}$ ) to get

$$\mathbf{r}^{-1} |\Psi_{OUT}\rangle = \mathbf{r}^{-1} \mathbf{T} |\Psi_{IN}\rangle = \mathbf{r}^{-1} \mathbf{T} \mathbf{r} \mathbf{r}^{-1} |\Psi_{IN}\rangle . \tag{8.1.3a}$$

This reduces to an expression *similar* to the original  $|\Psi_{OUT}\rangle = \mathbf{T} |\Psi_{IN}\rangle$

$$|\Psi_{OUT(r^{-1})}\rangle = \mathbf{r}^{-1} \mathbf{T} |\Psi_{IN}\rangle = \mathbf{r}^{-1} \mathbf{T} \mathbf{r} |\Psi_{IN(r^{-1})}\rangle = \mathbf{T}_{(r^{-1})} |\Psi_{IN(r^{-1})}\rangle \tag{8.1.3b}$$

where  $\mathbf{T}_{(r^{-1})}$  is a *similarity transformation*  $\mathbf{r}^{-1}\mathbf{T}\mathbf{r}$  of  $\mathbf{T}$ . (This is an active transformation; devices move.)

$$\mathbf{T}_{(r^{-1})} = \mathbf{r}^{-1} \mathbf{T} \mathbf{r} \tag{8.1.3c}$$

These relations hold true for any analyzer operator  $\mathbf{T}$  whether it has symmetry or not.

For  $\mathbf{T}$  to have  $\mathbf{r}$ -symmetry it is necessary that the similarity transformation leaves  $\mathbf{T}$  unchanged or invariant ( $\mathbf{T}_{(r^{-1})} = \mathbf{T}$ ), as in (8.1.2d). To recap

*An analyzer has  $\mathbf{r}$ -symmetry if and only if its operator  $\mathbf{T}$  commutes with  $\mathbf{r}$ , that is ( $\mathbf{T} \mathbf{r} = \mathbf{r} \mathbf{T}$ ).*

### (b) $C_N$ Symmetry groups and representations

Now, the janitor, having fooled the physicists once, does it again the next night, by rotating by  $\mathbf{r}$  one more time giving the same positions as if  $\mathbf{r}^2$  had been done the first night. Then a combination of  $\mathbf{r}^2$  and  $\mathbf{r}^3$  is tried. (This just gives  $\mathbf{r}^{-1} = \mathbf{r}^5$  the inverse of which was tried on the first night.) All of these products are symmetries if the factors are. (So the physicists end up getting fooled night after night for almost a week of different positions! Saturday, they have to take off since they read right-to-left. )

If operators  $\mathbf{a}$  and  $\mathbf{b}$  commute with an analyzer  $\mathbf{T}$ -matrix then so do all their products

$$\text{If: } \mathbf{aT} = \mathbf{Ta} \quad \text{and} \quad \mathbf{bT} = \mathbf{Tb} \quad \text{then} \quad \mathbf{abT} = \mathbf{Tab} \quad \text{and} \quad \mathbf{baT} = \mathbf{Tba} \tag{8.1.4a}$$

$$\text{and inverses. If: } \mathbf{aT} = \mathbf{Ta} \quad \text{then} \quad \mathbf{a}^{-1}\mathbf{T} = \mathbf{Ta}^{-1} \tag{8.1.4b}$$

This shows that the set of unitary operators that commute with a particular  $\mathbf{T}$ -operator must satisfy the group axioms (1-4) stated in Sec. 2.2. This set is called a *symmetry group*  $G = \{ \mathbf{a}, \mathbf{b}, \mathbf{c}, \dots, \mathbf{g}, \dots \}$  of the operator  $\mathbf{T}$ . We are supposing that the analyzer matrix  $\mathbf{T}$  associated with the experiment in Fig. 8.1.1 has an  $N$ -cyclic symmetry group  $C_6 = \{ \mathbf{1}, \mathbf{r}, \mathbf{r}^2, \mathbf{r}^3, \mathbf{r}^4, \mathbf{r}^5 \}$  of six ( $N=6$ ) operators that have the following *group multiplication table*. We put the inverses of the first column in the top row so  $\mathbf{1}$  is on the diagonal.

$C_6$	$\mathbf{1}$	$\mathbf{r}^5$	$\mathbf{r}^4$	$\mathbf{r}^3$	$\mathbf{r}^2$	$\mathbf{r}$
$\mathbf{1}$	$\mathbf{1}$	$\mathbf{r}^5$	$\mathbf{r}^4$	$\mathbf{r}^3$	$\mathbf{r}^2$	$\mathbf{r}$
$\mathbf{r}$	$\mathbf{r}$	$\mathbf{1}$	$\mathbf{r}^5$	$\mathbf{r}^4$	$\mathbf{r}^3$	$\mathbf{r}^2$
$\mathbf{r}^2$	$\mathbf{r}^2$	$\mathbf{r}$	$\mathbf{1}$	$\mathbf{r}^5$	$\mathbf{r}^4$	$\mathbf{r}^3$
$\mathbf{r}^3$	$\mathbf{r}^3$	$\mathbf{r}^2$	$\mathbf{r}$	$\mathbf{1}$	$\mathbf{r}^5$	$\mathbf{r}^4$
$\mathbf{r}^4$	$\mathbf{r}^4$	$\mathbf{r}^3$	$\mathbf{r}^2$	$\mathbf{r}$	$\mathbf{1}$	$\mathbf{r}^5$
$\mathbf{r}^5$	$\mathbf{r}^5$	$\mathbf{r}^4$	$\mathbf{r}^3$	$\mathbf{r}^2$	$\mathbf{r}$	$\mathbf{1}$

(8.1.5a)

$$\mathbf{1} = \begin{pmatrix} 1 & \cdot & \cdot & \cdot & \cdot & \cdot \\ \cdot & 1 & \cdot & \cdot & \cdot & \cdot \\ \cdot & \cdot & 1 & \cdot & \cdot & \cdot \\ \cdot & \cdot & \cdot & 1 & \cdot & \cdot \\ \cdot & \cdot & \cdot & \cdot & 1 & \cdot \\ \cdot & \cdot & \cdot & \cdot & \cdot & 1 \end{pmatrix} \tag{8.1.5b}$$

Think of the table as a matrix in a basis  $\{|0\rangle|1\rangle|2\rangle|3\rangle|4\rangle|5\rangle\}$  defined by operators  $\{\mathbf{1}, \mathbf{r}, \mathbf{r}^2, \mathbf{r}^3, \mathbf{r}^4, \mathbf{r}^5\}$ .

This makes a matrix representation for each operator using the channel states as a basis by simply replacing each operator's table entry by a "1" in that position of its matrix and "0" or "dot" (·) elsewhere.



## 8.2 $C_N$ Spectral Decomposition: Solving a $C_6$ transfer matrix

The main analyzer of Fig. 8.1.1 is supposed to have  $C_6$  symmetry. However, it is also supposed to do some things that we haven't let single analyzers do to an incoming base state  $|\Psi_{IN}\rangle = |p\rangle$ , and that is, *mix it up!* No longer will a base state  $|1\rangle$  or  $|2\rangle$  just fly on through with nothing more than an extra phase attached, so it just comes out  $e^{i\Omega_1}|1\rangle$  or  $e^{i\Omega_2}|2\rangle$ . From now on, each base state  $|p\rangle$  is going to get treated to a full-blown transformation matrix  $\mathbf{T}$  that is not necessarily diagonal. A general base state  $|\Psi_{IN}\rangle$  will be output as  $|\Psi_{OUT}\rangle$ , as follows,

$$\begin{pmatrix} \langle 0|\Psi_{OUT}\rangle \\ \langle 1|\Psi_{OUT}\rangle \\ \langle 2|\Psi_{OUT}\rangle \\ \langle 3|\Psi_{OUT}\rangle \\ \langle 4|\Psi_{OUT}\rangle \\ \langle 5|\Psi_{OUT}\rangle \end{pmatrix} = \begin{pmatrix} T_{00} & T_{01} & T_{02} & T_{03} & T_{04} & T_{05} \\ T_{10} & T_{11} & T_{12} & T_{13} & T_{14} & T_{15} \\ T_{20} & T_{21} & T_{22} & T_{23} & T_{24} & T_{25} \\ T_{30} & T_{31} & T_{32} & T_{33} & T_{34} & T_{35} \\ T_{40} & T_{41} & T_{42} & T_{43} & T_{44} & T_{45} \\ T_{50} & T_{51} & T_{52} & T_{53} & T_{54} & T_{55} \end{pmatrix} \cdot \begin{pmatrix} \langle 0|\Psi_{IN}\rangle \\ \langle 1|\Psi_{IN}\rangle \\ \langle 2|\Psi_{IN}\rangle \\ \langle 3|\Psi_{IN}\rangle \\ \langle 4|\Psi_{IN}\rangle \\ \langle 5|\Psi_{IN}\rangle \end{pmatrix} \quad (8.2.1a)$$

where off-diagonal ( $p \neq q$ ) matrix elements

$$T_{pq} = \langle p|\mathbf{T}|q\rangle \quad (8.2.1b)$$

of  $\mathbf{T}$  are not all zero if  $|p\rangle$  and  $|q\rangle$  do not belong to  $\mathbf{T}$ 's "own" eigenbasis. (Bilingual redundancy, again.)

So, are we ready to diagonalize a general six-by-six matrix? No way, Jose! But, here is where symmetry analysis rides to the rescue. If we can diagonalize the  $\mathbf{r}$ -matrix in (8.1.5) then, barring appearance of nilpotents or other obnoxious gremlins, we may be able to also diagonalize the  $\mathbf{T}$ -matrix (8.2.1). This is because (8.2.1) isn't just any old six-by-six matrix; it has  $C_6$  symmetry and must therefore commute with each of its symmetry operators like  $\mathbf{r}$ . Recall  $\mathbf{T}\mathbf{r} = \mathbf{r}\mathbf{T}$  in (8.1.2). This means that  $\mathbf{T}$  and  $\mathbf{r}$  share projectors  $\mathbf{P}_k$  as shown in (3.1.37). Diagonalize  $\mathbf{r}$  and you may have diagonalized  $\mathbf{T}$  as well!

### (a) Spectral decomposition of symmetry operators $\mathbf{r}^p$

The problem of analyzing (8.2.1) is then reduced to diagonalizing  $\mathbf{r}$  in (8.1.5a), another six-by-six matrix, albeit a simpler one. But wait! No matrix need bother us. The minimal equation for  $\mathbf{r}$  is simply

$$\mathbf{r}^N = \mathbf{1} \quad (N=6, \text{ here.}) \quad (8.2.2)$$

and all its eigenvalues are the roots of unity given before by (7.3.5) and displayed in Fig. 7.3.3.

$$\chi_m = (r_N)^m = \left( e^{-i2\pi/N} \right)^m = e^{-i2\pi m/N} \quad \text{where: } m = 0, 1, 2, \dots, N-1 \quad (8.2.3)$$

(Again,  $N=6$ ). The spectral projectors of  $\mathbf{r}$  follow easily. To help understand this recall that a spectral decomposition of any matrix  $\mathbf{M}$  come with beautiful and powerful consequential relations. First,  $\mathbf{M}$ 's *eigen-projector*  $\mathbf{P}_k$  satisfies:  $\mathbf{M}\mathbf{P}_k = \epsilon_k \mathbf{P}_k$  and *orthonormality*  $\mathbf{P}_j\mathbf{P}_k = \delta_{jk} \mathbf{P}_k$ . Then there is *completeness*

$$\mathbf{1} = \mathbf{P}_1 + \mathbf{P}_2 + \dots + \mathbf{P}_n. \quad (3.1.15d)\text{repeated}$$

and *spectral decomposition of operator*  $\mathbf{M}$ , and *functional spectral decomposition of an operator*  $\mathbf{M}$ .

$$\mathbf{M} = \epsilon_1 \mathbf{P}_1 + \epsilon_2 \mathbf{P}_2 + \dots + \epsilon_n \mathbf{P}_n \quad (3.1.15e)\text{repeated}$$

$$f(\mathbf{M}) = f(\epsilon_1) \mathbf{P}_1 + f(\epsilon_2) \mathbf{P}_2 + \dots + f(\epsilon_n) \mathbf{P}_n \quad (3.1.17)\text{repeated}$$

Applying the spectral relations using the eigenvalues (roots) in (8.2.3) gives a functional (power) spectral decomposition (3.1.17)repeated of all powers  $\mathbf{r}^p$  of rotation operator  $\mathbf{r}$  by putting  $(\chi_m)^p$  before each  $\mathbf{P}^m$ .

$$\begin{aligned} \mathbf{1} &= \mathbf{P}^0 + \mathbf{P}^1 + \mathbf{P}^2 + \mathbf{P}^3 + \mathbf{P}^4 + \mathbf{P}^5 \\ \mathbf{r} &= \mathbf{P}^0 + \chi_1 \mathbf{P}^1 + \chi_2 \mathbf{P}^2 + \chi_3 \mathbf{P}^3 + \chi_4 \mathbf{P}^4 + \chi_5 \mathbf{P}^5 \\ \mathbf{r}^2 &= \mathbf{P}^0 + \chi_1^2 \mathbf{P}^1 + \chi_2^2 \mathbf{P}^2 + \chi_3^2 \mathbf{P}^3 + \chi_4^2 \mathbf{P}^4 + \chi_5^2 \mathbf{P}^5 \\ \mathbf{r}^3 &= \mathbf{P}^0 + \chi_1^3 \mathbf{P}^1 + \chi_2^3 \mathbf{P}^2 + \chi_3^3 \mathbf{P}^3 + \chi_4^3 \mathbf{P}^4 + \chi_5^3 \mathbf{P}^5 \\ \mathbf{r}^4 &= \mathbf{P}^0 + \chi_1^4 \mathbf{P}^1 + \chi_2^4 \mathbf{P}^2 + \chi_3^4 \mathbf{P}^3 + \chi_4^4 \mathbf{P}^4 + \chi_5^4 \mathbf{P}^5 \\ \mathbf{r}^5 &= \mathbf{P}^0 + \chi_1^5 \mathbf{P}^1 + \chi_2^5 \mathbf{P}^2 + \chi_3^5 \mathbf{P}^3 + \chi_4^5 \mathbf{P}^4 + \chi_5^5 \mathbf{P}^5 \end{aligned} \quad \text{where: } \chi_m^p = (\chi_m)^p = e^{-i2\pi(mp)/N} \quad (8.2.4a)$$

Apart from the normalization, the  $\mathbf{P}^m$ -to- $\mathbf{r}^p$  relation above is a unitary linear combination having the same Fourier transformation coefficients  $\langle k_m | x_p \rangle$  as (7.3.10a). The inverse  $\mathbf{r}^p$ -to- $\mathbf{P}^m$  relation is obtained by transpose conjugating the coefficients  $\chi_m^p$  above to give coefficients just like  $\langle x_p | k_m \rangle$  in (7.3.10b).

$$(\chi_m^p)^* = \sqrt{N} \langle k_m | x_p \rangle^* = \sqrt{N} \langle x_p | k_m \rangle = e^{i2\pi(mp)/N} = \rho_p^m \quad (8.2.4b)$$

Then divide all by the norm  $N=6$  to make the following idempotent projectors.

$$\begin{aligned} \mathbf{P}^0 &= (\mathbf{1} + \mathbf{r} + \mathbf{r}^2 + \mathbf{r}^3 + \mathbf{r}^4 + \mathbf{r}^5) / 6 \\ \mathbf{P}^1 &= (\mathbf{1} + \rho_1 \mathbf{r} + \rho_2 \mathbf{r}^2 + \rho_3 \mathbf{r}^3 + \rho_4 \mathbf{r}^4 + \rho_5 \mathbf{r}^5) / 6 \\ \mathbf{P}^2 &= (\mathbf{1} + \rho_1^2 \mathbf{r} + \rho_2^2 \mathbf{r}^2 + \rho_3^2 \mathbf{r}^3 + \rho_4^2 \mathbf{r}^4 + \rho_5^2 \mathbf{r}^5) / 6 \\ \mathbf{P}^3 &= (\mathbf{1} + \rho_1^3 \mathbf{r} + \rho_2^3 \mathbf{r}^2 + \rho_3^3 \mathbf{r}^3 + \rho_4^3 \mathbf{r}^4 + \rho_5^3 \mathbf{r}^5) / 6 \\ \mathbf{P}^4 &= (\mathbf{1} + \rho_1^4 \mathbf{r} + \rho_2^4 \mathbf{r}^2 + \rho_3^4 \mathbf{r}^3 + \rho_4^4 \mathbf{r}^4 + \rho_5^4 \mathbf{r}^5) / 6 \\ \mathbf{P}^5 &= (\mathbf{1} + \rho_1^5 \mathbf{r} + \rho_2^5 \mathbf{r}^2 + \rho_3^5 \mathbf{r}^3 + \rho_4^5 \mathbf{r}^4 + \rho_5^5 \mathbf{r}^5) / 6 \end{aligned} \quad \text{where: } \rho_p^m = \chi_m^p = e^{i2\pi(pm)/N} \quad (8.2.4c)$$

Operating on the first position state with these projectors gives the desired eigenstates of the  $\mathbf{T}$ -matrix. The norm is  $\langle \mathbf{1} | \mathbf{P}^m | \mathbf{1} \rangle = 1/N$ . (Recall (3.1.13)example) Its root  $1/\sqrt{N}$  results to give normalized eigenkets.

$$|k_m\rangle = \mathbf{P}^m |0\rangle \sqrt{N} = \sum_{p=0}^{N-1} \rho_p^m \mathbf{r}^p |0\rangle \sqrt{N} / N = \sum_{p=0}^{N-1} e^{i2\pi(pm)/N} |p\rangle / \sqrt{N} \quad (8.2.5a)$$

The inverse ket relations give position states  $|x_p\rangle=|p\rangle$  in terms of wave  $|k_m\rangle$  eigenkets.

$$|p\rangle = \mathbf{r}^p |0\rangle = \sum_{m=0}^{N-1} \chi_m^p \mathbf{P}^m |0\rangle \sqrt{N} = \sum_{m=0}^{N-1} e^{-i2\pi(mp)/N} |k_m\rangle / \sqrt{N} \quad (8.2.5b)$$

The preceding ket relations (8.2.5) and their operator equivalents (8.2.4) are the discrete- $N$  Fourier transformations whose  $N$ -by- $N$  transformation matrices are pictured for  $N=1, 2, 3, 4, 5$ , and  $6$  in Fig. 7.3.3 and for  $N=24$  in Fig. 7.3.5. The physical transformation is between  $N$  “quantum-dot” position point  $|p\rangle$ -states ( $|x_p\rangle=|p\rangle$ ) and their  $N$  quantum momentum Fourier-wave  $|k_m\rangle$ -states. Much of the above is mathematical “legalese” which gets short-circuited in the calculations that are described next.

### (b) Writing transfer operator $\mathbf{T}$ in terms of symmetry operators $\mathbf{r}^p$

In order for main analyzer  $\mathbf{T}$ -matrix (8.2.1) to have  $C_N$  symmetry, it must commute with all the rotation operator  $\mathbf{r}$ -matrices in (2.7.5).  $\mathbf{T}$  does this by being a linear combination of  $\mathbf{r}^p$  as follows.

$$\mathbf{T} = A \mathbf{1} + B \mathbf{r} + C \mathbf{r}^2 + D \mathbf{r}^3 + C' \mathbf{r}^4 + B' \mathbf{r}^5, \quad (8.2.6)$$

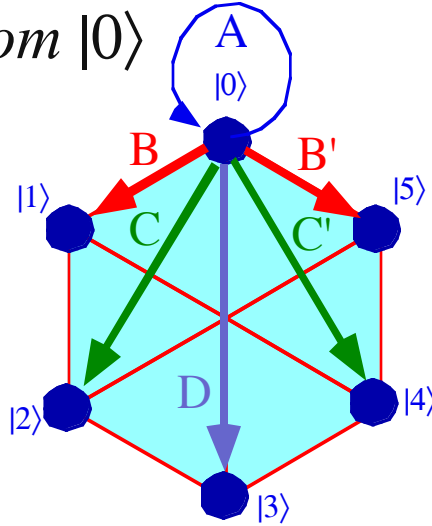
The  $\mathbf{r}^p$ -matrices in (2.7.5) are thus combined to give the general  $C_6$ -symmetric  $\mathbf{T}$ -matrix relation (8.2.1).

$$\begin{pmatrix} \langle 0 | \Psi_{\text{OUT}} \rangle \\ \langle 1 | \Psi_{\text{OUT}} \rangle \\ \langle 2 | \Psi_{\text{OUT}} \rangle \\ \langle 3 | \Psi_{\text{OUT}} \rangle \\ \langle 4 | \Psi_{\text{OUT}} \rangle \\ \langle 5 | \Psi_{\text{OUT}} \rangle \end{pmatrix} = \begin{pmatrix} A & B' & C' & D & C & B \\ B & A & B' & C' & D & C \\ C & B & A & B' & C' & D \\ D & C & B & A & B' & C' \\ C' & D & C & B & A & B' \\ B' & C' & D & C & B & A \end{pmatrix} \cdot \begin{pmatrix} \langle 0 | \Psi_{\text{IN}} \rangle \\ \langle 1 | \Psi_{\text{IN}} \rangle \\ \langle 2 | \Psi_{\text{IN}} \rangle \\ \langle 3 | \Psi_{\text{IN}} \rangle \\ \langle 4 | \Psi_{\text{IN}} \rangle \\ \langle 5 | \Psi_{\text{IN}} \rangle \end{pmatrix} \quad (8.2.7)$$

The undetermined coefficients  $A$ ,  $B$ ,  $C$ ,  $D$ ,  $C'$ , and  $B'$  correspond to all the *transition amplitudes* that state  $|0\rangle$  could possibly have to other states  $|0\rangle$ ,  $|1\rangle$ ,  $|2\rangle$ ,  $|3\rangle$ ,  $|4\rangle$ , and  $|5\rangle$  as indicated by arrows in Fig. 8.2.1a.

#### (a) Paths from $|0\rangle$

$$\begin{aligned} A &= \langle 0 | \mathbf{T} | 0 \rangle \\ B &= \langle 1 | \mathbf{T} | 0 \rangle \\ C &= \langle 2 | \mathbf{T} | 0 \rangle \\ D &= \langle 3 | \mathbf{T} | 0 \rangle \\ C' &= \langle 4 | \mathbf{T} | 0 \rangle \\ B' &= \langle 5 | \mathbf{T} | 0 \rangle \end{aligned}$$



#### (b) All Paths

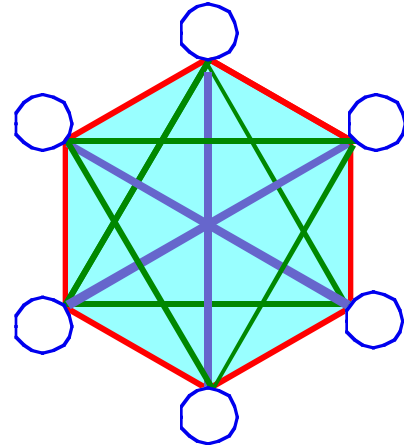


Fig. 8.2.1 Generic 6-channel ( $C_6$ ) beam transitions (a) Amplitudes (b) Paths

In order that the system really have  $C_6$  symmetry, the next state  $|1\rangle$  must make the same amplitudes to the states  $|1\rangle$ ,  $|2\rangle$ ,  $|3\rangle$ ,  $|4\rangle$ ,  $|5\rangle$ , and  $|6\rangle$ , respectively, and so on for  $|2\rangle$ ,  $|3\rangle$ ,  $|4\rangle$ , and  $|5\rangle$ . All the equivalent paths are indicated in Fig. 8.2.1b.

The expression of a quantum operator, such as the analyzer transfer matrix  $\mathbf{T}$ , in terms of its symmetry operators, such as the  $\mathbf{r}^p$ , is a deep and important idea which will be used a lot in the rest of this text. It is useful if, as the case is here, the  $\mathbf{r}^p$  and  $\mathbf{T}$  have the same set of eigenstates or projectors so that a (presumably!) easy spectral decomposition of the former also solves the latter. Also, it is useful to label by symmetry operators both the system coordinate base states, as in (8.1.6), and the transfer or transition amplitudes or *paths* between the base states, as in Fig. 8.2.1.

**(c) Spectral decomposition of transfer operator T**

Now a  $C_6$ -symmetric **T** operator equation with these  $A, B, C,..$  amplitudes must be diagonalized if represented in the symmetry projected  $|k_m\rangle$  basis (8.2.5).

$$\begin{pmatrix} \langle k_0 | \Psi_{OUT} \rangle \\ \langle k_1 | \Psi_{OUT} \rangle \\ \langle k_2 | \Psi_{OUT} \rangle \\ \langle k_3 | \Psi_{OUT} \rangle \\ \langle k_4 | \Psi_{OUT} \rangle \\ \langle k_5 | \Psi_{OUT} \rangle \end{pmatrix} = \begin{pmatrix} \varepsilon(k_0) & 0 & 0 & 0 & 0 & 0 \\ 0 & \varepsilon(k_1) & 0 & 0 & 0 & 0 \\ 0 & 0 & \varepsilon(k_2) & B & 0 & 0 \\ 0 & 0 & 0 & \varepsilon(k_3) & 0 & 0 \\ 0 & 0 & 0 & 0 & \varepsilon(k_4) & 0 \\ 0 & 0 & 0 & 0 & 0 & \varepsilon(k_5) \end{pmatrix} \cdot \begin{pmatrix} \langle k_0 | \Psi_{IN} \rangle \\ \langle k_1 | \Psi_{IN} \rangle \\ \langle k_2 | \Psi_{IN} \rangle \\ \langle k_3 | \Psi_{IN} \rangle \\ \langle k_4 | \Psi_{IN} \rangle \\ \langle k_5 | \Psi_{IN} \rangle \end{pmatrix} \quad (8.2.8)$$

This is because **T** in (8.2.6) is a combination of symmetry operators (2.7.5) and all the symmetry operators have  $|k_m\rangle$  as eigenvectors with eigenvalues (8.2.3).

$$\mathbf{r}^p |k_m\rangle = \mathbf{r}^p \mathbf{P}^m |1\rangle = e^{-i2\pi mp/N} \mathbf{P}^m |1\rangle = e^{-i2\pi mp/6} |k_m\rangle \quad (8.2.9)$$

Eigensolutions for **r**-operators are examples of elementary *Bloch symmetry conditions*.

$$\mathbf{r} |k_m\rangle = e^{-ik_m a} |k_m\rangle = e^{-i2\pi m/6} |k_m\rangle \text{ where: } k_m = \frac{2\pi}{Na} m \quad (8.2.10)$$

It says that a translation by distance  $a$  ( $60^\circ$  rotation **r** along analyzer circumference) sees each phase timer advance forward by  $k_m a$  consistent with pictures Fig. 7.3.3 of Bloch  $(m)_N$  waves. (Remember: phasor clocks turn clockwise with time, a negative angle.) Bloch symmetry is based upon the **r** -eigenoperator relation  $\mathbf{r} \mathbf{P}^m = \chi_m \mathbf{P}^m$  with  $(m)$ -th-root-of-unity eigenvalues  $\chi_m = e^{-i2\pi m/N}$  of **r** from (8.2.3).

An eigenvalue formula for all possible  $C_6$  symmetric T-matrices

To compute the **T**-eigenvalues we just have to substitute the **r**-values of (8.2.9) into (8.2.6)!

$$\begin{aligned} \langle k_m | \mathbf{T} | k_m \rangle &= A \langle k_m | \mathbf{1} | k_m \rangle + B \langle k_m | \mathbf{r} | k_m \rangle + C \langle k_m | \mathbf{r}^2 | k_m \rangle + D \langle k_m | \mathbf{r}^3 | k_m \rangle + C' \langle k_m | \mathbf{r}^4 | k_m \rangle + B' \langle k_m | \mathbf{r}^5 | k_m \rangle \\ &= A + B e^{-ik_m a} + C e^{-i2k_m a} + D e^{-i3k_m a} + C' e^{i2k_m a} + B' e^{ik_m a} \end{aligned} \quad (8.2.11a)$$

(Note:  $e^{-i4k_m a} = e^{i2k_m a}$  since  $-4 \bmod 6 = 2 \bmod 6$ . Also,  $e^{-i5k_m a} = e^{ik_m a}$  since  $-5 \bmod 6 = 1 \bmod 6$ ) Another way to derive eigenvalues is to put  $|k_m\rangle$  into a matrix eigenequation (8.2.7) for **T**.

$$\begin{pmatrix} A & B' & C' & D & C & B \\ B & A & B' & C' & D & C \\ C & B & A & B' & C' & D \\ D & C & B & A & B' & C' \\ C' & D & C & B & A & B' \\ B' & C' & D & C & B & A \end{pmatrix} \cdot \begin{pmatrix} 1 \\ e^{ik_m a} \\ e^{i2k_m a} \\ e^{i3k_m a} \\ e^{-i2k_m a} \\ e^{-ik_m a} \end{pmatrix} = \varepsilon(k_m) \begin{pmatrix} 1 \\ e^{ik_m a} \\ e^{i2k_m a} \\ e^{i3k_m a} \\ e^{-i2k_m a} \\ e^{-ik_m a} \end{pmatrix} \quad (8.2.11b)$$

The first row multiplication shows gives the same eigenvalue.

$$\varepsilon(k_m) = A + B e^{-ik_m a} + C e^{-i2k_m a} + D e^{-i3k_m a} + C' e^{i2k_m a} + B' e^{ik_m a} \quad (8.2.11c)$$

It is important to understand what has been accomplished. A general eigenvalue and eigenvector formula has been derived *for all possible matrices T that have the symmetry C6* of this particular “thought-experimental” problem. That is pretty neat, and it is just the beginning of a powerful set of symmetry tools!

What do the  $k_m$ -eigenstates mean?

The physical interpretation of  $C_N$  eigenstates is well known to electrical engineers. The ket in (8.2.11b) is a 6-phase generalization of the voltage in 3-phase wires commonly used to transport 220V power. A  $C_3$  example shown in Fig. 8.2.2 resembles the  $2_3=-1_3$ -row of the  $C_3$  table in Fig.7.3.3 with a time-phase of  $t=5\pi/6$ . (The  $2_3=-1_3$ -bra (row) is the  $\dagger$ -conjugate of a  $1_3=-2_3$ -ket (column) eigenvector.) The result is a ( $k=1$ )-wave moving left to right in Fig. 8.2.2a or clockwise in Fig. 8.2.2b. (Recall: phasor-ahead feeds into phasor-behind. Imaginary  $\text{Im}\Psi$  precedes the real  $\text{Re}\Psi$  in time since phasors turn like clocks.)

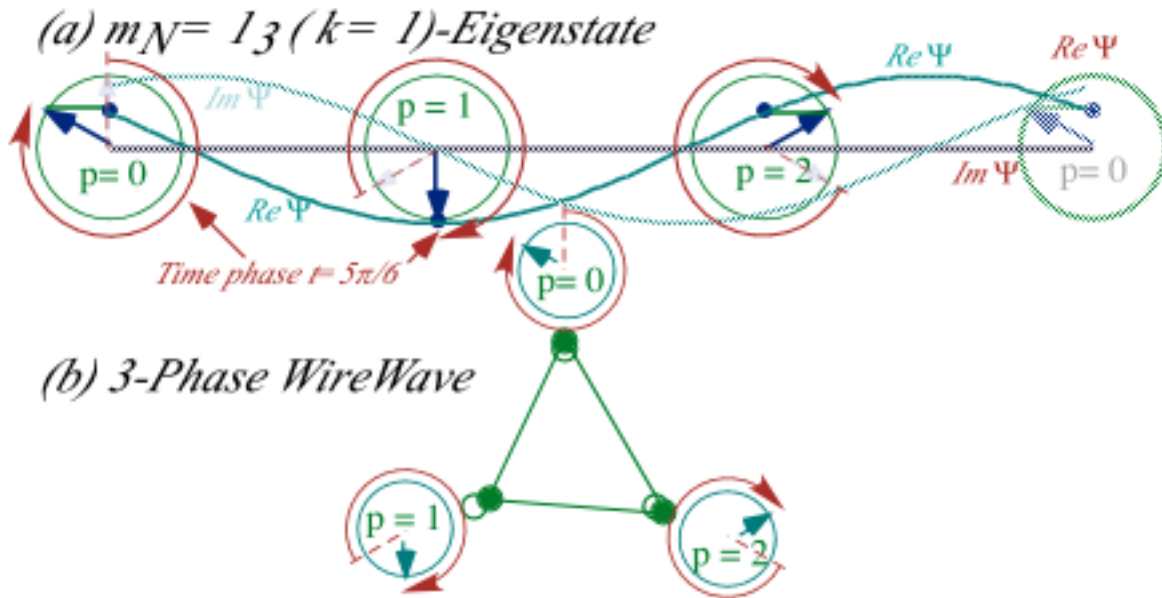


Fig. 8.2.2 ( $k=1$ ) 3-channel ( $C_3$ ) wave eigenstate (a) Real and imaginary waves (b) Phasors

A beam with all amplitudes equally dephased from their next neighbor is a  $|k_m\rangle$ -state that is not changed by a cyclically wired device that has  $C_N$  symmetry such as the  $C_6$  analyzer sketched in Fig. 8.2.1. Also, if the  $\mathbf{T}$ -matrix is unitary ( $\mathbf{T}^\dagger=\mathbf{T}^{-1}$ ),  $|k_m\rangle$ -state eigenvalues  $\varepsilon(k_m)$  must be unitary, too.

$$\varepsilon(k_m)^* = 1/\varepsilon(k_m) \quad \text{or: } \varepsilon(k_m) = e^{i\phi_m} \tag{8.2.12}$$

So the effect of the analyzer on an *eigenchannel*  $|k_m\rangle$ -state can only be to add an overall phase  $\phi_m$  to it.

$$\mathbf{T} |k_m\rangle = e^{i\phi_m} |k_m\rangle \tag{8.2.13}$$

The phase  $\phi_m$  is sometimes called an *eigenchannel phase-shift* or *eigenphase*  $\phi_m$ . Below we write the *eigenchannel basis representation* of the  $\mathbf{T} |k_m\rangle$ -equation for a general input state  $|\Psi_{IN}\rangle$  with arbitrary values for its  $N$ -*eigenchannel-amplitudes*  $\langle k_m|\Psi_{IN}\rangle$  of (8.2.7). (This means the  $N$ -*channel-amplitudes*  $\langle p|\Psi_{IN}\rangle$  in the original representation (8.2.6) are arbitrary, too.) Below is for general  $|\Psi_{IN}\rangle$ .

$$\begin{pmatrix} \langle k_0|\Psi_{OUT}\rangle \\ \langle k_1|\Psi_{OUT}\rangle \\ \langle k_2|\Psi_{OUT}\rangle \\ \langle k_3|\Psi_{OUT}\rangle \\ \langle k_4|\Psi_{OUT}\rangle \\ \langle k_5|\Psi_{OUT}\rangle \end{pmatrix} = \begin{pmatrix} e^{i\phi_0} & 0 & 0 & 0 & 0 & 0 \\ 0 & e^{i\phi_1} & 0 & 0 & 0 & 0 \\ 0 & 0 & e^{i\phi_2} & 0 & 0 & 0 \\ 0 & 0 & 0 & e^{i\phi_3} & 0 & 0 \\ 0 & 0 & 0 & 0 & e^{i\phi_4} & 0 \\ 0 & 0 & 0 & 0 & 0 & e^{i\phi_5} \end{pmatrix} \cdot \begin{pmatrix} \langle k_0|\Psi_{IN}\rangle \\ \langle k_1|\Psi_{IN}\rangle \\ \langle k_2|\Psi_{IN}\rangle \\ \langle k_3|\Psi_{IN}\rangle \\ \langle k_4|\Psi_{IN}\rangle \\ \langle k_5|\Psi_{IN}\rangle \end{pmatrix} \tag{8.2.14}$$

**(d) OK, where did those  $e^{ikx}$  wavefunctions come from?**

Every student of differential equations is told early on to try the exponential solutions  $e^{At}$  or  $e^{iat}$  in independent variable  $t$  with little reason given except, "It works!...sometimes." Now we can see why and when such solutions work. The key to our exponential eigenfunctions  $\Psi_{k_m}(x_p) = e^{ik_m x_p} / \sqrt{N}$  was  $C_N$  symmetry which demanded in (2.7.5) that we use roots of unity, that is, the roots of the minimal equation  $\mathbf{r}^N = \mathbf{1}$  for symmetry operator  $\mathbf{r}$ .

If we let  $N$  approach infinity ( $N \rightarrow \infty$ ) the symmetry approaches continuous translation symmetry  $C_\infty$ , and the eigenfunctions  $\Psi_{k_m}(x_p)$  approach plane waves  $\Psi_k(x) = e^{ikx} / \sqrt{2\pi}$  such as given by (2.6.20b) in Sec. 2.6b. Symmetry demands independence or invariance to translation of the independent variable  $x$ . In other words, you should get the same differential equation no matter whether you let the origin be at  $x=0$  or at  $x=2,517$  in Timbuktu. For example, the differential equation

$$\frac{d^2 \psi}{dx^2} + 2\gamma \frac{d\psi}{dx} + k^2 \psi = 0 \quad (8.2.15)$$

does have  $C_\infty$  symmetry so  $e^{ikx}$  will work, but an equation like

$$\frac{d^2 \psi}{dx^2} + 2\gamma x \frac{d\psi}{dx} + k^2 x^2 \psi = 0 \quad (8.2.16)$$

does not have  $C_\infty$  symmetry because of the  $x$ -dependence; it's not the same equation in Timbuktu. An example of a  $C_N$ -symmetric differential equation is Matieu's equation for waves in a periodic solid.

$$\frac{d^2 \psi}{dx^2} + k^2 \cos(Nx) \psi = 0$$

All that we have said applies as well when the independent variable is time  $t$ . For example, the differential equation

$$\frac{d^2 \psi}{dt^2} + 2\Gamma \frac{d\psi}{dt} + \omega^2 \psi = 0$$

does have  $C_\infty$  symmetry so  $e^{i\omega t}$  will work. An example of a  $C_N$ -symmetric time differential equation is Mathieu's equation for a periodic force. Later we use  $C_N$ -symmetry to help solve this type of equation.

$$\frac{d^2 \psi}{dt^2} + k^2 \cos(Nt) \psi = 0$$

### 8.3 Related Symmetry Analysis Examples

The homo-cyclic two-dot  $C_2$  and three-dot  $C_3$  systems are sketched below in the way the  $C_6$  system was sketched in Fig. 8.2.1. The transfer matrix equations (8.3.1) have eigenket tables (8.3.2).

$$\begin{pmatrix} \langle 0 | \Psi_{\text{OUT}} \rangle \\ \langle 1 | \Psi_{\text{OUT}} \rangle \end{pmatrix} = \begin{pmatrix} A & B \\ B & A \end{pmatrix} \begin{pmatrix} \langle 0 | \Psi_{\text{IN}} \rangle \\ \langle 1 | \Psi_{\text{IN}} \rangle \end{pmatrix} \quad (8.3.1a)$$

$$\begin{pmatrix} \langle 0 | \Psi_{\text{OUT}} \rangle \\ \langle 1 | \Psi_{\text{OUT}} \rangle \\ \langle 2 | \Psi_{\text{OUT}} \rangle \end{pmatrix} = \begin{pmatrix} A & B' & B \\ B & A & B' \\ B' & B & A \end{pmatrix} \begin{pmatrix} \langle 0 | \Psi_{\text{IN}} \rangle \\ \langle 1 | \Psi_{\text{IN}} \rangle \\ \langle 2 | \Psi_{\text{IN}} \rangle \end{pmatrix} \quad (8.3.1b)$$

(a)  $C_2$  System

(b)  $C_3$  System

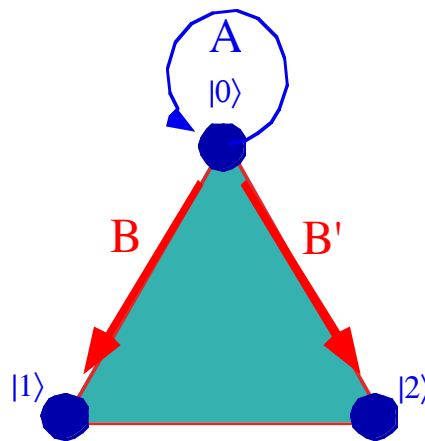
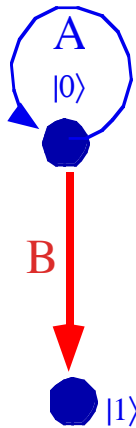


Fig. 8.3.1 Generic  $N$ -channel ( $C_N$ ) quantum dot systems. (a)  $N=2$  (b)  $N=3$

(8.3.2a)

(8.3.2b)

$C_2$	$ x_0\rangle = \mathbf{R}^0  0\rangle$	$ x_1\rangle = \mathbf{R}^1  0\rangle$	
$ (0)_2\rangle$	1	1	$1/\sqrt{2}$
$ (1)_2\rangle$	1	-1	$1/\sqrt{2}$

$C_3$	$ x_0\rangle = \mathbf{r}^0  0\rangle$	$ x_1\rangle = \mathbf{r}^1  0\rangle$	$ x_2\rangle = \mathbf{r}^2  0\rangle$	
$ (0)_3\rangle$	1	1	1	$1/\sqrt{3}$
$ (1)_3\rangle$	1	$e^{2\pi i/3}$	$e^{-2\pi i/3}$	$1/\sqrt{3}$
$ (2)_3\rangle$	1	$e^{-2\pi i/3}$	$e^{2\pi i/3}$	$1/\sqrt{3}$

The eigenket tables are from Fig. 7.3.3. Each phasor in the  $\langle \text{bra} |$  table for  $C_3$  in Fig. 7.3.3 is replaced by its complex conjugate to make kets. A preceding Fig. 8.2.2 shows a  $|(1)_3\rangle$  wave with eigen-phase shift of  $-5\pi/6$ . The corresponding transfer matrix eigenvalues  $\langle m_N | \mathbf{T} | m_N \rangle$  in terms of parameters  $A, B, \dots$  are left as exercises.

Besides such cyclic  $C_N$  systems there are an enormous number of ways to connect  $N$ -dots in ways that have more or less symmetry. A few of these are considered below and in problems. Most of the interesting (Also, read “doable!”) quantum problems have an underlying symmetry.

**(a) Dihedral symmetry  $D_2$**

Two 4-dot symmetries are shown in Fig. 8.3.2 below with transfer matrix relations.

$$\begin{pmatrix} \langle 0 | \Psi_{OUT} \rangle \\ \langle 1 | \Psi_{OUT} \rangle \\ \langle 2 | \Psi_{OUT} \rangle \\ \langle 3 | \Psi_{OUT} \rangle \end{pmatrix} = \begin{pmatrix} A & B & C & C \\ B & A & C & C \\ C & C & A' & B' \\ C & C & B' & A' \end{pmatrix} \begin{pmatrix} \langle 0 | \Psi_{IN} \rangle \\ \langle 1 | \Psi_{IN} \rangle \\ \langle 2 | \Psi_{IN} \rangle \\ \langle 3 | \Psi_{IN} \rangle \end{pmatrix} \quad (8.3.3a)$$

$$\begin{pmatrix} \langle 0 | \Psi_{OUT} \rangle \\ \langle 1 | \Psi_{OUT} \rangle \\ \langle 2 | \Psi_{OUT} \rangle \\ \langle 3 | \Psi_{OUT} \rangle \end{pmatrix} = \begin{pmatrix} A & B & B' & C \\ B & A & C & B' \\ B' & C & A & B \\ C & B' & B & A \end{pmatrix} \begin{pmatrix} \langle 0 | \Psi_{IN} \rangle \\ \langle 1 | \Psi_{IN} \rangle \\ \langle 2 | \Psi_{IN} \rangle \\ \langle 3 | \Psi_{IN} \rangle \end{pmatrix} \quad (8.3.3b)$$

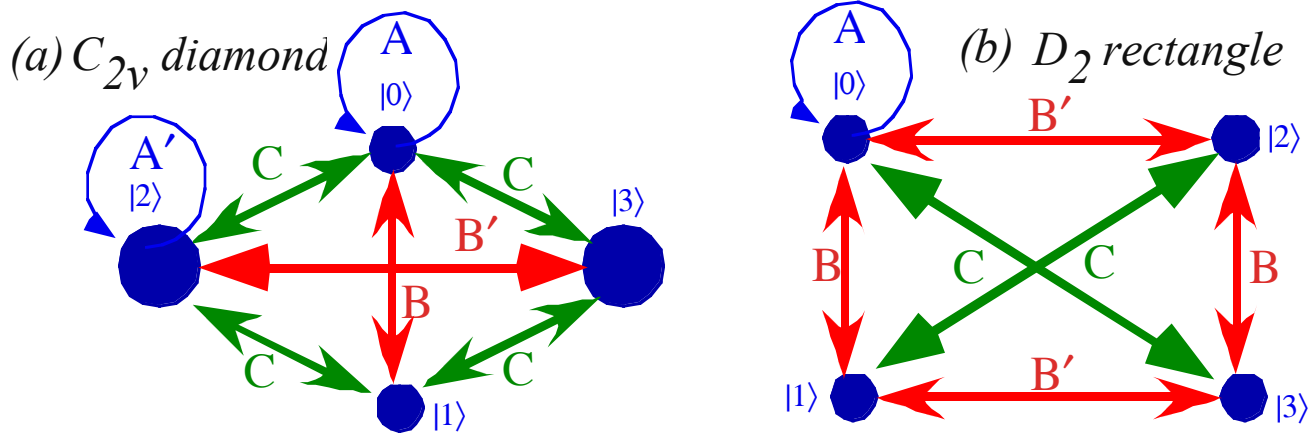


Fig. 8.3.2 Generic 4-channel ( $D_2$ ) quantum dot systems. (a)Diamond  $C_{2v}$  (b) Rectangular  $D_2$ .

Consider the rectangular  $D_2$  system. Its transfer matrix may be written in terms of four operators.

$$\mathbf{T} = A \mathbf{1} + B \mathbf{R}_x + B' \mathbf{R}_y + C \mathbf{R}_z \quad (8.3.4)$$

$$\begin{pmatrix} A & B & B' & C \\ B & A & C & B' \\ B' & C & A & B \\ C & B' & B & A \end{pmatrix} = A \begin{pmatrix} 1 & 0 & 0 & 0 \\ 0 & 1 & 0 & 0 \\ 0 & 0 & 1 & 0 \\ 0 & 0 & 0 & 1 \end{pmatrix} + B \begin{pmatrix} 0 & 1 & 0 & 0 \\ 1 & 0 & 0 & 0 \\ 0 & 0 & 0 & 1 \\ 0 & 0 & 1 & 0 \end{pmatrix} + B' \begin{pmatrix} 0 & 0 & 1 & 0 \\ 0 & 0 & 0 & 1 \\ 1 & 0 & 0 & 0 \\ 0 & 1 & 0 & 0 \end{pmatrix} + C \begin{pmatrix} 0 & 0 & 0 & 1 \\ 0 & 0 & 1 & 0 \\ 0 & 1 & 0 & 0 \\ 1 & 0 & 0 & 0 \end{pmatrix}$$

Each of the operators  $\mathbf{R}_x$ ,  $\mathbf{R}_y$ , or  $\mathbf{R}_z$ , corresponds to  $180^\circ$ -rotations around  $x$ ,  $y$ , or  $z$  axes, respectively, the effect of which is indicated in Fig. 8.3.1b by transfer path arrows labeled  $B$ ,  $B'$ , and  $C$ , respectively. A transfer path  $B'$  along the  $x$ -direction is done by a  $y$ -rotation  $\mathbf{R}_y$ , while  $B$  along  $y$  is done by  $\mathbf{R}_x$ .

*$D_2$  group structure*

The multiplication table for the *Verrgruppe* (4-group) is quite famous and relevant to quantum theory.

1	$R_x$	$R_y$	$R_z$
$R_x$	1	$R_z$	$R_y$
$R_y$	$R_z$	1	$R_x$
$R_z$	$R_y$	$R_x$	1

(8.3.5a)

Its structure reduces to a few simple products. The first is ( $xyz$ )-cyclic: It holds for ( $zxy$ ) and ( $yzx$ ), too.

$$\mathbf{R}_x \mathbf{R}_y = \mathbf{R}_y \mathbf{R}_x = \mathbf{R}_z, \quad (8.3.5b)$$

$$\mathbf{R}_x^2 = \mathbf{R}_y^2 = \mathbf{R}_z^2 = \mathbf{1}. \quad (8.3.5c)$$

$D_2$  spectral decomposition: The old “ $1=1 \cdot 1$  trick” again

The latter (8.3.5c) are of immediate interest to a quantum algebraist because they give minimal equations.

$$\mathbf{R}_x^2 - \mathbf{1} = \mathbf{0}, \quad (8.3.5d) \qquad \mathbf{R}_y^2 - \mathbf{1} = \mathbf{0}. \quad (8.3.5e)$$

From the roots ( $\pm 1$ ) of each minimal equation is constructed a spectral decomposition of  $\mathbf{R}_x$  and  $\mathbf{R}_y$ . This is the simplest application of the Chapter 3 projector formula (3.1.15a) you will probably ever see.

$$\begin{aligned} \mathbf{P}_x^+ &= \frac{\mathbf{1} + \mathbf{R}_x}{2} & \mathbf{P}_y^+ &= \frac{\mathbf{1} + \mathbf{R}_y}{2} \\ \mathbf{P}_x^- &= \frac{\mathbf{1} - \mathbf{R}_x}{2} & \mathbf{P}_y^- &= \frac{\mathbf{1} - \mathbf{R}_y}{2} \end{aligned} \quad (8.3.6a) \qquad (8.3.6b)$$

This spectrally decomposes  $\mathbf{R}_x$  and  $\mathbf{R}_y$  separately. We can do  $\mathbf{R}_z$ , too, but all three must be done *together*.

$$\begin{aligned} \mathbf{1} &= \mathbf{P}_x^+ + \mathbf{P}_x^- & \mathbf{1} &= \mathbf{P}_y^+ + \mathbf{P}_y^- \\ \mathbf{R}_x &= \mathbf{P}_x^+ - \mathbf{P}_x^- & \mathbf{R}_y &= \mathbf{P}_y^+ - \mathbf{P}_y^- \end{aligned} \quad (8.3.7a) \qquad (8.3.7b)$$

To make projectors for the whole  $D_2$  symmetry together we use the old “ $\mathbf{1}=\mathbf{1} \cdot \mathbf{1}$  trick” from (3.1.36).

$$\mathbf{1} = \mathbf{1} \cdot \mathbf{1} = (\mathbf{P}_x^+ + \mathbf{P}_x^-) \cdot (\mathbf{P}_y^+ + \mathbf{P}_y^-) = \mathbf{P}_x^+ \cdot \mathbf{P}_y^+ + \mathbf{P}_x^- \cdot \mathbf{P}_y^+ + \mathbf{P}_x^+ \cdot \mathbf{P}_y^- + \mathbf{P}_x^- \cdot \mathbf{P}_y^- \quad (8.3.8)$$

The result are *irreducible* projectors  $\mathbf{P}^{(i)}$  for the whole  $D_2$  symmetry. Irreducible means  $\text{Trace}(\mathbf{P}^{(i)}) = 1$ .

$$\begin{aligned} \mathbf{P}^{++} &\equiv \mathbf{P}_x^+ \cdot \mathbf{P}_y^+ = \frac{(\mathbf{1} + \mathbf{R}_x) \cdot (\mathbf{1} + \mathbf{R}_y)}{2 \cdot 2} = \frac{1}{4} (\mathbf{1} + \mathbf{R}_x + \mathbf{R}_y + \mathbf{R}_z) \\ \mathbf{P}^{-+} &\equiv \mathbf{P}_x^- \cdot \mathbf{P}_y^+ = \frac{(\mathbf{1} - \mathbf{R}_x) \cdot (\mathbf{1} + \mathbf{R}_y)}{2 \cdot 2} = \frac{1}{4} (\mathbf{1} - \mathbf{R}_x + \mathbf{R}_y - \mathbf{R}_z) \\ \mathbf{P}^{+-} &\equiv \mathbf{P}_x^+ \cdot \mathbf{P}_y^- = \frac{(\mathbf{1} + \mathbf{R}_x) \cdot (\mathbf{1} - \mathbf{R}_y)}{2 \cdot 2} = \frac{1}{4} (\mathbf{1} + \mathbf{R}_x - \mathbf{R}_y - \mathbf{R}_z) \\ \mathbf{P}^{--} &\equiv \mathbf{P}_x^- \cdot \mathbf{P}_y^- = \frac{(\mathbf{1} - \mathbf{R}_x) \cdot (\mathbf{1} - \mathbf{R}_y)}{2 \cdot 2} = \frac{1}{4} (\mathbf{1} - \mathbf{R}_x - \mathbf{R}_y + \mathbf{R}_z) \end{aligned} \quad (8.3.9a)$$

Each  $\mathbf{P}$  is multiplied by its own eigenvalue ( $\pm 1$ ) of  $\mathbf{1}$ ,  $\mathbf{R}_x$ ,  $\mathbf{R}_y$ , and  $\mathbf{R}_z$  in the  $D_2$  spectral decomposition.

$$\begin{aligned} \mathbf{1} &= (+1)\mathbf{P}^{++} + (+1)\mathbf{P}^{-+} + (+1)\mathbf{P}^{+-} + (+1)\mathbf{P}^{--} \quad (\text{completeness}) \\ \mathbf{R}_x &= (+1)\mathbf{P}^{++} + (-1)\mathbf{P}^{-+} + (+1)\mathbf{P}^{+-} + (-1)\mathbf{P}^{--} \\ \mathbf{R}_y &= (+1)\mathbf{P}^{++} + (+1)\mathbf{P}^{-+} + (-1)\mathbf{P}^{+-} + (-1)\mathbf{P}^{--} \\ \mathbf{R}_z &= (+1)\mathbf{P}^{++} + (-1)\mathbf{P}^{-+} + (-1)\mathbf{P}^{+-} + (+1)\mathbf{P}^{--} \end{aligned} \quad (8.3.9b)$$

*Spectral decomposition of  $D_2$  transfer matrices*

Spectral decomposition applies to transfer matrix (8.3.4) and yields its eigenvalue spectrum.

$$\begin{aligned} \langle ++ | \mathbf{T} | ++ \rangle &= \varepsilon^{++} = A \langle \mathbf{1} \rangle + B \langle \mathbf{R}_x \rangle + B' \langle \mathbf{R}_y \rangle + C \langle \mathbf{R}_z \rangle = A + B + B' + C \\ \langle -+ | \mathbf{T} | -+ \rangle &= \varepsilon^{-+} = A \langle \mathbf{1} \rangle + B \langle \mathbf{R}_x \rangle + B' \langle \mathbf{R}_y \rangle + C \langle \mathbf{R}_z \rangle = A - B + B' - C \\ \langle +- | \mathbf{T} | +- \rangle &= \varepsilon^{+-} = A \langle \mathbf{1} \rangle + B \langle \mathbf{R}_x \rangle + B' \langle \mathbf{R}_y \rangle + C \langle \mathbf{R}_z \rangle = A + B - B' - C \\ \langle -- | \mathbf{T} | -- \rangle &= \varepsilon^{--} = A \langle \mathbf{1} \rangle + B \langle \mathbf{R}_x \rangle + B' \langle \mathbf{R}_y \rangle + C \langle \mathbf{R}_z \rangle = A - B - B' + C \end{aligned} \quad (8.3.10)$$

Again, this is a formula for *all possible*  $D_2$ -symmetric operators in this device space of Fig. 8.3.2b. Higher symmetry, such as “square” or *tetragonal*  $D_4$ -symmetry is obtained if parameters  $B$  and  $B'$  are equal. Then the

eigenvalues  $\epsilon^{+-}$  and  $\epsilon^{-+}$  become equal or *degenerate*. Such a symmetry is non-commutative or *non-Abelian* and requires further theory which will be taken up in a later chapter.

**(b) Outer product structure: Double qubit registers**

One of the things that makes group algebra powerful is the concept of an *outer* ( $\times$ ) *product* of two groups. You may have noticed that the  $D_2$  group multiplication table was divided up so that the  $C_2$  subgroup  $\{1, \mathbf{R}_x\}$  was isolated from the rest. The outer product is appropriate when two isolated “factors” correspond to orthogonal or independent systems such as two separate particles or two dimensions or two qubits.

$D_2$  is product  $C_2 \times C_2$

An outer product of the eigenvalue tables in (8.3.2a) yields the  $D_2$  eigenvalue table. This is basically what was happening in the algebraic maneuver of (8.3.8) based upon the old “ $1=1 \cdot 1$ ” trick.

$$\begin{array}{c|cc} C_2^x & 1 & \mathbf{R}_x \\ \hline + & 1 & 1 \\ - & 1 & -1 \end{array} \times \begin{array}{c|cc} C_2^y & 1 & \mathbf{R}_y \\ \hline + & 1 & 1 \\ - & 1 & -1 \end{array} = \begin{array}{c|ccc|cc} C_2^x \times C_2^y & 1 \cdot 1 & \mathbf{R}_x \cdot 1 & 1 \cdot \mathbf{R}_y & \mathbf{R}_x \cdot \mathbf{R}_y \\ \hline ++ & 1 \cdot 1 & 1 \cdot 1 & 1 \cdot 1 & 1 \cdot 1 \\ +- & 1 \cdot 1 & -1 \cdot 1 & 1 \cdot 1 & -1 \cdot 1 \\ -+ & 1 \cdot 1 & 1 \cdot 1 & 1 \cdot (-1) & 1 \cdot (-1) \\ -- & 1 \cdot 1 & -1 \cdot 1 & 1 \cdot (-1) & -1 \cdot (-1) \end{array} \tag{8.3.11a}$$

$$= \begin{array}{c|ccc|cc} D_2 & 1 & \mathbf{R}_x & \mathbf{R}_y & \mathbf{R}_z \\ \hline ++ & 1 & 1 & 1 & 1 \\ +- & 1 & -1 & 1 & -1 \\ -+ & 1 & 1 & -1 & -1 \\ -- & 1 & -1 & -1 & 1 \end{array} \tag{8.3.11b}$$

Note that the numbers in (8.3.11b) are exactly the coefficients of  $A, B, B',$  and  $C$  in the eigenvalue formulas for  $\epsilon^{++}, \epsilon^{-+}, \epsilon^{+-},$  and  $\epsilon^{--}$  in (8.3.10). So the  $\times$ -product makes this calculation very easy indeed.

The outer product requires every operator in  $D_2$  to be *uniquely* a product of one element in  $C_2^x$  and one element in  $C_2^y$ . The elements in  $C_2^x$  must commute with all those in  $C_2^y$  so each product is unique.

$$\begin{aligned} C_2^x \times C_2^y &= \{1, \mathbf{R}_x\} \times \{1, \mathbf{R}_y\} = \begin{array}{c|ccc} C_2^x \times C_2^y & 1 & \mathbf{R}_y \\ \hline 1 & 1 \cdot 1 & 1 \cdot \mathbf{R}_y \\ \mathbf{R}_x & \mathbf{R}_x \cdot 1 & \mathbf{R}_x \cdot \mathbf{R}_y \end{array} \\ &= \{1, \mathbf{R}_x, \mathbf{R}_y, \mathbf{R}_z\} = D_2 \end{aligned} \tag{8.3.11c}$$

If a group  $G$  has  $g$  operators and a group  $H$  has  $h$  members, then  $G \times H$  must have exactly  $gh$  members. It can be a great help to find a symmetry group is an outer product of its parts.

Multiple outer products are possible. The  $D_2 = C_2 \times C_2$  system is like a double-binary or 4-bit register. A  $C_2 \times C_2 \times C_2$  system is a triple-binary or 8-bit register known as *1-byte*. A double-binary  $D_2$  register differs from a quadrary ( $C_4$ ) register as a 1-byte binary system is not a single octal ( $C_8$ ) system.

*Big-endian versus Little-endian*

Computer scientists differ on whether the right ending bit should be the most significant bit (and least rapidly changing) or least significant bit and most often changing. (The former is called the Big-Endian

convention while the latter is called the Little-Endian convention after a perjorative folk-song.) The sequence (00, 01, 10, 11) is Little-Endian and more like our decimal numbering system. The sequence (00, 10, 01, 11) or in (8.3.11) (++, +-, +-, --) is Big-Endian and what we are using here.

$C_6$  is product  $C_3 \times C_2$  (but  $C_4$  is NOT  $C_2 \times C_2$ )

Our first example, the cyclic group  $C_6$ , is a composite  $C_3 \times C_2$  of two of its subgroups  $C_2$  and  $C_3$  as shown below. Here the eigenvalue table (8.3.2a) of  $C_2$  is crossed with the  $C_3$  table (8.3.2b).

$C_3$	<b>1</b>	<b>r</b>	<b>r<sup>2</sup></b>	×	$C_2$	<b>1</b>	<b>R</b>	=	$C_3 \times C_2$	<b>1</b>	<b>r</b>	<b>r<sup>2</sup></b>	<b>1 · R</b>	<b>r · R</b>	<b>r<sup>2</sup> · R</b>	
$(0)_3$	1	1	1		$(0)_2$	1	1		$(0)_3 \cdot (0)_2$	1 · 1	1 · 1	1 · 1	1 · 1	1 · 1	1 · 1	1 · 1
$(1)_3$	1	$e^{2\pi i/3}$	$e^{-2\pi i/3}$		$(1)_2$	1	-1		$(1)_3 \cdot (0)_2$	1 · 1	$e^{2\pi i/3} \cdot 1$	$e^{-2\pi i/3} \cdot 1$	$e^{2\pi i/3} \cdot 1$	$e^{2\pi i/3} \cdot 1$	$e^{-2\pi i/3} \cdot 1$	$e^{2\pi i/3} \cdot 1$
$(2)_3$	1	$e^{-2\pi i/3}$	$e^{2\pi i/3}$		$(1)_2$	1	-1		$(2)_3 \cdot (0)_2$	1 · 1	$e^{-2\pi i/3} \cdot 1$	$e^{2\pi i/3} \cdot 1$	$e^{2\pi i/3} \cdot 1$	$e^{-2\pi i/3} \cdot 1$	$e^{-2\pi i/3} \cdot 1$	$e^{2\pi i/3} \cdot 1$
									$(0)_3 \cdot (1)_2$	1 · 1	1 · 1	1 · 1	1 · (-1)	1 · (-1)	1 · (-1)	1 · (-1)
									$(1)_3 \cdot (1)_2$	1 · 1	1 · 1	$e^{-2\pi i/3} \cdot 1$	1 · (-1)	$e^{2\pi i/3} \cdot (-1)$	$e^{-2\pi i/3} \cdot (-1)$	$e^{-2\pi i/3} \cdot (-1)$
									$(2)_3 \cdot (1)_2$	1 · 1	$e^{-2\pi i/3} \cdot 1$	1 · 1	1 · (-1)	$e^{-2\pi i/3} \cdot (-1)$	$e^{2\pi i/3} \cdot (-1)$	$e^{2\pi i/3} \cdot (-1)$

$C_3 \times C_2 = C_6$	<b>1</b>	<b>r = h<sup>2</sup></b>	<b>r<sup>2</sup> = h<sup>4</sup></b>	<b>R = h<sup>3</sup></b>	<b>r · R = h</b>	<b>r<sup>2</sup> · R = h<sup>5</sup></b>	=		<b>1</b>	<b>r = h<sup>2</sup></b>	<b>r<sup>2</sup> = h<sup>4</sup></b>		<b>R = h<sup>3</sup></b>	<b>r · R = h</b>	<b>r<sup>2</sup> · R = h<sup>5</sup></b>	(8.3.12)
$(0)_3 \cdot (0)_2 = (0)_6$	1	1	1		1	1		$(0)_3 \cdot (1)_2 = (3)_6$	1	1	1		-1	-1	-1	
$(1)_3 \cdot (0)_2 = (2)_6$	1	$e^{2\pi i/3}$	$e^{-2\pi i/3}$		1	$e^{2\pi i/3}$		$(1)_3 \cdot (1)_2 = (5)_6$	1	$e^{2\pi i/3}$	$e^{-2\pi i/3}$		-1	$-e^{2\pi i/3}$	$-e^{-2\pi i/3}$	
$(2)_3 \cdot (0)_2 = (4)_6$	1	$e^{-2\pi i/3}$	$e^{2\pi i/3}$		1	$e^{-2\pi i/3}$		$(2)_3 \cdot (1)_2 = (1)_6$	1	$e^{-2\pi i/3}$	$e^{2\pi i/3}$		-1	$-e^{-2\pi i/3}$	$-e^{2\pi i/3}$	

The tricky part is to identify the  $C_6$  waves  $(k)_6$  that belong to a each product  $(m)_3 \cdot (n)_2$ . That is,

$$e^{i(k)_6 x} = e^{i(m)_3 x} e^{i(n)_2 x} = e^{i\left(m\frac{2\pi}{3} + n\frac{2\pi}{2}\right)x} = e^{i(2m+3n)\frac{2\pi}{6}x} \tag{8.3.13a}$$

The desired k-value is:  $k = (2m + 3n) \bmod 6$  (8.3.13b)

For, example, the last row of (8.3.12) belongs to  $C_6$  wave  $k=(2 \cdot 2 + 3 \cdot 1) \bmod 6 = 7 \bmod 6 = 1$  or  $(1)_6$ . The result is a reordered  $C_6$  table, but otherwise it is the same as the one first drawn in Fig. 7.3.3. Verify!

*Symmetry Catalog*

Cataloging the number of symmetry groups of a given order  $N$  is a difficult problem with a long history. But, for commutative or Abelian groups considered so far, it reduces to finding all the distinct outer products  $C_p \times C_q \times C_r \times C_s \times C_t \dots$  of cyclic groups such that  $N = pqrst\dots$  is a product of primes. Product  $C_p \times C_q$  is the same as  $C_{pq}$  if  $p$  and  $q$  share no factor in common so we don't include  $C_{pq}$  in the catalog if  $p$  and  $q$  are prime since then  $C_{pq} = C_p \times C_q$  as in the case of  $C_6 = C_2 \times C_3$  above. But we do include both  $C_p \times C_p$  and  $C_{pp}$  which are distinct as were  $C_2 \times C_2$  and  $C_4$  above. If  $N = p^P$  is a power of a prime such as  $N = 8 = 2^3$ , then a distinct group exists for each *partition* of the power  $P$ . For example,  $P = 3 = 1 + 2 = 1 + 1 + 1$  has three distinct prime base- $(p = 2)$  groups:  $C_8$  and  $C_4 \times C_2$  and  $C_2 \times C_2 \times C_2$  are all distinct symmetries.

## Problems for Chapter 8.

### Subgroup soup

- 8.1.1 (a) The  $C_6$  symmetry group has subgroups. List all of them except  $C_6$  itself.  
 (b) Do the same for the symmetry groups  $C_3$ ,  $C_4$ , and  $C_5$ . What is special about groups  $C_N$  of prime order  $N$ ?

### Trace'og

- 8.1.2 (a) By group axioms (Sec. 2.2) show each row and column of a group table has an operator  $\mathbf{g}$  only once.  
 (b) Use (a) to show that the regular representation trace  $\text{Trace}R(\mathbf{g})$  is zero for all but “do-nothing” unit operator  $\mathbf{g}=\mathbf{1}$ .

### Turn-about's fair play

- 8.2.1 Suppose we are given the eigenvalues  $\{\tau_0, \tau_1, \tau_2, \tau_3, \tau_4, \tau_5\}$  of a unitary  $C_6$  transfer matrix  $\mathbf{T}$  in (8.2.1).  
 (a) Can the  $\{\tau_0, \tau_1, \tau_2, \tau_3, \tau_4, \tau_5\}$  be any old complex numbers? What restrictions, if any, apply?  
 (b) Can one give a formula for all 36 components  $T_{pq}$  of  $\mathbf{T}$  in terms of  $\{\tau_0, \tau_1, \tau_2, \tau_3, \tau_4, \tau_5\}$ ? If so do it. If not explain why not and under what conditions you may be able to do it.

### A Hex on pairing

- 8.2.2 Suppose the  $C_6$  transfer matrix  $\mathbf{T}$  is the form of the *Pairing operator*, that is all components equal  $T_{pq} = T$ .  
 (a) Derive the resulting eigenvalue spectrum.  
 (b) What, if any, limitations need to be placed on parameter  $T$ ?  
 (c) Discuss which waves belong to which eigenvalues

### Phase o'Hex

- 8.2.3 (a) Could the hexagonal  $C_6$  analyzer be wired so input  $|even\ sites\rangle=(1,0,1,0,1,0)$  comes out  $e^{i\phi}|even\rangle$ ?  
 What  $k_m$ -eigenstates make up  $|even\ sites\rangle$ ? Does your “rewiring” maintain  $C_6$  symmetry?  
 (b) Could the  $C_6$  analyzer be wired so input  $|even\ sites\rangle$  comes out  $e^{i\phi}|odd\ sites\rangle=(0,1,0,1,0,1)$ ?  
 What  $k_m$ -eigenstates make up  $|odd\ sites\rangle$ ? Does your “rewiring” maintain  $C_6$  symmetry?  
 (c) Could the  $C_6$  analyzer be wired so input  $|odd\ symm\rangle=(1,-1,1,-1,1,-1)$  comes out  $e^{i\phi}|odd\ symm\rangle$ ?  
 What  $k_m$ -eigenstates make up  $|odd\ symm\rangle$ ? Does your “rewiring” maintain  $C_6$  symmetry?  
 (d) Could the  $C_6$  analyzer be wired so input  $|odd\ symm\rangle$  comes out  $e^{i\phi}|even\ symm\rangle=(1,1,1,1,1,1)$ ?  
 What  $k_m$ -eigenstates make up  $|even\ symm\rangle$ ? Does your “rewiring” maintain  $C_6$  symmetry?

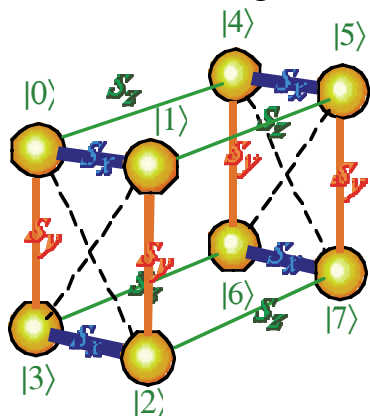
### Little diamond

- 8.3.1. The symmetry eigensolution analysis of the  $C_{2v}$  diamond quantum dot device in Fig. 8.3.2(a) is a little different than its  $D_2$  cousin in Fig. 8.3.2(b). Symmetry multiplication table and spectral decomposition is essentially the same but the transfer  $\mathbf{T}$ -operator is not such a simple linear combination of symmetry operators. Represent the symmetry and give a decomposition of symmetry and  $\mathbf{T}$ -matrix. (Note that x and y-plane mirror reflections are symmetry operators, too. There was no distinction between rotations and reflections in the  $D_2$  problem.)

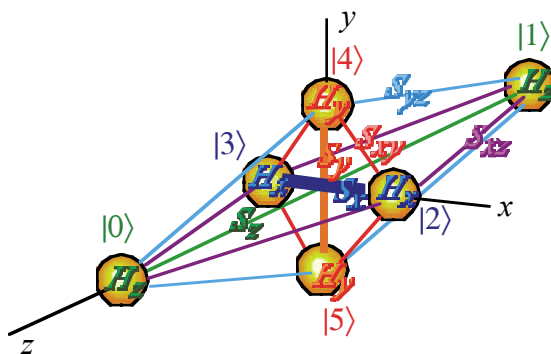
### Double Crossed

- 8.3.2. Complete a symmetry catalog of commutative (Abelian) groups in terms of distinct  $C_p \times C_q \times \dots$  cross products.  
 (a) for order  $N=8$ . (b)  $N=9$ . (c)  $N=10$ . (d)  $N=11$ . (e)  $N=12$ . (f)  $N=16$ .

Problem 8.3.3 “Big box”



Problem 8.3.4 “Big diamond”



Big box

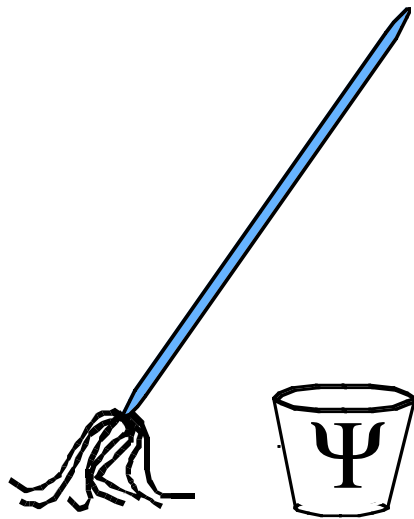
8.3.3. Give a complete symmetry eigensolution analysis of the  $D_{2h}$  device pictured here. First show that the full symmetry with horizontal reflection group  $C_h = \{1, \sigma_{xy}(\text{thru } z\text{-axis})\}$  is  $C_2 \times C_2 \times C_h = C_2 \times C_2 \times C_2$  which is called  $D_{2h}$ . Derive character table of  $D_{2h}$  using the cross product trick of (8.3.11).

Big diamond

8.3.4. Give a complete symmetry eigensolution analysis of the  $D_{2h}$  device pictured above.

Trace'o P

8.3.5. Before (8.3.9a) it is noted that  $\text{Trace}R(\mathbf{P})=1$  means projector  $\mathbf{P}$  is irreducible, that is, not a sum  $\mathbf{P} = \mathbf{P}_1 + \mathbf{P}_2$  of other “smaller” projectors. Explain this and verify by constructing the representation of the  $\mathbf{P}^{++}$ , ... in (8.3.9).



# QM for AMOP

## Chapter 9

### Time Evolution and Fourier Dynamics

**W. G. Harter**

Now we consider the transfer operator from Hell, the time evolution operator  $U$ . This “grim-reaper” of the quantum world determines everything that happens in a non-relativistic (Schrodinger) system. Nothing escapes  $U$ -action including you! So learn  $U$  well, and pay particular attention to  $U$ 's generator  $H$  which is called the Hamiltonian. The expression  $e^{-iHt}$  (for constant  $H$ ) is an icon of modern quantum theory. Quantum dot systems from Chapters 7 and 8 will be used as examples and provide our first introduction to quantum periodic band theory and quantum “revival” beats. (Yes, some waves can survive the grim reaper by reviving repeatedly while doing arithmetic, too!)

<b>CHAPTER 9. TIME EVOLUTION AND FOURIER DYNAMICS .....</b>	<b>1</b>
<b>9.1 Time Evolution Operator .....</b>	<b>1</b>
(a) Planck's oscillation hypothesis .....	1
<b>9.2 Schrodinger Time Equations .....</b>	<b>3</b>
(a) Schrodinger's time equations. Hamiltonian time generators .....	3
(b) Schrodinger's matrix equations.....	4
(c) Writing Hamiltonian $H$ in terms of symmetry operators $r^p$ .....	4
Unitary $U$ implies Hermitian $H$ .....	5
<b>9.3 Schrodinger Eigen-Equations .....</b>	<b>6</b>
(a) Solving Schrodinger's eigen-equations for $C_6$ system .....	7
(b) Energy spectrum and tunneling rates .....	7
Bloch's waves vs. Bohr's .....	9
(c) Brillouin's boundary .....	9
Effective mass: Another quantum view of inertia.....	11
(d) Bohr wavepacket dynamics: Uncertainty and revival .....	15
Semi-classical Theory: Farey Sums and Quantum Speed Limits .....	15
<b>9.4 Homo-cyclic <math>C_n</math> Revivals.....</b>	<b>19</b>
(a) Two-state $C_2$ systems: Beats.....	19
(b) $C_n$ group structure: $n=3, 4, \dots, 6$ Eigenstates.....	21
(c) $C_n$ dynamics: $n=3, 4, \dots, 6$ Fractional Revivals.....	23
Bohr vs. Bloch dispersion .....	28
<b>Problems for Chapter 9. ....</b>	<b>30</b>
<b>REVIEW TOPICS &amp; FORMULAS FOR UNIT 3.....</b>	<b>33</b>

## Chapter 9. Time Evolution and Fourier Dynamics

### 9.1 Time Evolution Operator

It is often said that nothing that is more demanding than the test of time. All the analyzer experiments considered so far have required time to do, lots and lots of time. Never forget that all our fancy theory of analyzers and wave mechanics is just giving us probabilities; not too different from odds posted at the racetrack. Millions of counts need to be registered before those fancy predictions are seen in a laboratory, and all that counting takes time.

Now we consider a very demanding kind of analyzer, good old Father Time, in the form of *the time evolution operator*  $U(t_{FINAL} ; t_{INITIAL})$ . This "grim reaper" is supposed to be able to take any state at an initial time and transform it into what the state will be at a later time.

$$|\Psi(t_{FINAL})\rangle = U(t_{FINAL} ; t_{INITIAL}) |\Psi(t_{INITIAL})\rangle \tag{9.1.1}$$

The main task of this section will be to begin theory and derivation of  $U$  operators. This is the main problem of quantum theory, so we won't finish the job here. In fact, we won't be done with  $U$  operators until the twelfth hour of never!

Let's first suppose *time translation symmetry* is present. By that I mean there is no one (such as perfidious janitors) "messing" with our analyzers. So, the experiments run the same day and night. Then we can often simplify the evolution operator equation by just having one time variable as follows

$$|\Psi(t)\rangle = U(t ; 0) |\Psi(0)\rangle, \tag{9.1.2}$$

so you may pick a "time origin" ( $t=0$ ) arbitrarily.

#### (a) Planck's oscillation hypothesis

At first, the time evolution problem looks formidable, even for a little six-state beam analyzer problem that was studied in Chapter 8. Its evolution equation (9.1.2) looks like the following at any point  $z$  in the beam and varies with  $z$ . We will put off discussing  $z$ -dependence until a later chapter.

$$\begin{pmatrix} \langle 1 | \Psi(t) \rangle \\ \langle 2 | \Psi(t) \rangle \\ \langle 3 | \Psi(t) \rangle \\ \langle 4 | \Psi(t) \rangle \\ \langle 5 | \Psi(t) \rangle \\ \langle 6 | \Psi(t) \rangle \end{pmatrix} = \begin{pmatrix} U_{11} & U_{12} & U_{13} & U_{14} & U_{15} & U_{16} \\ U_{21} & U_{22} & U_{23} & U_{24} & U_{25} & U_{26} \\ U_{31} & U_{32} & U_{33} & U_{34} & U_{35} & U_{36} \\ U_{41} & U_{42} & U_{43} & U_{44} & U_{45} & U_{46} \\ U_{51} & U_{52} & U_{53} & U_{54} & U_{55} & U_{56} \\ U_{61} & U_{62} & U_{63} & U_{64} & U_{65} & U_{66} \end{pmatrix} \cdot \begin{pmatrix} \langle 1 | \Psi(0) \rangle \\ \langle 2 | \Psi(0) \rangle \\ \langle 3 | \Psi(0) \rangle \\ \langle 4 | \Psi(0) \rangle \\ \langle 5 | \Psi(0) \rangle \\ \langle 6 | \Psi(0) \rangle \end{pmatrix} \tag{9.1.3a}$$

Here the matrix elements are

$$U_{pq} = \langle p | U(t ; 0) | q \rangle \tag{9.1.3b}$$

How in the world can one derive all those  $N^2=36$  time functions  $U_{pq}$  ? Woe is us!

But wait! The  $U$ -operator and any matrix representing it should have the  $C_N$  symmetry of the analyzer system shown in Fig. 9.1.1. And, like the analyzer  $T$ -operator, it should be reduced by the Fourier  $C_N$ -symmetry

$|k_m\rangle$  basis to a diagonal matrix made of phase factors  $e^{i\phi_m}$  as in (9.1.17b). Furthermore, the Planck hypothesis indicates that the phase factors should have the time phasor "clock" form  $e^{-i\omega_m t}$  that is conventional clockwise phasor rotation. Then the  $\mathbf{U}$ -operator in (9.1.3) can be made to have a much simpler form if the basis is changed to its eigenbasis  $|k_m\rangle$  as shown below.

$$\begin{pmatrix} \langle k_0 | \Psi(t) \rangle \\ \langle k_1 | \Psi(t) \rangle \\ \langle k_2 | \Psi(t) \rangle \\ \langle k_3 | \Psi(t) \rangle \\ \langle k_4 | \Psi(t) \rangle \\ \langle k_5 | \Psi(t) \rangle \end{pmatrix} = \begin{pmatrix} e^{-i\omega_0 t} & 0 & 0 & 0 & 0 & 0 \\ 0 & e^{-i\omega_1 t} & 0 & 0 & 0 & 0 \\ 0 & 0 & e^{-i\omega_2 t} & 0 & 0 & 0 \\ 0 & 0 & 0 & e^{-i\omega_3 t} & 0 & 0 \\ 0 & 0 & 0 & 0 & e^{-i\omega_4 t} & 0 \\ 0 & 0 & 0 & 0 & 0 & e^{-i\omega_5 t} \end{pmatrix} \cdot \begin{pmatrix} \langle k_0 | \Psi(0) \rangle \\ \langle k_1 | \Psi(0) \rangle \\ \langle k_2 | \Psi(0) \rangle \\ \langle k_3 | \Psi(0) \rangle \\ \langle k_4 | \Psi(0) \rangle \\ \langle k_5 | \Psi(0) \rangle \end{pmatrix} \quad (9.1.4)$$

Now, instead of  $N^2=36$  unknown  $U_{pq}$  functions we have only  $N=6$  frequency values  $\omega_m$  to derive.

This is quite a simplification, if true. It is also a reasonable one since the evolution operators need to form a group called the *time evolution group* that multiplies as follows. (Recall (1.4.12d).)

$$\mathbf{U}(t_3; t_1) = \mathbf{U}(t_3; t_2) \cdot \mathbf{U}(t_2; t_1) \quad (9.1.5a)$$

Also, axioms 1-4 require  $\mathbf{U}(t_2; t_1)$  to be unitary operators. (Recall (1.5.5b).)

$$\mathbf{U}^\dagger(t_2; t_1) = \mathbf{U}^{-1}(t_2; t_1) = \mathbf{U}(t_1; t_2) \quad (9.1.5b)$$

These requirements are satisfied by the Planck phasor forms in the diagonal matrix (9.1.4) or as follows,

$$\mathbf{U}(t_2; t_1) = \text{diag} \{ e^{-i\omega_0(t_2 - t_1)}, e^{-i\omega_1(t_2 - t_1)}, \dots, e^{-i\omega_m(t_2 - t_1)}, \dots \} \quad (9.1.6a)$$

since

$$e^{-i\omega_m(t_3 - t_1)} = e^{-i\omega_m(t_3 - t_2)} e^{-i\omega_m(t_2 - t_1)}, \text{ and } (e^{-i\omega_m(t_2 - t_1)})^* = e^{-i\omega_m(t_1 - t_2)} \quad (9.1.6b)$$

which depends only on relative time difference  $(t_1 - t_2)$ :  $\mathbf{U}(t_1; t_2) = \mathbf{U}(t_1 - t_2; 0) = \mathbf{U}(0; t_2 - t_1)$

Indeed, we shall demand that a  $\mathbf{U}$ -eigenbasis  $\{ |\omega_0\rangle, |\omega_1\rangle, \dots, |\omega_m\rangle, \dots \}$  shall exist even for asymmetric evolution operators for which a convenient symmetry basis  $\{ |k_0\rangle, |k_1\rangle, \dots, |k_m\rangle, \dots \}$  is not available to give "instant" diagonalization. We shall describe how to generally find eigenkets  $|\omega_m\rangle$  so that

$$\mathbf{U}(t_2; t_1) |\omega_m\rangle = e^{-i\omega_m(t_2 - t_1)} |\omega_m\rangle \quad (9.1.7)$$

This is always possible in principle since we know that all unitary operators are diagonalizable. (Recall exercises in Ch. 3.) However, in practice the problem of diagonalization can be a bit of a chore for large systems consisting of millions, billions, or more states! We will need all the help that symmetry analysis can give us.

## 9.2 Schrodinger Time Equations

Time evolution operators and the states they evolve satisfy time differential equations known as *Schrodinger equations*. This is a common way to restate Planck's oscillation axiom in differential form.

### (a) Schrodinger's time equations. Hamiltonian time generators

If time evolution equation (9.1.4) can predict the quantum state future far in advance, then it should certainly give the *rate* of evolution correctly. The time derivative of (9.1.4) is the following.

$$\frac{\partial}{\partial t} \begin{pmatrix} \langle k_0 | \Psi(t) \rangle \\ \langle k_1 | \Psi(t) \rangle \\ \langle k_2 | \Psi(t) \rangle \\ \langle k_3 | \Psi(t) \rangle \\ \langle k_4 | \Psi(t) \rangle \\ \langle k_5 | \Psi(t) \rangle \end{pmatrix} = -i \begin{pmatrix} \omega_0 e^{-i\omega_0 t} & 0 & 0 & 0 & 0 & 0 \\ 0 & \omega_1 e^{-i\omega_1 t} & 0 & 0 & 0 & 0 \\ 0 & 0 & \omega_2 e^{-i\omega_2 t} & 0 & 0 & 0 \\ 0 & 0 & 0 & \omega_3 e^{-i\omega_3 t} & 0 & 0 \\ 0 & 0 & 0 & 0 & \omega_4 e^{-i\omega_4 t} & 0 \\ 0 & 0 & 0 & 0 & 0 & \omega_5 e^{-i\omega_5 t} \end{pmatrix} \cdot \begin{pmatrix} \langle k_0 | \Psi(0) \rangle \\ \langle k_1 | \Psi(0) \rangle \\ \langle k_2 | \Psi(0) \rangle \\ \langle k_3 | \Psi(0) \rangle \\ \langle k_4 | \Psi(0) \rangle \\ \langle k_5 | \Psi(0) \rangle \end{pmatrix} \tag{9.2.1}$$

Simplifying the notation and factoring gives

$$\frac{\partial}{\partial t} \begin{pmatrix} \Psi_{k_0}(t) \\ \Psi_{k_1}(t) \\ \Psi_{k_2}(t) \\ \Psi_{k_3}(t) \\ \Psi_{k_4}(t) \\ \Psi_{k_5}(t) \end{pmatrix} = -i \begin{pmatrix} \omega_0 & 0 & 0 & 0 & 0 & 0 \\ 0 & \omega_1 & 0 & 0 & 0 & 0 \\ 0 & 0 & \omega_2 & 0 & 0 & 0 \\ 0 & 0 & 0 & \omega_3 & 0 & 0 \\ 0 & 0 & 0 & 0 & \omega_4 & 0 \\ 0 & 0 & 0 & 0 & 0 & \omega_5 \end{pmatrix} \cdot \begin{pmatrix} e^{-i\omega_0 t} \Psi_{k_0}(0) \\ e^{-i\omega_1 t} \Psi_{k_1}(0) \\ e^{-i\omega_2 t} \Psi_{k_2}(0) \\ e^{-i\omega_3 t} \Psi_{k_3}(0) \\ e^{-i\omega_4 t} \Psi_{k_4}(0) \\ e^{-i\omega_5 t} \Psi_{k_5}(0) \end{pmatrix} \tag{9.2.2}$$

Here we lose the Dirac notation briefly with

$$\Psi_{k_m}(t) = \langle k_m | \Psi(t) \rangle = e^{-i\omega_m t} \langle k_m | \Psi(0) \rangle = e^{-i\omega_m t} \Psi_{k_m}(0) . \tag{9.2.3}$$

Multiplying by  $i\hbar$  and then putting back the Dirac notation gives the following.

$$i\hbar \frac{\partial}{\partial t} \begin{pmatrix} \Psi_{k_0}(t) \\ \Psi_{k_1}(t) \\ \Psi_{k_2}(t) \\ \Psi_{k_3}(t) \\ \Psi_{k_4}(t) \\ \Psi_{k_5}(t) \end{pmatrix} = \begin{pmatrix} \hbar\omega_0 & 0 & 0 & 0 & 0 & 0 \\ 0 & \hbar\omega_1 & 0 & 0 & 0 & 0 \\ 0 & 0 & \hbar\omega_2 & 0 & 0 & 0 \\ 0 & 0 & 0 & \hbar\omega_3 & 0 & 0 \\ 0 & 0 & 0 & 0 & \hbar\omega_4 & 0 \\ 0 & 0 & 0 & 0 & 0 & \hbar\omega_5 \end{pmatrix} \cdot \begin{pmatrix} \Psi_{k_0}(t) \\ \Psi_{k_1}(t) \\ \Psi_{k_2}(t) \\ \Psi_{k_3}(t) \\ \Psi_{k_4}(t) \\ \Psi_{k_5}(t) \end{pmatrix} , \tag{9.2.4a}$$

$$i\hbar \frac{\partial}{\partial t} \begin{pmatrix} \langle k_0 | \Psi(t) \rangle \\ \langle k_1 | \Psi(t) \rangle \\ \langle k_2 | \Psi(t) \rangle \\ \langle k_3 | \Psi(t) \rangle \\ \langle k_4 | \Psi(t) \rangle \\ \langle k_5 | \Psi(t) \rangle \end{pmatrix} = \begin{pmatrix} \hbar\omega_0 & 0 & 0 & 0 & 0 & 0 \\ 0 & \hbar\omega_1 & 0 & 0 & 0 & 0 \\ 0 & 0 & \hbar\omega_2 & 0 & 0 & 0 \\ 0 & 0 & 0 & \hbar\omega_3 & 0 & 0 \\ 0 & 0 & 0 & 0 & \hbar\omega_4 & 0 \\ 0 & 0 & 0 & 0 & 0 & \hbar\omega_5 \end{pmatrix} \cdot \begin{pmatrix} \langle k_0 | \Psi(t) \rangle \\ \langle k_1 | \Psi(t) \rangle \\ \langle k_2 | \Psi(t) \rangle \\ \langle k_3 | \Psi(t) \rangle \\ \langle k_4 | \Psi(t) \rangle \\ \langle k_5 | \Psi(t) \rangle \end{pmatrix}, \quad (9.2.4b)$$

which is called *Schrodinger's time equation*. Its abstract Dirac form is the following

$$i\hbar \frac{\partial}{\partial t} |\Psi(t)\rangle = \mathbf{H} |\Psi(t)\rangle \quad (9.2.5a)$$

where the *Hamiltonian energy operator*  $\mathbf{H}$  is related to  $i\hbar$  times the time evolution operator derivative by

$$i\hbar \frac{\partial}{\partial t} \mathbf{U}(t,0) = \mathbf{H} \mathbf{U}(t,0) \quad (9.2.5b)$$

and is  $\mathbf{H}$  also called the *generator of time translation*. An exponential solution to (9.1.5b) is

$$\mathbf{U}(t,0) = e^{-i\mathbf{H}t/\hbar} \mathbf{U}(0,0) = e^{-i\mathbf{H}t/\hbar} \quad \text{where: } \mathbf{U}(0,0) = \mathbf{1} \quad (9.2.5c)$$

if  $\mathbf{H}$  is an  $N$ -by- $N$  constant matrix operator as it is in (9.1.4a-b). (It must be constant if there is time translation symmetry. Remember, it is time translation symmetry that permits exponential solutions.)

All of the above "derivations" of Schrodinger's equations (9.2.5) are really only Planck's frequency and energy axiom, starting with (9.1.4) and restated in many fancy ways for an  $N$ -state system for  $N=6$ .

## (b) Schrodinger's matrix equations

The thing that makes a Hamiltonian  $\mathbf{H}$  powerful is that it may be easily derived in some other basis like the original channel basis  $\{|1\rangle, |2\rangle, \dots, |N\rangle\}$  and then diagonalized using symmetry techniques or numerical methods to find its eigenvectors  $\{|\omega_0\rangle, |\omega_1\rangle, \dots, |\omega_{N-1}\rangle\}$  known as *energy eigenstates* and eigenvalues  $\{\hbar\omega_0, \hbar\omega_1, \dots, \hbar\omega_{N-1}\}$  known as *energy or frequency spectra*  $\varepsilon_m = \hbar\omega_m$ . This time, the word *spectra* is used as it was intended by the pioneering spectroscopists who first saw atomic spectral lines in laboratory and in astrophysical observations. (Mathematicians co-opt the term *spectra* other ways.)

Rewriting Schrodinger's time equation (9.2.5a)

$$i\hbar \frac{\partial}{\partial t} |\Psi(t)\rangle = \mathbf{H} |\Psi(t)\rangle \quad (9.2.6a)$$

in an arbitrary basis gives

$$i\hbar \frac{\partial}{\partial t} \begin{pmatrix} \langle 0 | \Psi(t) \rangle \\ \langle 1 | \Psi(t) \rangle \\ \langle 2 | \Psi(t) \rangle \\ \langle 3 | \Psi(t) \rangle \\ \langle 4 | \Psi(t) \rangle \\ \langle 5 | \Psi(t) \rangle \end{pmatrix} = \begin{pmatrix} H_{00} & H_{01} & H_{02} & H_{03} & H_{04} & H_{05} \\ H_{10} & H_{11} & H_{12} & H_{13} & H_{14} & H_{15} \\ H_{20} & H_{21} & H_{22} & H_{23} & H_{24} & H_{25} \\ H_{30} & H_{31} & H_{32} & H_{33} & H_{34} & H_{35} \\ H_{40} & H_{41} & H_{42} & H_{43} & H_{44} & H_{45} \\ H_{50} & H_{51} & H_{52} & H_{53} & H_{54} & H_{55} \end{pmatrix} \cdot \begin{pmatrix} \langle 0 | \Psi(t) \rangle \\ \langle 1 | \Psi(t) \rangle \\ \langle 2 | \Psi(t) \rangle \\ \langle 3 | \Psi(t) \rangle \\ \langle 4 | \Psi(t) \rangle \\ \langle 5 | \Psi(t) \rangle \end{pmatrix}, \quad (9.2.6b)$$

where the matrix elements

$$H_{pq} = \langle p | \mathbf{H} | q \rangle \tag{9.2.6c}$$

are generally non-diagonal except in  $\mathbf{H}$ 's or  $\mathbf{U}$ 's own (eigen) basis  $|k_m\rangle$  as in (9.2.4).

**(c) Writing Hamiltonian  $\mathbf{H}$  in terms of symmetry operators  $\mathbf{r}^p$**

If analyzer  $\mathbf{H}$  -matrix (8.2.1) has  $C_6$  symmetry, it commutes with all the rotation operator  $\mathbf{r}$ -matrices in (2.7.5) and is a linear combination of  $\mathbf{r}^p$  as follows.

$$\mathbf{H} = H \mathbf{1} + S \mathbf{r} + T \mathbf{r}^2 + U \mathbf{r}^3 + T^* \mathbf{r}^4 + S^* \mathbf{r}^5, \tag{9.2.6}$$

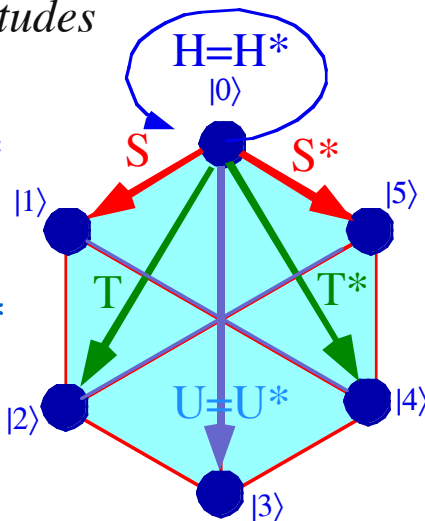
The  $\mathbf{r}^p$ -matrices in (2.7.5) combine to give a  $C_6$  -symmetric  $\mathbf{H}$ -matrix Schrodinger equation (9.2.7) in analogy to the  $\mathbf{T}$ -matrix transfer equation (8.2.7), and label its *tunneling paths* from point-to-point.

$$i\hbar \frac{\partial}{\partial t} \begin{pmatrix} \langle 0 | \Psi(t) \rangle \\ \langle 1 | \Psi(t) \rangle \\ \langle 2 | \Psi(t) \rangle \\ \langle 3 | \Psi(t) \rangle \\ \langle 4 | \Psi(t) \rangle \\ \langle 5 | \Psi(t) \rangle \end{pmatrix} = \begin{pmatrix} H & S^* & T^* & U & T & S \\ S & H & S^* & T^* & U & T \\ T & S & H & S^* & T^* & U \\ U & T & S & H & S^* & T^* \\ T^* & U & T & S & H & S^* \\ S^* & T^* & U & T & S & H \end{pmatrix} \cdot \begin{pmatrix} \langle 0 | \Psi(t) \rangle \\ \langle 1 | \Psi(t) \rangle \\ \langle 2 | \Psi(t) \rangle \\ \langle 3 | \Psi(t) \rangle \\ \langle 4 | \Psi(t) \rangle \\ \langle 5 | \Psi(t) \rangle \end{pmatrix}, \tag{9.2.7}$$

The undetermined coefficients  $H, S, T, U, T^*$ , and  $S^*$  correspond to all the *tunneling amplitudes* that state  $|0\rangle$  could possibly have to other states  $|0\rangle, |1\rangle, |2\rangle, |3\rangle, |4\rangle$ , and  $|5\rangle$  as indicated by arrows in Fig. 9.2.1 which are analogous to the transfer amplitude paths for the  $\mathbf{T}$  -matrix (or of a  $\mathbf{U}$ -matrix) in Fig. 8.2.1.

*(a) Tunneling Amplitudes from  $|0\rangle$*

$$\begin{aligned} H &= \langle 0 | \mathbf{H} | 0 \rangle = H^* \\ S &= \langle 1 | \mathbf{H} | 0 \rangle \\ T &= \langle 2 | \mathbf{H} | 0 \rangle \\ U &= \langle 3 | \mathbf{H} | 0 \rangle = U^* \\ T^* &= \langle 4 | \mathbf{H} | 0 \rangle \\ S^* &= \langle 5 | \mathbf{H} | 0 \rangle \end{aligned}$$



*(b) All  $C_6$  Tunneling Paths*

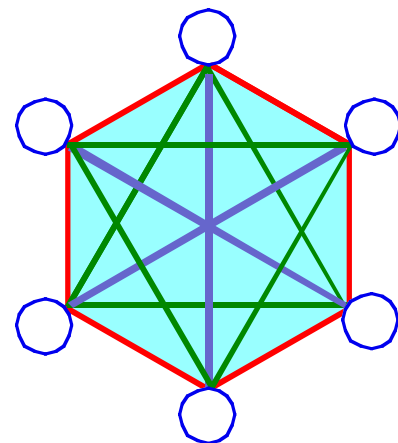


Fig. 9.2.1 Generic 6-channel ( $C_6$ )Hamiltonian tunneling (a) Amplitudes (b) Paths

But, there is one important difference. Hamiltonian matrices must be *Hermitian* (self-conjugate:  $\mathbf{H}^\dagger = \mathbf{H}$ ).

$$H_{pq} = \langle p | \mathbf{H} | q \rangle = \langle p | \mathbf{H}^\dagger | q \rangle = H_{qp}^* \tag{9.2.8a}$$

Unitary  $\mathbf{U}$  implies Hermitian  $\mathbf{H}$

Hamiltonian  $\mathbf{H}$  is Hermitian because the time evolution operator is unitary by definition (9.2.5).

$$\mathbf{U}(t,0)^\dagger = \left( e^{-i\mathbf{H}t/\hbar} \right)^\dagger = e^{i\mathbf{H}^\dagger t/\hbar} = \mathbf{U}(t,0)^{-1} = \mathbf{U}(-t,0) = e^{i\mathbf{H}t/\hbar} \quad (9.2.8b)$$

So, an inverse tunneling amplitude such as  $S^*$  is the complex conjugate of the forward one  $S$ . Also, diagonal components of a Hamiltonian matrix are thus always real.

$$H_{pp} = H_{pp}^* \quad (9.2.8c)$$

This means the eigenvalues are also real since relations (9.2.8) are true in any basis including the  $\mathbf{H}$  operator's own basis or eigenbasis where  $\mathbf{H}$  is diagonal.

Note that a diametric tunneling amplitude such as  $U=U^*$  also is real because its operator  $\mathbf{r}^3$  is its own inverse ( $\mathbf{r}^3 = \mathbf{r}^{3\dagger} = \mathbf{r}^{-3}$ ). Conjugation reverses direction of rotation for all  $C_6$  operators except  $\mathbf{1}$  and  $\mathbf{r}^3$ .  $\dagger$ -conjugation is time reversal for Schrodinger equation (9.2.6). Axiom-2 says bra-clocks run backwards.

### 9.3 Schrodinger Eigen-Equations

Time evolution is simple for eigenstates  $|\omega_m\rangle$  because only a single eigenfrequency  $\omega_m$  is present. Energy or frequency eigenstates and eigenvalues satisfy *Schrodinger's eigenvalue equation*, also called the *Schrodinger time-independent equation*.

$$\mathbf{H} |\omega_m\rangle = \hbar\omega_m |\omega_m\rangle = \varepsilon_m |\omega_m\rangle \quad (9.3.1a)$$

In a “quantum-dot” basis this is a matrix eigenvalue problem such as the following for  $N=6$ .

$$\begin{pmatrix} H_{00} & H_{01} & H_{02} & H_{03} & H_{04} & H_{05} \\ H_{10} & H_{11} & H_{12} & H_{13} & H_{14} & H_{15} \\ H_{20} & H_{21} & H_{22} & H_{23} & H_{24} & H_{25} \\ H_{30} & H_{31} & H_{32} & H_{33} & H_{34} & H_{35} \\ H_{40} & H_{41} & H_{42} & H_{43} & H_{44} & H_{45} \\ H_{50} & H_{51} & H_{52} & H_{53} & H_{54} & H_{55} \end{pmatrix} \cdot \begin{pmatrix} \langle 0|\omega_m\rangle \\ \langle 1|\omega_m\rangle \\ \langle 2|\omega_m\rangle \\ \langle 3|\omega_m\rangle \\ \langle 4|\omega_m\rangle \\ \langle 5|\omega_m\rangle \end{pmatrix} = \hbar\omega_m \begin{pmatrix} \langle 0|\omega_m\rangle \\ \langle 1|\omega_m\rangle \\ \langle 2|\omega_m\rangle \\ \langle 3|\omega_m\rangle \\ \langle 4|\omega_m\rangle \\ \langle 5|\omega_m\rangle \end{pmatrix}, \quad (9.3.1b)$$

The Schrodinger time equation (9.2.6b) is a simple 1-dimensional relation for each amplitude.

$$i\hbar \frac{\partial}{\partial t} \langle p|\omega_m\rangle = \langle p|\mathbf{H}|\omega_m\rangle = \hbar\omega_m \langle p|\omega_m\rangle \quad (9.3.2)$$

Its solution has each amplitude  $\langle p|\omega_m\rangle$  spinning its clock at the same rate  $\omega_m$  at constant size  $|\langle p|\omega_m\rangle|^2$ .

$$\langle p|\omega_m(t)\rangle = \langle p|\omega_m(0)\rangle e^{-i\omega_m t} \quad (9.3.3)$$

$$\left| \langle p|\omega_m(t)\rangle \right|^2 = \left| \langle p|\omega_m(0)\rangle \right|^2 = \text{const.} \quad (9.3.4)$$

Such is the fate of an eigenstate or stationary state. Its observable probability distribution is forever fixed.

But, how does one find just the right  $\langle p|\omega_m\rangle$  amplitudes to solve (9.3.1)? Aren't we back in hot water again with  $N^2=36$  unknown constants  $H_{pq}$  and a big diagonalization job facing us? Woe is us, again! But, fortunately, there are all kinds of techniques and approximation tricks to find the Hamiltonian matrix elements and then find the energy spectrum. That is what most of the rest of the book is about!

Chief among the eigensolution techniques is symmetry analysis. The time evolution matrix  $\mathbf{U}$  and the Hamiltonian matrix  $\mathbf{H}$  for the  $C_6$ -analyzer in Fig. 8.1.1 can be treated to the same techniques that worked for the analyzer  $\mathbf{T}$ -matrix. Again, all possible  $C_6$ -symmetric Hamiltonian matrices are given with a single complete set

of eigensolutions. Then all possible motions are obtained from combinations of eigensolutions, which, by their completeness are able to produce an arbitrary initial condition.

After that, the motion is just the interference beating between all the eigenfrequencies that participate in producing a given initial state. Remember, it takes two to tango! At least two eigenstates with different eigenfrequencies need to be up and spinning to have observable motion. Otherwise, nothin's happening!

It turns out that while it takes two to tango, three's a crowd! Two state systems are unique in their harmonic simplicity. At the end of this unit we will see how to understand more complicated 3, 4, 5, ... level excitations for some simple systems.

### (a) Solving Schrodinger's eigen-equations for $C_6$ system

$\mathbf{H}$ -eigenvalues use  $\mathbf{r}$ -expansion (9.2.6) of  $\mathbf{H}$  and  $C_6$  symmetry  $\mathbf{r}^p$ -eigenvalues from (8.2.9).

$$\langle k_m | \mathbf{r}^p | k_m \rangle = e^{-ipk_m a} = e^{-ipm2\pi/N} \quad \text{where: } k_m = m(2\pi/Na)$$

$$\begin{aligned} \langle k_m | \mathbf{H} | k_m \rangle &= H \langle k_m | \mathbf{1} | k_m \rangle + S \langle k_m | \mathbf{r} | k_m \rangle + T \langle k_m | \mathbf{r}^2 | k_m \rangle + U \langle k_m | \mathbf{r}^3 | k_m \rangle + T^* \langle k_m | \mathbf{r}^4 | k_m \rangle + S^* \langle k_m | \mathbf{r}^5 | k_m \rangle \\ &= H + S e^{-ik_m a} + T e^{-i2k_m a} + U e^{-i3k_m a} + T^* e^{i2k_m a} + S^* e^{ik_m a} \end{aligned} \quad (9.3.5a)$$

Again we check that  $\mathbf{H}$  eigenvectors  $|\omega_m\rangle$  are the  $|k_m\rangle$  in (8.2.11) which solved transfer matrix  $\mathbf{T}$ .

$$\begin{pmatrix} H & S^* & T^* & U & T & S \\ S & H & S^* & T^* & U & T \\ T & S & H & S^* & T^* & U \\ U & T & S & H & S^* & T^* \\ T^* & U & T & S & H & S^* \\ S^* & T^* & U & T & S & H \end{pmatrix} \cdot \begin{pmatrix} 1 \\ e^{ik_m a} \\ e^{i2k_m a} \\ e^{i3k_m a} \\ e^{-i2k_m a} \\ e^{-ik_m a} \end{pmatrix} = \hbar\omega_m \begin{pmatrix} 1 \\ e^{ik_m a} \\ e^{i2k_m a} \\ e^{i3k_m a} \\ e^{-i2k_m a} \\ e^{-ik_m a} \end{pmatrix} \quad (9.3.5b)$$

Because of Hermiticity ( $\mathbf{H}^\dagger = \mathbf{H}$ ) eigenvalues  $\omega_m$  or  $\varepsilon_m$  will be real eigenfrequency and energy spectra.

$$\hbar\omega_m = \varepsilon_m = H + S e^{-ik_m a} + T e^{-i2k_m a} + U e^{-i3k_m a} + T^* e^{i2k_m a} + S^* e^{ik_m a} \quad (9.3.5c)$$

$$\hbar\omega_m = \varepsilon_m = H + 2|S| \cos(k_m a - \sigma) + 2|T| \cos(2k_m a - \tau) - U (-1)^m \quad (9.3.5d)$$

Here we note:  $e^{-i3k_m a} = e^{-i3\pi m} = (-1)^m$  for  $N=6$ . Also, let the complex parameters be in polar form.

$$S = |S| e^{i\sigma}, \quad T = |T| e^{i\tau} \quad (9.3.5e)$$

Their phase angles  $\sigma$  and  $\tau$  correspond to what is sometimes called a *gauge symmetry breaking* or *Zeeman splitting* parameters. To begin the discussion, we shall let the phase angles be zero or pi.

A little physical intuition helps to make some sense of the energy eigenvalues. The parameters  $S$ ,  $T$ , and  $U$  are called *tunneling amplitudes* because they are "sneak factors" that tell how rapidly (and with what phase  $\sigma$ ,  $\tilde{\tau}$ ) an evanescent wave in one channel can sneak or tunnel over to one of its neighbors as indicated in Fig. 9.2.1. The  $S$ ,  $T$ ,  $U$  give *rates* at which the  $A$ ,  $B$ ,  $C$  amplitudes of a  $\mathbf{T}$  or  $\mathbf{U}$  matrix grow.

### (b) Energy spectrum and tunneling rates

We saw how the evanescent waves in (6.3.10a) of Sec. 6.3c(3) decay exponentially and die off with distance. Channel waves are like this, a channel wave state  $|0\rangle$  will be exponentially more likely to tunnel to its nearest neighbor channels  $|1\rangle$  or  $|5\rangle$  than to more distant channels  $|2\rangle$ ,  $|3\rangle$ , or  $|4\rangle$  in Fig. 9.2.1. So, the distant tunneling amplitudes  $U$  and  $T$  might be approximated by zero in (9.3.5d) to give

$$\hbar\omega_m = \varepsilon_m = H + 2|S| \cos(k_m a - \sigma). \quad (9.3.5f)$$

This is an elementary *Bloch dispersion relation*. If wavevector  $k_m$  were a continuous variable  $k$  the dispersion function  $\omega(k)$  would trace a cosine as shown in Fig. 9.3.1 where the gauge phase is set to pi ( $\sigma=\pi$ ) to make the  $k_0$  state lowest. Now the spectra correspond to hexagonal projections of  $e^{i2\pi m/6}$ .

$$\hbar\omega_m = \varepsilon_m = H - 2|S| \cos(k_m a). \quad (\sigma=\pi) \quad (9.3.5g)$$

Note that while the eigenvalues ( $\hbar\omega_m = \varepsilon_m$ ) vary with parameters  $H$ ,  $S$ ,  $T$ , or  $U$ , the eigenvectors  $|\omega_m\rangle$  or eigenfunctions  $\psi_m(x_p)$  are the same for all values of parameters due to  $C_N$ -symmetry.

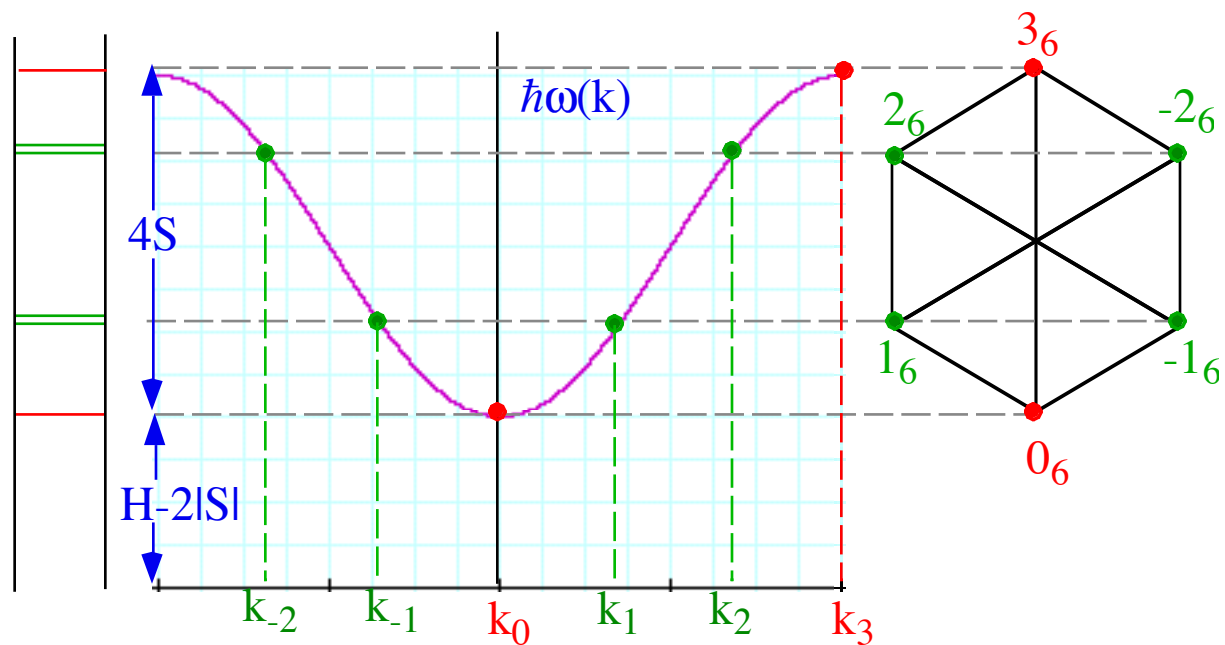


Fig. 9.3.1 Generic 6-channel ( $C_6$ ) tunneling spectra and Bloch dispersion.

If the tunneling phase  $\sigma$  increases by  $\pi/12$  it shifts the dispersion relation to the right by  $\pi/12$  in  $k$ -space. It rotates the hexagonal spectral diagram by  $\pi/12$  or  $15^\circ$  as shown in Fig. 9.3.2. The resulting spectra shifts and splits the degenerate doublets  $\pm 1_6$  and  $\pm 2_6$ .

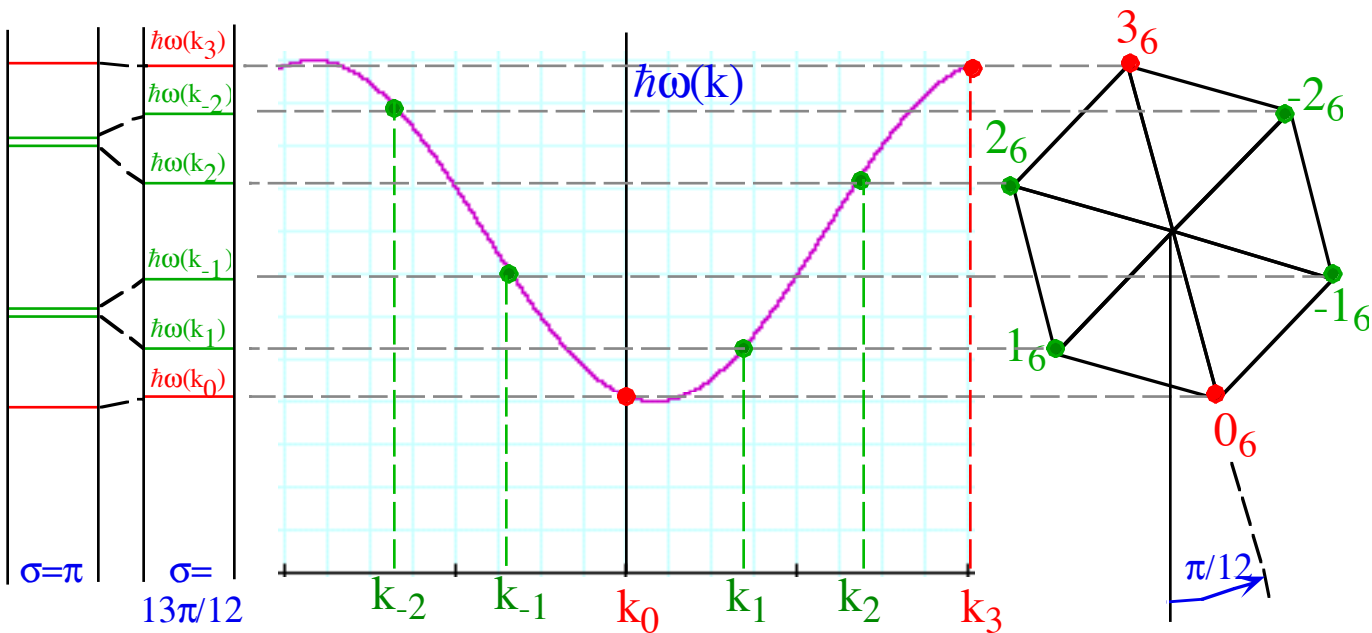


Fig.9.3.2 Same 6-channel ( $C_6$ ) tunneling spectra with broken symmetry and doublet splitting

This is equivalent to rotating the analyzer disk in Fig. 8.1.1 at a constant negative or clockwise velocity so negatively moving waves increase in energy while the positively moving ones have less energy.

Such a tunneling phase or gauge factor causes a *right-left symmetry breaking* so right-handed and left-handed waves are no longer degenerate in energy. It is analogous to the Doppler shift that is observed by an observer moving through a monochromatic standing wave and sees red-shifted and blue-shifted frequencies while the stationary observer sees equal frequencies. (Recall Sec. 4.2.)

A similar effect occurs if a magnetic field is applied perpendicular to the plane of the analyzer along a beam of charged particles. Then the splitting of doublets is called *Zeeman splitting* which is a very well known atomic spectral effect that will be studied later.

Bloch's waves vs. Bohr's

One should compare the discrete Bloch spectra and dispersion in Fig. 9.3.1 here to the simple Bohr spectra in Fig. 7.1.1. The orbital wavefunctions for both have a plane-wave form of "Bohr's ghost" waves.

$$\Psi_m(x) = e^{ik_m x} \quad (9.3.6a)$$

However, Bloch waves for  $C_6$  are discretized into  $N=6$  phasors at discrete points  $x_p$ . ( $p=1, 2, \dots, 6$ )

$$\Psi_m(x_p) = e^{ik_m x_p} = e^{i2\pi m p/N} \quad (9.3.6b)$$

Each Bloch quantum number  $m=0, 1, 2, \dots, 5$ , is a number *m-modulo-6* as in (7.3.7) and in Fig. 7.3.3.

Bloch eigenvalues, however, differ from Bohr's. Bohr orbital dispersion or energy is a simple parabola (7.1.16) as follows using momentum quantization  $p_m = \hbar k_m = \hbar 2\pi m/L$  with:  $m=0, \pm 1, \pm 2, \dots$

$$E_m = (\hbar k_m)^2 / 2M = m^2 [h^2 / 2ML^2] \quad (9.3.7)$$

This parabola is a low-energy approximation to the relativistic hyperbola in Fig. 5.2.1. In contrast, the Bloch curve is a flipped cosine function (9.3.5g) as plotted in Fig. 9.3.3 and superimposed upon the Bohr parabola. For larger  $N$  (Fig. 9.3.3 it is  $N=24$ ) and small  $m$  the cosine curve is approximated by a Bloch-like parabola given by a Taylor expansion at the origin ( $k=0=k_0$ ) in  $k$ -space.

$$\hbar\omega_m = E_m = H - 2|S| \cos(k_m a) = H - 2|S| + |S|(k_m a)^2 + \dots \quad (9.3.8)$$

In this limit the Bloch dispersion is approximated by the simple Bohr parabola.

In the limit of large number  $N$  of "quantum dot" coordinates  $x_p$ . ( $p=1, 2, 3, 4, \dots, N$ ) the continuum coordinate  $x$  of the Bohr orbitals is approached. As long as the waves considered have low  $k_m$ , that is, are long compared to the lattice interval  $a=L/N$  that divides up the Bohr coordinate range  $L$ , then Bohr and Bloch waves have nearly the same dispersion  $\omega_m(k_m)$  and will behave the same.

### (c) Brillouin's boundary

For larger wavevector  $k_m$  the wavelength becomes shorter until its waves begin to "fall through the cracks" in the lattice. Recall the difficulty in following the "Bohr's ghost" wave through the  $C_6$  phasors in Fig. 7.3.3 for the higher waves  $(m)_N = (4)_6$  or  $(5)_6$ , or even  $(2)_6$ . A break occurs when a half-wave length matches the lattice spacing  $a$ . This is when  $(m)_N = (N/2)_N = (3)_6$ , a "half-way point" known as the *first Brillouin zone boundary (BZB-1)*. It is at  $k_{12}$  or  $(m)_N = (12)_{24}$  in Fig. 9.3.3 ( $N=24$ ).

$$(m)_{BZB-1} = (N/2) \quad \text{or:} \quad k_{BZB-1} = \pi/a \quad \text{or:} \quad \lambda_{BZB-1} = 2a \quad (9.3.9a)$$

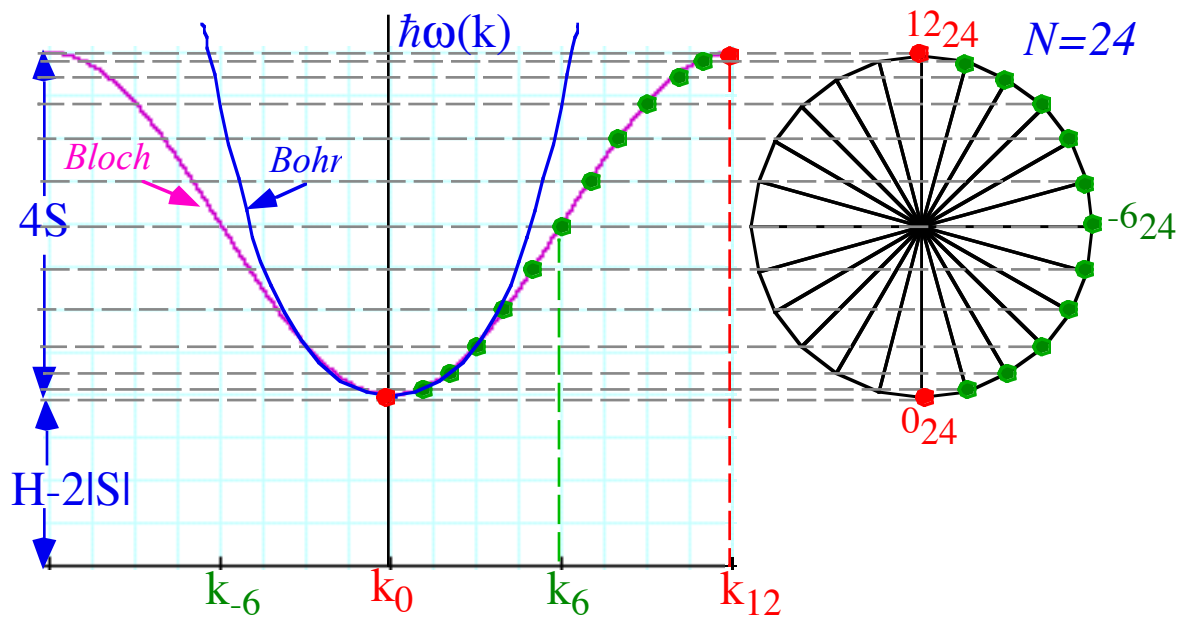


Fig.9.3.3 Generic 24-channel ( $C_{24}$ ) tunneling spectra and Bohr vs. Bloch dispersion.

At this  $m$ -number or  $k$ -value the wave amplitudes are alternating  $\pm 1$  at the lattice points  $x_p$ .

$$\Psi_{N/2}(x_p) = e^{ikN/2x_p} = e^{i2\pi(N/2)p/N} = e^{i\pi p} = (-1)^p \tag{9.3.9b}$$

Phases that are in or  $\pi$ -out of phase make a standing wave with zero group velocity as in Fig. 9.3.4.

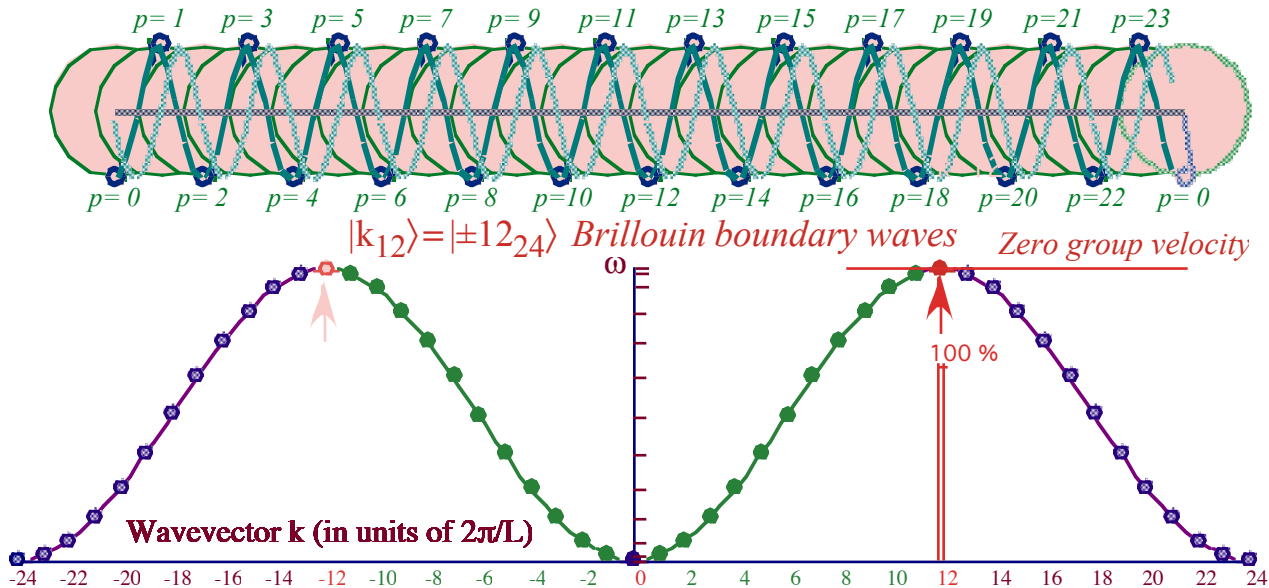


Fig.9.3.4 ( $C_{24}$ ) Brillouin boundary wave must be standing. (No group velocity)

Positive or negative ( $k=\pm 12$ ) waves have the same effect on the 24 lattice points; both give standing wave motion with no transmission one way or the other. In  $C_{24}$  symmetry  $+12 \text{ mod } 24 = -12 \text{ mod } 24$ .

The wave group velocity is the velocity  $V_{group}$  associated with classical particle or "message" velocity. (Recall discussions in Sec. 4.4 (b-c).) From (9.3.8) the  $V_{group}$  for Bloch (or for low- $k$  Bohr) is

$$V_{group} = \frac{d\omega_m}{dk_m} = 2 \frac{|S|}{\hbar} a \sin(k_m a) \left( \cong 2 \frac{|S|}{\hbar} k_m a^2, \text{ for: } k_m \ll \pi / a \right) \quad (9.3.10)$$

The group velocity goes to zero at the origin ( $k_m=0$ ) and at the Brillouin zone boundary ( $k_m=k_{BZB}$ ). This is consistent with our picture Fig. 9.3.4 of a standing wave. It just goes nowhere but up and down.

#### Effective mass: Another quantum view of inertia

Low velocity ( $u \ll c$ ) particle momentum is mass times particle velocity:  $Mu = MV_{group}$ . DeBroglie relation (5.2.5c) gives momentum as  $\hbar k_m$ . For low- $k_m$ -Bloch waves (Bohr waves), (9.3.10) gives  $V_{group}$  proportional to the tunneling amplitude  $S$  implying an *effective mass*  $M_{eff}$  inversely proportional to  $S$ .

$$M_{eff}(0) = \hbar^2 / (2|S| a^2) \quad (9.3.11a)$$

This is consistent with a comparison of Bohr energy values  $\epsilon_m = 1/2(\hbar k_m)^2/M$  and the low- $k_m$  Bloch energy eigenvalues (9.3.8). Recall the quantum effective mass introduced in (5.3.13) and repeated here.

$$M_{eff} = \frac{F}{a} = \frac{\hbar \dot{k}}{\left( \frac{dV_{group}}{dt} \right)} = \frac{\hbar \dot{k}}{\left( \frac{dV_{group}}{dk} \frac{dk}{dt} \right)} = \frac{\hbar}{\left( \frac{d^2\omega}{dk^2} \right)} \quad \text{where: } V_{group} = \frac{d\omega}{dk} \quad (9.3.11b)$$

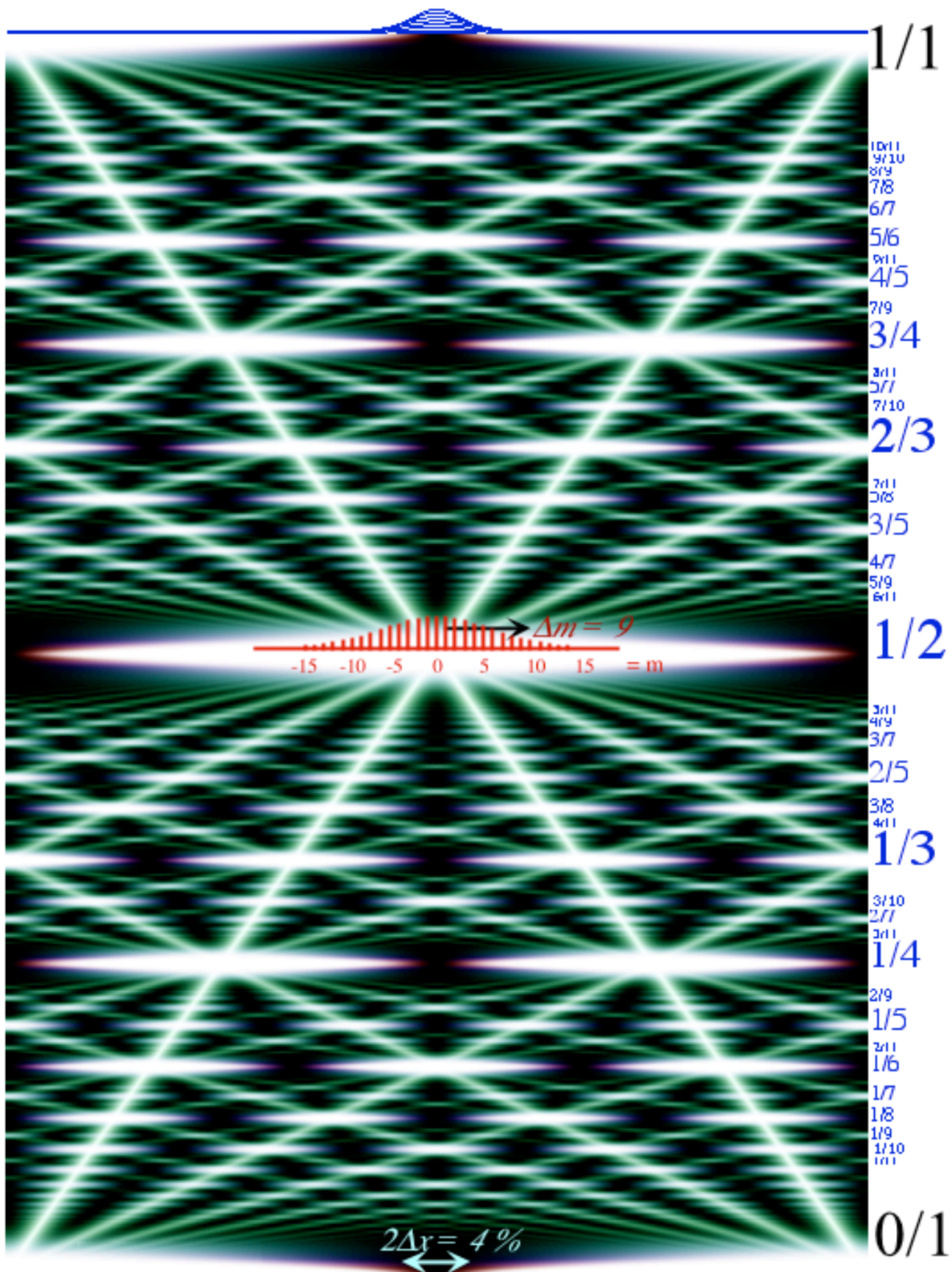
Effective mass is inversely proportional to the curvature of the dispersion relation. As  $k_m$  increases in Fig. 9.3.3 the effective mass starts out at  $k=0$  with the  $M_{eff}(0)$  value (9.3.11a). Then it increases until it goes to infinity at  $k_m = k_{N/4} = k_6$ . Then it comes back from negative infinity losing much of its negativity to end up at  $(M_{eff}(k_{12}) = -M_{eff}(0))$  on the Brillouin zone boundary  $k_m = k_{N/2} = k_{12}$ . There  $\omega_{Bloch}(k)$  is a downward curving dispersion like Dirac negative-energy anti-particle band in the lower half of Fig. 5.4.1. But,  $\omega_{Bloch}(k)$  in Fig. 9.3.3 differs from a continuum relativistic dispersion relation (5.2.8)

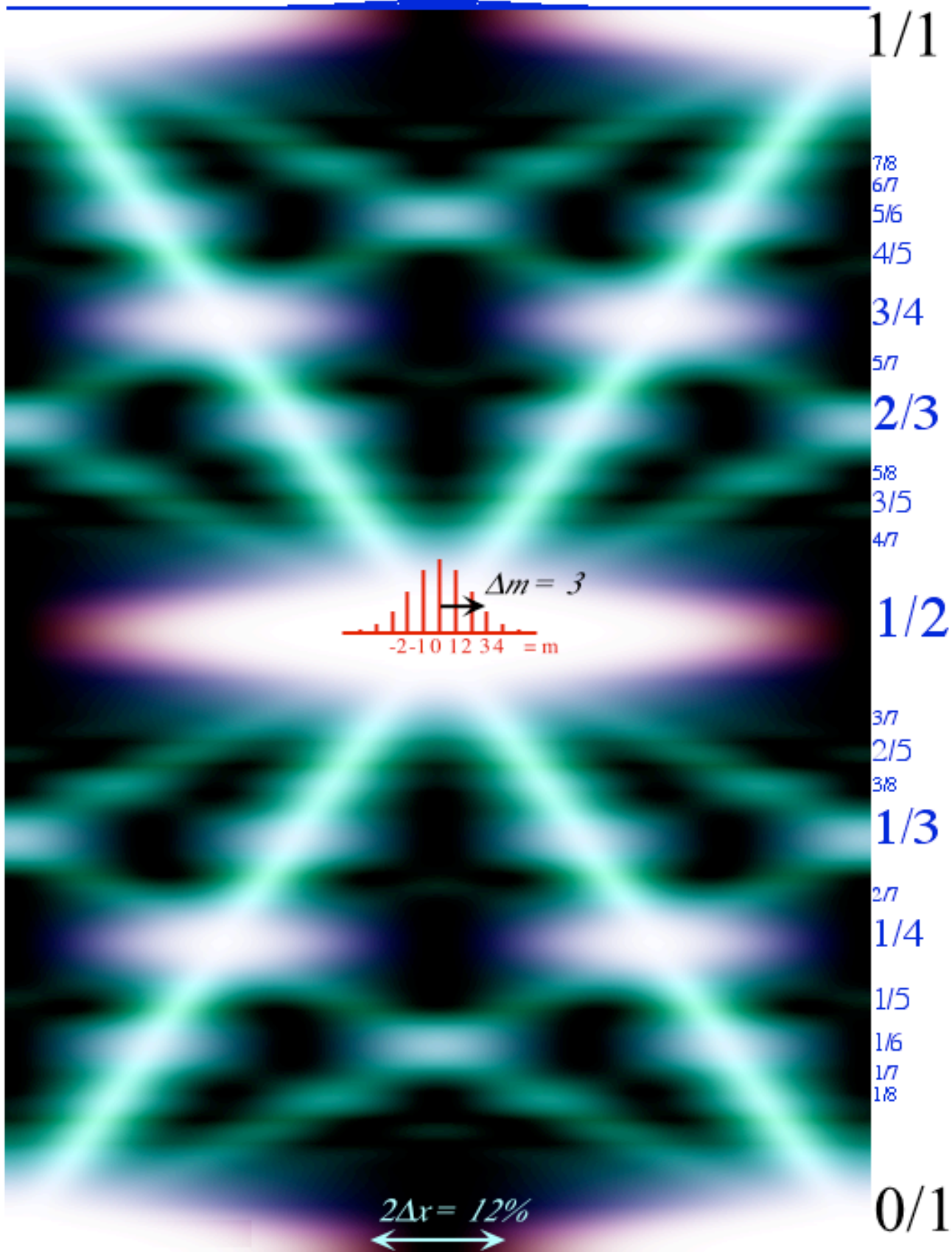
$$E = \hbar \omega_{relativistic} = \pm \sqrt{(Mc^2)^2 + (c\hbar k)^2} \quad (5.2.8)_{repeated}$$

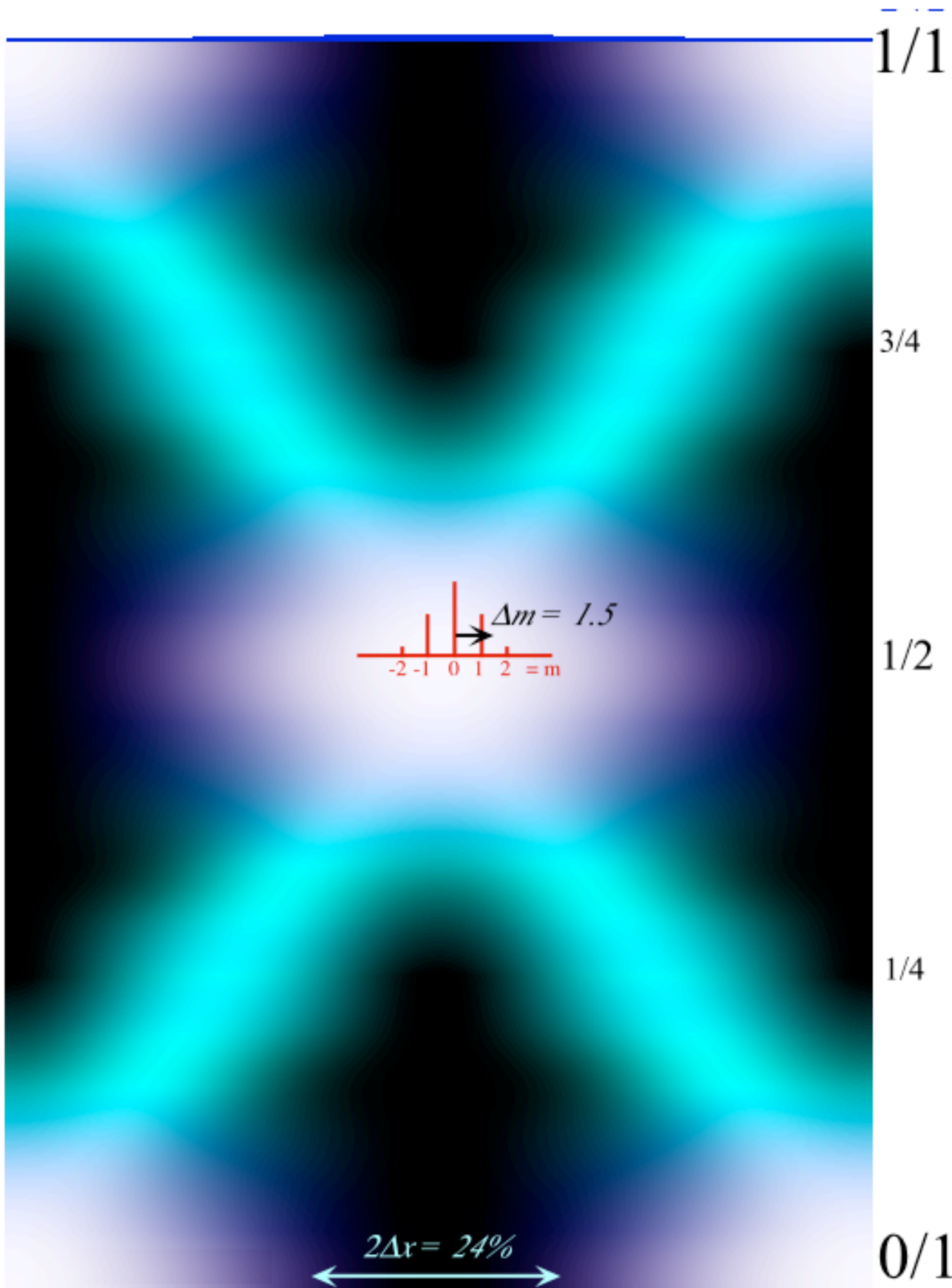
For  $\omega_{rela.}(k)$  effective mass approaches infinity only as the momentum or  $k$  becomes large. For a vacuum, a constant applied electric field would cause  $k$  to increase uniformly. But, for a  $C_N$  lattice  $k$ -space is periodic so a field causes a charged particle to just oscillate back and forth each time  $k$  passes through another Brillouin zone. Based on this, relativistic symmetry appears quite different from that of a Bloch lattice. But then, have we really looked closely enough at that vacuum continuum? It may take some pretty high  $k$ -values to do so!

The final sections of this unit are devoted to dynamics of Bohr waves shown in space-time plots of the following Fig. 9.3.5-6. Recall also Fig. 5.5.5-6. The interference anti-nodes that spring up and then vanish are called *revivals*, a term coined by Joe Eberly to describe atom-laser simulations he noticed around 1976. Much of the intricate structure are called *fractional revivals* first noticed in molecular rotor simulations around 1980. Much of the first analyses of fractional revivals, done during the 1990's, involves particle-in-a-box and atomic Rydberg states. However, Bohr orbitals provide the clearest understanding of revivals because of their underlying  $C_N$  symmetry.

(Next pages: Figs. 9.3.5a-c)







(Preceding pages: Figs. 9.3.5a-c Bohr wavepacket revivals in space-time)

### (d) Bohr wavepacket dynamics: Uncertainty and revival

We now study Bohr waves that are a Gaussian combination of momentum- $m$  plane waves.

$$\Psi(\phi, 0) = \langle \phi, 0 | \Psi \rangle = \frac{1}{2\pi} \sum_{m=-\infty}^{\infty} e^{-m^2/\Delta m^2} e^{im\phi} \quad (9.3.12a)$$

Here,  $m=0, \pm 1, \pm 2, \pm 3, \dots$  are momentum quantum numbers in Bohr energy formula (9.3.7).

$$E_m = (\hbar k_m)^2/2M = m^2 [h^2/2ML^2] = m^2 \hbar \omega_I = m^2 \hbar \omega_1 \quad (9.3.12b)$$

The *fundamental Bohr frequency*  $\omega_I = 2\pi \nu_I$  is the lowest *transition (beat) frequency*  $\nu_I = (E_I - E_0)/h$ .

Completing the square of the exponent provides a simpler  $\phi$ -angle wavefunction.

$$\Psi(\phi, 0) = \frac{1}{2\pi} \sum_{m=-\infty}^{\infty} e^{-\left(\frac{m}{\Delta m} - i\frac{\Delta m}{2}\phi\right)^2 - \left(\frac{\Delta m}{2}\phi\right)^2} = \frac{A(\Delta m, \phi)}{2\pi} e^{-\left(\frac{\Delta m}{2}\phi\right)^2} \quad (9.3.13a)$$

Only the lower- $m$  terms with  $m < \Delta m$  in the sum  $A(\Delta m, \phi)$  have significant  $e^{-(m/\Delta m)^2}$  values, but for larger  $\Delta m$  the number of significant terms grows until sum  $A$  approaches a Gaussian integral independent of  $\phi$ .

$$A(\Delta m, \phi) = \sum_{m=-\infty}^{\infty} e^{-\left(\frac{m}{\Delta m} - i\frac{\Delta m}{2}\phi\right)^2} \xrightarrow{\Delta m \gg 1} \int_{-\infty}^{\infty} dk e^{-\left(\frac{k}{\Delta m}\right)^2} = \sqrt{\pi} \Delta m \quad (9.3.13b)$$

The variable factor  $e^{-(\Delta m \phi/2)^2}$  is a Gaussian function of angle  $\phi$  or position  $x$ . It is remarkable that the Fourier transform of a Gaussian  $e^{-(m/\Delta m)^2}$  momentum distribution is a Gaussian  $e^{-(\phi/\Delta \phi)^2}$  in coordinate  $\phi$ .

$$\langle m | \Psi \rangle = e^{-(m/\Delta m)^2} \quad \text{implies:} \quad \langle \phi | \Psi \rangle = e^{-(\phi/\Delta \phi)^2} \quad (9.3.14)$$

The relation between *momentum uncertainty*  $\Delta m$  and *coordinate uncertainty*  $\Delta \phi$  is a *Heisenberg relation*.

$$\Delta m/2 = 1/\Delta \phi, \text{ or:} \quad \Delta m \Delta \phi = 2 \quad (9.3.15)$$

A Gaussian is an eigenvector of the Fourier  $C_n$  transformation matrix. (More about this later.)

Three space-time plots are given in Fig. 9.3.5a, b, and c, respectively, with decreasing momentum half-width  $\Delta m=9, 3, \text{ and } 1.5$  and coarser spatial resolution  $\Delta \phi/2\pi=2\%, 6\%, \text{ and } 12\%$ . Each is plotted for a full time period  $\tau_I = 1/\nu_I = 2\pi/\omega_I$  after which it repeats. The first Fig. 9.3.5a uses fine spatial resolution  $\Delta x=0.02$  which requires 9-quantum excitation ( $\Delta m=9$ ). It shows a labyrinth of increasingly fine self-similar X-patterns of wave *revivals*. In the second and third figures (9.3.5b and c), of lower excitation ( $\Delta m=3, \text{ and } 1.5$ , respectively), the finer X-patterns begin to disappear leaving one big X over Fig. 9.3.5c.

*Semi-classical Theory: Farey Sums and Quantum Speed Limits*

Fig. 9.3.5c provides a clue to the theory of revivals. Its X is like a zero crossing in the Lorentz grid in Fig. 4.2.9, but with momentum values restricted by  $\Delta m=1.5$  to the first two levels  $m=0, \pm 1$ , leaving two group (or phase) velocities  $V_{\pm 1} = \pm L/\tau_I$  by (4.2.20), that is, a Bohr length  $L$  per Bohr time unit  $\tau_I$ .

$$V_{\text{group}}^{Bohr}(m \leftrightarrow n) = \frac{\omega_m - \omega_n}{k_m - k_n} = \frac{(m^2 - n^2) \hbar \nu_1}{(m - n) h / L} = (m + n) \frac{L}{\tau_I} = (m + n) V_1 \quad (9.3.16)$$

The X in Fig. 9.3.5c has two zeros doing one lap in opposite directions around the Bohr ring in a Bohr period  $\tau_I$ . The packet anti-nodes or "particles" do laps, too, but their paths are not as contiguous.

Fig. 4

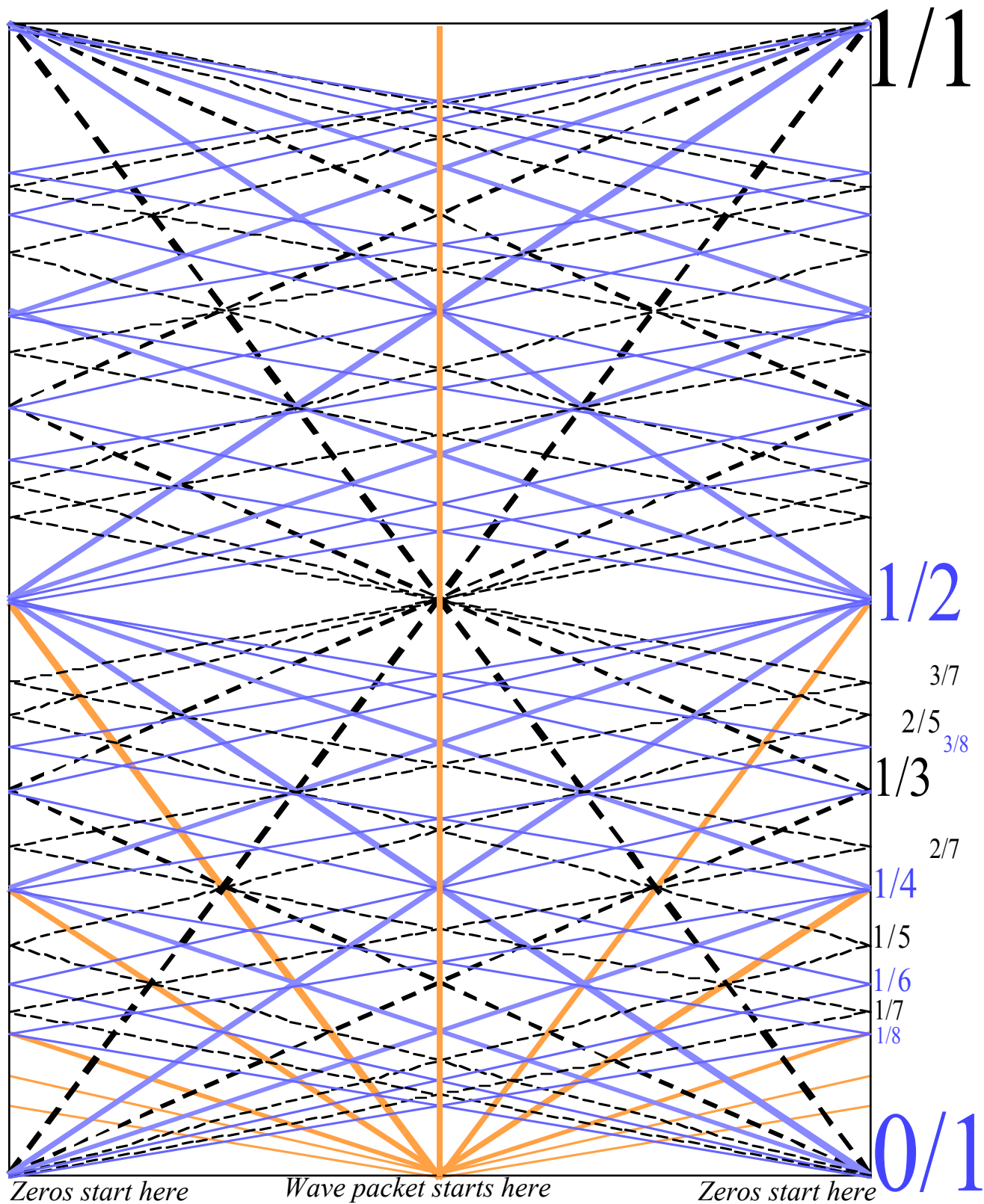


Fig. 9.3.6 Intersecting wave space-time X-path trajectories of nodes and anti-nodes.

(Anti-nodal revival peaks and phases are discussed later.)  $|\Psi\rangle$ -nodes, being virtually dead, have an indestructibility not had by zeros of  $Re\Psi$  that annihilate and re-create as they gallop through Fig. 4.2.9.

Relaxing the momentum uncertainty  $\Delta m$  allows more  $m$ -values and wave velocities:  $\pm V_1, \pm 2V_1, \pm 3V_1, \dots$  ranging up to  $2\Delta m V_1$ . By (9.3.16) the maximum lap rate or *quantum speed limit* is  $2\Delta m$ , i.e., twice the maximum  $|m|$ . Each velocity gives a fractional lap time of  $1/1, 1/2, 1/3, \dots, 1/(2\Delta m)$  of the Bohr period. Such fractions are written in the margin of Fig. 9.3.5 at the point where a lap trajectory passes the point  $\phi = \pm\pi$  opposite the origin  $\phi = 0$  of the wave packet. An  $n$ -th multiple  $n/D$  of an allowed fraction  $1/D$  corresponds to the  $n$ -th lap of a wave node ("zero") if  $D$  is odd or the  $n$ -th lap of a wave anti-node ("particle") if  $D$  is even.

The  $n/D$  fractional lines in Fig. 9.3.6 highlight the wave paths in Fig. 9.3.5a. As excitation  $\Delta m$  increases, even- $D$  "particle" paths show up as dark shadows in between the odd- $D$  "zero" paths in Fig. 9.3.5a. Also seen in a high- $\Delta m$  plot (Fig. 9.3.5a) are "particle" paths with odd *and* even fractional slopes emanating from the origin  $\phi = 0$  of the wave packet. This is indicated in Fig. 9.3.6, too.

The geometry of generic group velocity rays is sketched in Fig. 9.3.7 using two rays to form an asymmetric X around an intersection. (A symmetric X has equal group speeds  $d_1$  and  $d_2$ .) Fig. 9.3.5a is a patchwork of self-similar X patterns of nodal (*odd- $d_k$* ) or anti-nodal (*even- $d_k$* ) rays. The equations for the two lines in Fig. 9.3.6 are

$$\phi = -d_1 t + n_1 + 1/2 \qquad \phi = d_2 t - n_2 + 1/2 \qquad (9.3.17)$$

Subtracting the first  $\phi$  equation from the second gives the intersection time for the center of the X.

$$t_{12\text{-intersection}} = \frac{n_2 + n_1}{d_2 + d_1} = \frac{n_2}{d_2} \oplus_F \frac{n_1}{d_1} \qquad (9.3.18)$$

The resulting combination is called a *Farey Sum*  $\oplus_F$  of the rational fractions  $n_1/d_1$  and  $n_2/d_2$  after John Farey, an 1800's geologist.

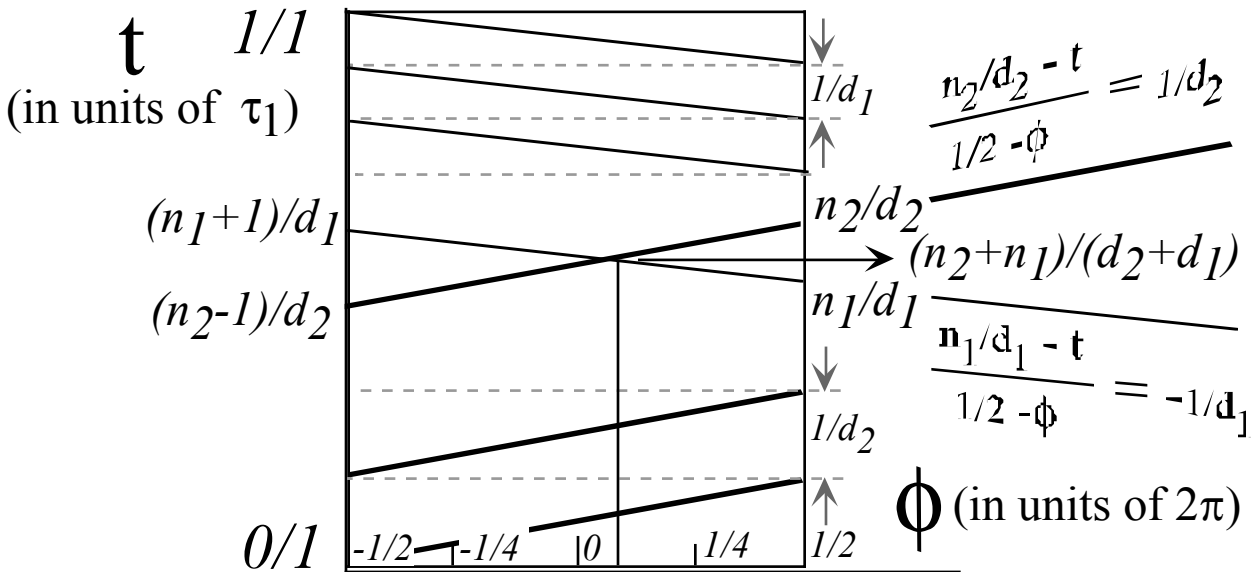


Fig. 9.3.7 Farey-sum geometry and algebra of intersecting wave space-time trajectories.

The Farey sum has been used to analyze classically "chaotic" or "fractal" structures , but its use in organizing quantum resonance structure is new. It begins with a fundamental Farey sum relating the beginning fraction (0/1) and ending fraction (1/1) of the (0↔1)-quantum beat or fundamental revival.

$$\frac{0}{1} \oplus_F \frac{1}{1} = \frac{1}{2} \tag{9.3.19}$$

This is the instant  $t/\tau_I=1/2$  for a half-time revival and the zero at the center of the fundamental X in Fig. 9.3.5c. The fundamental sum makes up the second row of a *Farey Tree* of such sums shown in (9.3.20). The sums in the *D*-th row of a Farey tree are an ordered set of all reduced fractions with denominator equal to *D* or less. The tree need not go beyond  $D>2\Delta m$  where denominator *D* exceeds the wave quantum speed limit  $2\Delta m$  of (9.3.16). Finer revivals will be unresolvable. More energy is needed to see finer X's.

$D \leq 1$	$\frac{0}{1}$																			$\frac{1}{1}$																									
$D \leq 2$	$\frac{0}{1}$																			$\frac{1}{2}$	$\frac{1}{1}$																								
$D \leq 3$	$\frac{0}{1}$																			$\frac{1}{3}$	$\frac{1}{2}$	$\frac{2}{3}$	$\frac{1}{1}$																						
$D \leq 4$	$\frac{0}{1}$																				$\frac{1}{4}$	$\frac{1}{3}$	$\frac{1}{2}$	$\frac{2}{3}$	$\frac{3}{4}$	$\frac{1}{1}$																			
$D \leq 5$	$\frac{0}{1}$																					$\frac{1}{5}$	$\frac{1}{4}$	$\frac{1}{3}$	$\frac{2}{5}$	$\frac{1}{2}$	$\frac{3}{5}$	$\frac{2}{3}$	$\frac{3}{4}$	$\frac{4}{5}$	$\frac{1}{1}$														
$D \leq 6$	$\frac{0}{1}$																						$\frac{1}{6}$	$\frac{1}{5}$	$\frac{1}{4}$	$\frac{1}{3}$	$\frac{2}{5}$	$\frac{1}{2}$	$\frac{3}{5}$	$\frac{2}{3}$	$\frac{3}{4}$	$\frac{4}{5}$	$\frac{5}{6}$	$\frac{1}{1}$											
$D \leq 7$	$\frac{0}{1}$																							$\frac{1}{7}$	$\frac{1}{6}$	$\frac{1}{5}$	$\frac{1}{4}$	$\frac{2}{7}$	$\frac{1}{3}$	$\frac{2}{5}$	$\frac{3}{7}$	$\frac{1}{2}$	$\frac{4}{7}$	$\frac{3}{5}$	$\frac{2}{3}$	$\frac{5}{7}$	$\frac{3}{4}$	$\frac{4}{5}$	$\frac{6}{7}$	$\frac{1}{1}$					
$D \leq 8$	$\frac{0}{1}$																								$\frac{1}{8}$	$\frac{1}{7}$	$\frac{1}{6}$	$\frac{1}{5}$	$\frac{1}{4}$	$\frac{2}{7}$	$\frac{1}{3}$	$\frac{3}{8}$	$\frac{2}{5}$	$\frac{3}{7}$	$\frac{1}{2}$	$\frac{4}{7}$	$\frac{3}{5}$	$\frac{5}{8}$	$\frac{2}{3}$	$\frac{5}{7}$	$\frac{3}{4}$	$\frac{4}{5}$	$\frac{6}{7}$	$\frac{7}{8}$	$\frac{1}{1}$

(9.3.20)

The tracking of crests or wave peaks yields information about classical particle-like or group-wave motion. It is comforting to see familiar classical paths in what is often bewildering quantum cacophony but, the clearest X-paths in Fig. 9.3.5a are *zeros* emanating from the point  $\phi=\pm\pi$  where the particle packet originally was *not*. Quantum wave dynamics differs from classical dynamics is that multiple Fourier components easily interfere much of a wave to death. Most path phases lead to *non*-existence except near (rare) stationary-phase paths that may be familiar classical ones. This is what is responsible for particle localization that allows us to enjoy a Newtonian world and largely conceals its quantum wave nature from us. Where the wave is *not* provides important quantum clues. One recalls Sherlock Holmes' revelation that it is the "dog that did *not* bark" which solved a mystery.

## 9.4 Homo-cyclic $C_N$ Revivals

Wave phase is key to the  $C_N$  dynamics beginning with the “beats” of two-state  $C_2$  system. As we have said, “It takes two to tango.” First we review the two-state-system dynamics with analogies to optical polarization from Chapter 1 and coupled pendulum dynamics. (Later chapters will use this analogy.)  $C_2$  holds the first key to analyzing the revivals introduced in the preceding section.

We have also said, “Three’s a crowd.” The dynamics associated with  $C_3$  systems is discussed after that of  $C_2$  and then that of  $C_4$ ,  $C_5$ ,  $C_6$ , and  $C_{15}$  systems. Each is part of the revival milieu of Fig. 9.3.5.

### (a) Two–state $C_2$ systems: Beats

Motion of anti-nodal revivals for a 2-level excitation such as Fig. 9.3.5c are like beats of coupled pendulums. Fig. 9.4.1a shows *phasor* pictures of 2-cyclic ( $C_2$ ) eigenstates. Phasor “clocks” are phase-space plots of  $Re\Psi$  vs.  $Im\Psi$  for wavefunction  $\Psi(p)$  at each spatial point  $p=0,1$ .  $Re\Psi$  is up,  $Im\Psi$  is to the left, and the area  $\pi|\Psi|^2$  of the phasor is proportional to probability  $|\Psi|^2$  at point  $p$ .

Each eigenstate phasor rotates clockwise at its Bohr eigenfrequency  $\omega_m = m^2\omega_1$ , that is,  $\Psi(t) = e^{-i\omega_m t}\Psi(0)$ . The  $C_2$  eigenstates are labeled *even* ( $0_2$ )= $(+)$  or *odd* ( $1_2$ )= $(-)$  as usual.

$$|+\rangle = (|0_2\rangle + |1_2\rangle) / \sqrt{2} \quad (9.4.1a)$$

$$|-\rangle = (|0_2\rangle - |1_2\rangle) / \sqrt{2} \quad (9.4.1b)$$

$$\text{Bohr eigenfrequency: } \omega_0 = 0 \quad (9.4.2a)$$

$$\text{Bohr eigenfrequency: } \omega_1 \quad (9.4.2b)$$

$|m_2\rangle$  eigenfrequencies  $\omega_m$  are  $\omega_0 = 0$  and  $\omega_1 = h/(2ML^2)$  by (9.3.12b). States  $|m_2\rangle$  are + or – combinations of a local oscillator base state labeled  $|x\rangle = |r^0\rangle$  (localized at spatial point  $p=0$  or  $\phi=0$ ) and a “flipped” base state  $|y\rangle = |r^1\rangle$  (localized at point  $p=1$  or  $\phi=\pi$ ). States  $|+\rangle$  and  $|-\rangle$  are also eigenstates of  $C_2$  “flip” operator  $\mathbf{r}$  defined by  $\mathbf{r}|x\rangle = |y\rangle$  and  $\mathbf{r}|y\rangle = |x\rangle$ , that is,  $\mathbf{r}|+\rangle = +|+\rangle$ , and  $\mathbf{r}|-\rangle = -|-\rangle$ . State  $|+\rangle$  is analogous to  $+45^\circ$  polarization which is the “slow” eigenstate. State  $|-\rangle$  is analogous to the “fast”  $-45^\circ$  optical axis.

An initial 50-50 combination of the  $|+\rangle$  and  $|-\rangle$  eigenstates briefly recovers the  $|x\rangle = |r^0\rangle$  local base

$$|x\rangle = (|+\rangle + |-\rangle) / \sqrt{2} = (|0_2\rangle + |1_2\rangle) / \sqrt{2}, \quad (\text{Time } t=0)$$

lying between  $|+\rangle$  and  $|-\rangle$  in Fig. 9.4.1b. The  $|1_2\rangle$ -eigenstate is faster than the  $|0_2\rangle$ -eigenstate (which does not move at all by (9.4.2a)) The  $|x\rangle$ -state is always a sum of  $0_2$  and  $1_2$  phasors. (Left and right  $0_2$  phasors are at 12 PM in Fig. a while the left  $1_2$  phasor starts at 12 PM and the right  $1_2$  phasor at 6 PM.) After 12 PM the  $1_2$  phasors “tick” but  $0_2$  phasors are stuck at 12PM. Their sum  $|x\rangle$  varies with time.

By  $1/4$  of beat period  $\tau_1$ , the fast  $|1_2\rangle$  clocks are  $90^\circ$  ahead of the stuck  $|0_2\rangle$ . (Clockwise is  $-i$ .)

$$|L\rangle = (|+\rangle - i|-\rangle) / \sqrt{2} = (|0_2\rangle - i|1_2\rangle) / \sqrt{2}. \quad (\text{Time } t=(1/4)\tau_1)$$

The left and right hand  $1_2$  clocks move to 3 PM and 9 PM, respectively, but  $0_2$  clocks are stuck at 12 PM. On the left: 12 PM plus 3 PM is half-size clock at 2:30 PM. On the right: 12 PM plus 9PM is a half-size clock at 10:30 PM. Note two half-phasors at  $-45^\circ$  (2:30 PM) and  $+45^\circ$  (10:30 PM) at  $1/4$ -period. The  $1/4$  period situation is analogous to optical  $1/4$ -wave plates that change  $|x\rangle$ -polarization to left-circular  $|L\rangle$ .

By  $\tau_1/2$  the fast  $1_2$ -clocks go  $180^\circ$  ahead to give the “flipped” local base state of  $y$ -polarization.

$$|y\rangle = (|+\rangle - |-\rangle) / \sqrt{2} = (|0_2\rangle - |1_2\rangle) / \sqrt{2} \quad (\text{Time } t=(1/2)\tau_1)$$

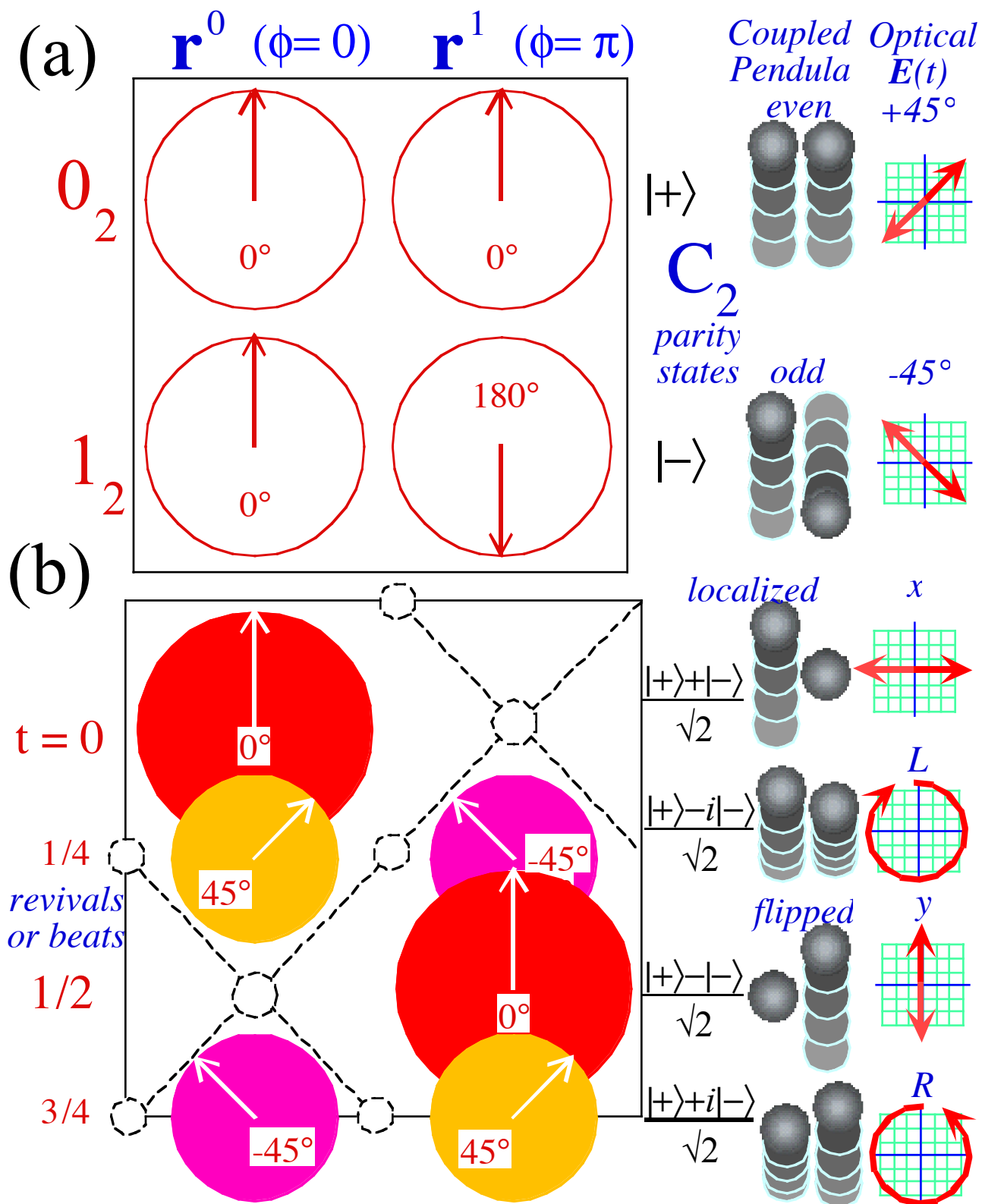


Fig. 9.4.1 (a)  $C_2$  eigenstate phasors. (b) 50% combination states de localizing and reviving.

At  $\tau_1/2$ , the left  $I_2$  clock is at 6 PM the right one at 12 PM, but both  $0_2$  clocks still read 12PM . On the left: 12 PM plus 6 PM is zero (a node). On the right: 12 PM plus 12PM is *big* 12 PM. All the wave flips to the  $|y\rangle$ -state. The  $1/2$ -period situation is like  $1/2$ -wave plate changing  $|x\rangle$ -polarization to  $|y\rangle$ .

Still later at  $(3\tau_1/4)$  the initial  $|x\rangle$ -state has become a right circular state. (Fig. 9.4.1b bottom)

$$|R\rangle = (|+\rangle + i|-\rangle) / \sqrt{2} = (|0_2\rangle + i|1_2\rangle) / \sqrt{2} \quad (\text{Time } t = (3/4)\tau_1)$$

Finally, at full-time  $(1/1)\tau_1$  the initial  $|x\rangle$  state (top of Fig. 9.4.1b) is once again back to being  $|x\rangle$  and would reappear beneath Fig. 9.4.1b to begin repeating the revival sequence.

In Fig. 9.4.1b, dotted lines making an X are drawn around the phasors to connect places where wave amplitude is low like the X-pattern in Fig. 9.3.5c. Low  $m$ -uncertainty ( $\Delta m = 1.5$ ) means the revival wave is mostly a combination of the first two Bohr eigenlevels  $m=0$  and  $|m|=1$  having just two group (or phase) velocities  $+V_1$  and  $-V_1$ . In other words, Fig. 9.3.5c is essentially just a two-state system, and the major half and full revivals are just binary beat of two coupled symmetric pendulums.

The  $1/4$  fractional revival corresponds to *transition state*  $|L\rangle = (|x\rangle - i|y\rangle) / \sqrt{2}$  (analogous to left circular polarization) between the major revivals. In  $|L\rangle$  the left hand position phasor is  $90^\circ$  ahead of the right hand one being resonantly pumped up. The roles of the two phasors are reversed at  $3\tau_1/4$ .

### (b) $C_n$ group structure: $n=3, 4, \dots, 6$ Eigenstates

To understand finer X-zero patterns and fractional revivals between zeros in Fig. 9.3.5 a-b we go beyond the binary  $\{|0_2\rangle|1_2\rangle\}$  basis to, at least, the base-3 basis  $\{|0_3\rangle|1_3\rangle|2_3\rangle\}$  of  $C_3$ . The bra state vectors  $\{\langle 0_3| \langle 1_3| \langle 2_3|\}$  were defined in Fig. 2.6.4 and are re-drawn in Fig. 9.4.2a. The  $C_3$  wave states have quantized momentum  $m=0, 1, \text{ and } 2 \text{ modulo } 3$ . Each  $m$  labels a row of three phasors in Fig. 9.4.2a which are a discrete sampling of the waves in the first three Bohr levels  $m=0, 1, \text{ and } 2$ .

In Fig. 9.4.2b are *4-nary*  $C_4$  base states of  $m=0, 1, 2 \text{ and } 3 \text{ modulo } 4$  quanta and Fig. 9.4.3a reintroduces *5-nary*  $C_5$  bases of  $m=0, 1, 2, 3, \text{ and } 4 \text{ modulo } 5$  quanta, and similarly in Fig. 9.4.3b for  $C_6$ . These systems are like counters; a binary  $C_2$  system can count only to two, that is,  $0$  to  $1$ , but each of the  $C_N$  systems are capable of counting to  $N$ , that is,  $0, 1, 2, 3, \dots, N-1$ .

Physically the  $C_N$  waves are bases of a finite and discrete Fourier analysis. Each  $C_N$  *character table* in Fig. 9.4.2a-b or 9.4.3a-b (if all divided by  $\sqrt{N}$ ) is the  $N$ -by- $N$  unitary ( $U(n)$ ) transformation matrix  $\langle p|m\rangle$  of *discrete Fourier transformation coefficients*. (Recall Fig. 7.3.3 and discussion.)

$$\langle p|(m)_N\rangle = e^{i p m / 2\pi N} / \sqrt{N} = \langle (m)_N | p \rangle^* \quad (p, m = 0, 1, 2, \dots, N-1) \quad (9.4.3a)$$

Each phasor in Fig. 9.4.2-12 sits at one of  $N$  equally spaced lattice points  $p=0, 1, \dots, N-1$ . Each phasor gives for a particular angular point  $p=0, 1, 2, 3, \dots, N-1$  the complex wave amplitude (7.3.10a)

$$\Psi_{\pm m}(2\pi p/N) = \langle p|(m)_N\rangle = \langle (m)_N | p \rangle^*$$

of a continuous running wave that is one of Bohr-Schrodinger eigenfunctions  $\Psi_{\pm m}(\phi)$ .

A real (cosine) part of the eigenfunction is drawn for each eigenstate  $|(m)_N\rangle$  in Fig. 9.4.2-3 to help connect it to the latter. The state notation  $(m)_N$  labels these waves and should be read *m-modulo-N* (or  $m\%N$  in C) meaning

that waves having  $m \pm nN$  wavelengths or quanta will give a physically and mathematically identical state  $(m)_N$ . (They are Fourier *aliases*  $(m)_N = (m \pm nN)_N$ , states differing only by reciprocal lattice vectors  $K = \pm nN$ .)

In Fig. 9.4.2-12 each one of  $N$  equally spaced lattice points  $p=0, 1, 2, 3, \dots, N-1$ , is labeled by a  $p$ -th power  $\mathbf{r}^p$  of a fundamental  $C_N$  group rotation  $\mathbf{r}$  by angle  $2\pi/N$ , that is, by  $\mathbf{r}^0=\mathbf{1}, \mathbf{r}^1, \mathbf{r}^2, \mathbf{r}^3 \dots, \mathbf{r}^{N-1}, \mathbf{r}^N=\mathbf{1}$  respectively. This labeling notation simply lists the operator elements of the cyclic  $C_N$  symmetry group as was done in equations (8.1.5a). The entries  $e^{-ipm/2\pi N}$  are  $m$ -th eigenvalues of  $\mathbf{r}^0, \mathbf{r}^1, \mathbf{r}^2, \dots, \mathbf{r}^p$ .

The phasors are graphical representations of the complex eigenvalues or *characters* of the various cyclic groups. It should be noted that the binary  $C_2$  phasor table (Fig. 9.4.1a) is embedded as a subset in the  $C_4$  table since  $C_2$  is a subgroup of  $C_4$ .  $C_2$  is also seen in the  $C_6$  table (Fig. 9.4.3b) or any  $C_N$  table of even- $N$  since  $C_2$  is a subgroup of all  $C_{2n}$ . The  $C_6$  table also has the  $C_3$  table (Fig. 9.4.2a) embedded. Symmetry embedding is of utmost importance for analyzing group algebra, their representations, and their physical applications. Here it is what gives the revival structure down to the finest observable details of revival wave phase or amplitude shown in Fig. 9.3.5 a.

The same numbers (without the  $\sqrt{N}$ ) serve triple or quadruple duty in algebraic group theory. Besides Fourier transforms they are *irreducible representations*  $D^m(\mathbf{r}^p)$  of  $C_N$

$$D^{(m)}_N(\mathbf{r}^p) = e^{-i \frac{pm}{2\pi N}} \tag{9.4.3b}$$

such that

$$D^m(\mathbf{a}) D^m(\mathbf{b}) = D^m(\mathbf{ab}) .$$

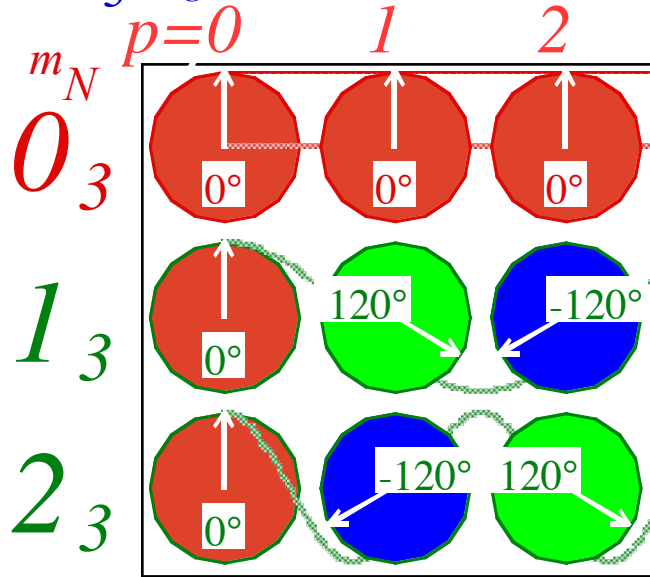
This goes along with the  $D^m(\mathbf{c})$  being eigenvalues of the group operators  $\mathbf{c}=\mathbf{r}^p$ . (Note  $(\mathbf{r}^p)^\dagger = \mathbf{r}^{-p}$ .)

$$\mathbf{r}^p |(m)_N\rangle = D^{(m)}_N(\mathbf{r}^p) |(m)_N\rangle = e^{-i \frac{pm}{2\pi N}} |(m)_N\rangle \tag{9.4.3c}$$

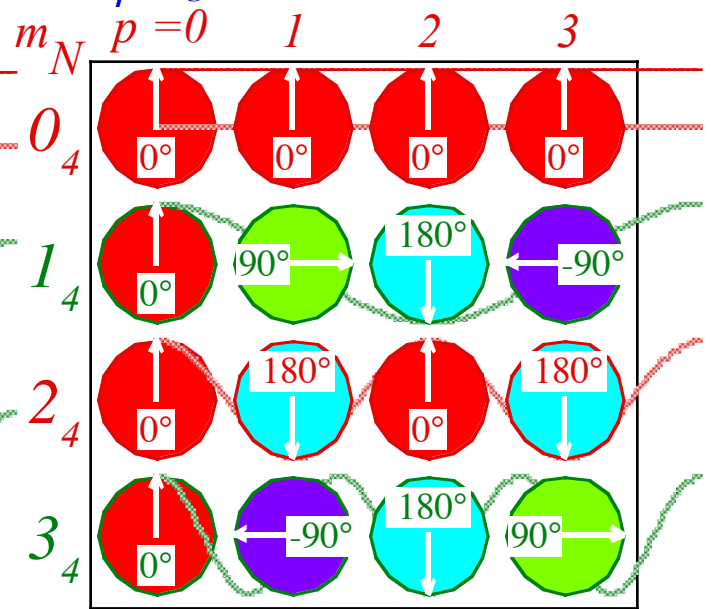
$$\langle (m)_N | \mathbf{r}^p = D^{(m)}_N(\mathbf{r}^p) \langle (m)_N | = e^{-i \frac{pm}{2\pi N}} \langle (m)_N | \tag{9.4.3d}$$

Also, each row of the character table in Fig. 9.4.2-3 is an eigen-bra-vector wavefunction of discrete points  $p$  or powers of  $\mathbf{r}^p$ . As shown in Sec. 9.2, each bra  $\langle (m)_N |$  and ket  $| (m)_N \rangle$  must also be an eigenvector of any Hamiltonian operator  $\mathbf{H}$  that commutes with  $C_N$ , *i.e.*, has  $C_N$  symmetry ( $\mathbf{H}\mathbf{r}^p = \mathbf{r}^p\mathbf{H}$ ). So the character tables serve finally as universal energy eigenvectors and eigenstates, too. All the above apply to the generic  $C_N$  groups and all their embedded subgroups which include all smaller  $C_n$  for which  $n$  is an integral divisor of  $N$ .

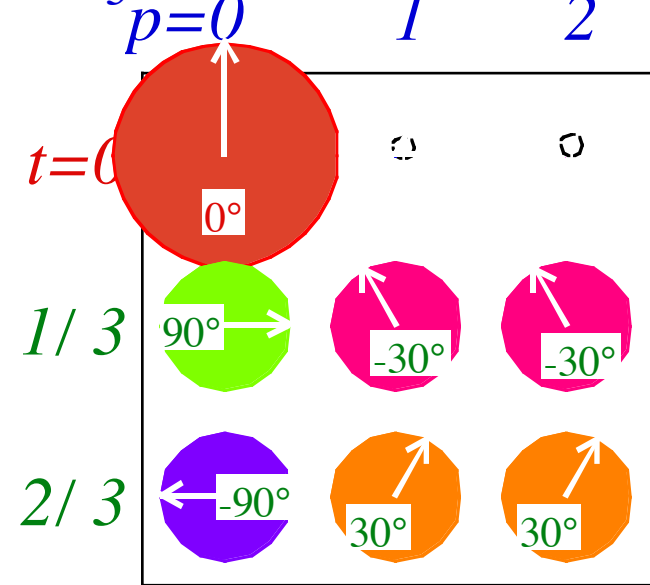
(a)  $C_3$  Eigenstate Characters



(b)  $C_4$  Eigenstate Characters



(c)  $C_3$  Revivals



(d)  $C_4$  Revivals

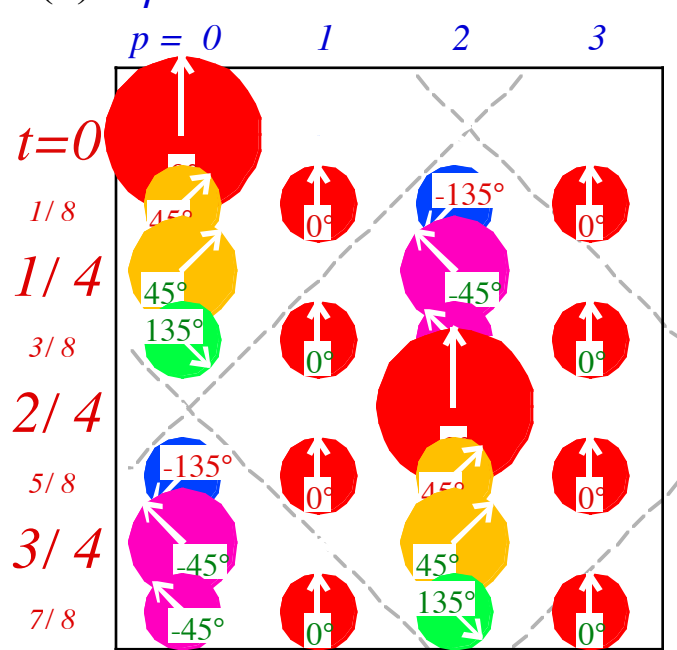


Fig. 9.4.2  $C_3$  and  $C_4$  eigenstates and revivals.

(a) and (b)  $C_3$  and  $C_4$  eigenstate characters.

(c) and (d)  $C_3$  and  $C_4$  revival space time patterns.

(c)  $C_n$  dynamics:  $n=3, 4, \dots, 6$  Fractional Revivals

For each subgroup embedding there is a corresponding embedding of the *revival tables* that are shown in Fig. 9.4.2c-d and 9.4.3c-d. Revival tables are obtained, as in Fig. 9.4.1b, by first summing all the rows of phasors in each character table  $C_3$ ,  $C_4$ ,  $C_5$ , or  $C_6$  of Fig. 9.4.2-3a-b. This localizes the initial wave 100% onto the first phasor position state  $|x_0\rangle$ . Because  $\langle(m)_N|x_0\rangle = 1$  identically, we have

$$|x_0\rangle = \sum_{m=0}^{N-1} |(m)_N\rangle \langle (m)_N | x_0 \rangle = \sum_{m=0}^{N-1} |(m)_N\rangle \quad (9.4.4a)$$

This is called a group *completeness relation* or *resolution of the identity*. All phasors are equivalent due to  $C_N$  symmetry, so arbitrarily picking the first column ( $\mathbf{r}^0=\mathbf{1}$ ) does not affect the general utility of Fig. 9.4.2-3.

Translation by  $\mathbf{r}^p$  rephases the sum (9.4.4a) according to (9.4.3c) and translates all waves rigidly.

$$|x_p\rangle = \mathbf{r}^p |x_0\rangle = \sum_{m=0}^{N-1} \mathbf{r}^p |(m)_N\rangle = \sum_{m=0}^{N-1} e^{-i\frac{pm}{2\pi N}} |(m)_N\rangle \quad (9.4.4b)$$

Then each term  $|(m)_N\rangle$  in the sum (9.4.3) is allowed to advance its Bohr phase  $e^{-i\omega_m t} = e^{-im^2\omega_1 t}$  in discrete time fractions  $1/N$  of  $\tau_1$  for  $N$ -odd or  $1/2N$  for  $N$ -even, that is, through *stroboscopic instants*  $t_v$ .

$$|x_0(t_v)\rangle = \sum_{m=0}^{N-1} e^{-im^2\omega_1 t_v} |(m)_N\rangle \quad t_v = \begin{cases} v \frac{\tau_1}{N} = \frac{2\pi v}{\omega_1 N} & (v = 1, 2, \dots, N-1) \text{ for } N - \text{odd} \\ v \frac{\tau_1}{2N} = \frac{\pi v}{\omega_1 N} & (v = 1, 2, \dots, 2N-1) \text{ for } N - \text{even} \end{cases} \quad (9.4.5)$$

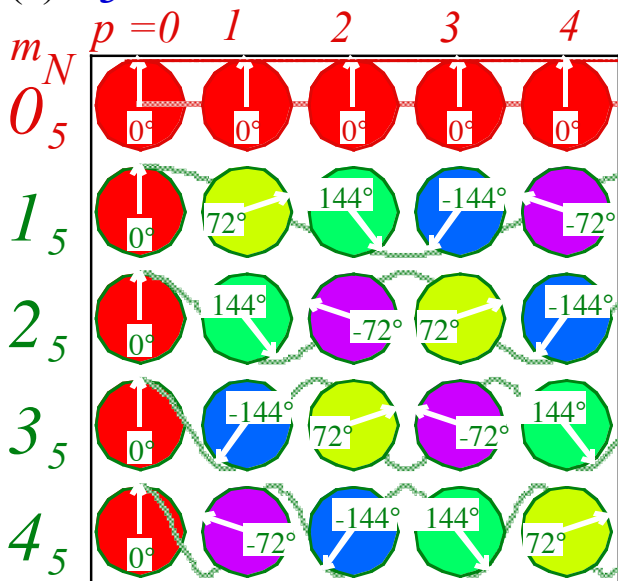
For each stroboscopic instant or row in Fig. 9.4.3 there is an array of equally-sized and equally-spaced phasors, that is, a *kaleidoscopic* phasor array. At each  $t_v$ , phasors are either revived or else zeroed-out.

An even- $N=2p$  revival table, such as  $N=4$  and  $N=6$  in Fig. Fig. 9.4.3 has embedded the  $N=2$  revival or "beat" table in Fig. Fig. 9.4.1b since  $C_2$  is a  $C_{2p}$  subgroup. So besides the obvious  $1/2$ -time revival halfway around, there must be  $1/4$ -time and  $3/4$ -time revivals for  $N=2$  at each of the  $1/4$ -lattice points, that is for  $N=6$ , at  $t=3/12$  and  $t=9/12$ , and for  $N=4$ , at  $t=2/8$  and  $t=6/8$ . Because  $N=6$  is also divisible by 3 there will be  $N=3$  revivals embedded at  $t=4/12=1/3$  and  $t=8/12=2/3$ . Also,  $N=3$  revivals embedded relative to the  $1/2$ -time revival at  $t=1/3-1/2=-1/6$  and  $t=1/3+1/2=5/6$  and  $t=2/3-1/2=1/6$  and at  $t=2/3+1/2=7/6$ . The phase angle "combinations" for each of the embedded phasors are reproduced perfectly and periodically as in a kind of quantum "odometer" or counter.

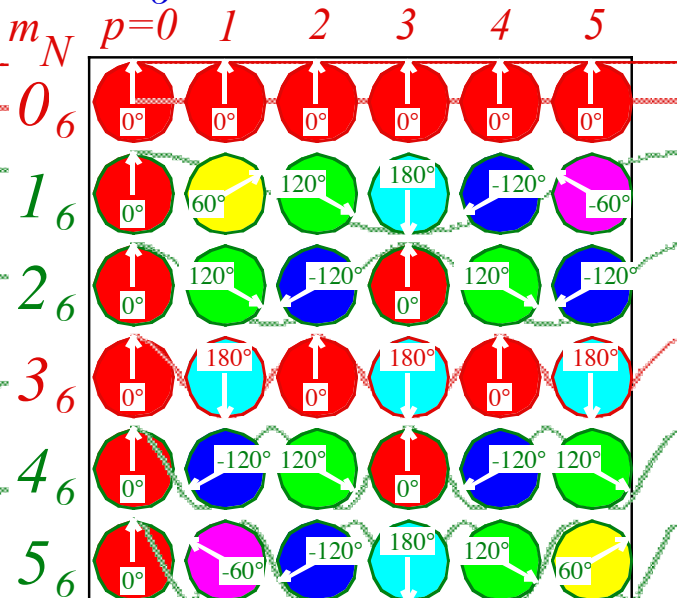
An even- $N$  revival table must start all over again at half-time, but from a point half-way around the ring at  $\phi=\pi$  if it started at  $\phi=0$ . This is required by  $C_N$  symmetry and by  $C_2$  half-time revival having 100% probability on the antipodal (half-way) point  $p=N/2$  if 100% probability starts on the initial  $p=0$  point. So the  $C_4$  phasors below the  $(p=2, t=2/4=1/2)$  point in Fig. Fig. 9.4.3b, namely,  $t=5/8, 3/4,$  and  $7/8$ , must have positions, amplitudes, and phases relative to the mid-point  $p=2$  that are identical to ones at  $t=1/8, 1/4,$  and  $3/8$ , respectively, below the initial  $t=0=p$  point. Similar repetition is seen for  $N=6$  in Fig. 9.4.3c and for any *even- $N$*  revival table below  $t=1/2$ .

A prime- $N$  revival table (like  $N=3$  in Fig. 9.4.2c or  $N=5$  in Fig. 9.4.3c) has no embedded structure because prime  $C_N$  has no subgroup but  $C_1$ . After the initial localized state each revival has probability distributed equally on all  $N$  lattice sites but with distinct phase combinations as in a kind of base- $N$  quantum odometer. In contrast, base- $N$  counters with  $N=2^p, p!$  or other composite numbers like  $N=4$  or  $6$  in Fig. 9.4.2d or 9.4.3d have the greatest variety of revival amplitudes.

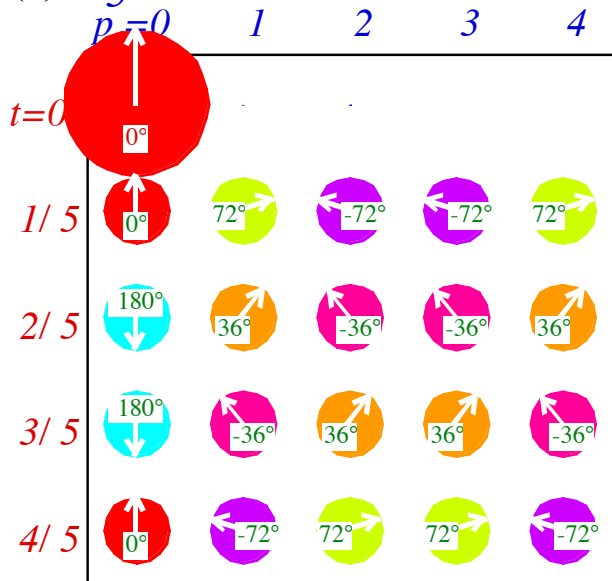
(a)  $C_5$  Eigenstate Characters



(b)  $C_6$  Eigenstate Characters



(c)  $C_5$  Revivals



(d)  $C_6$  Revivals

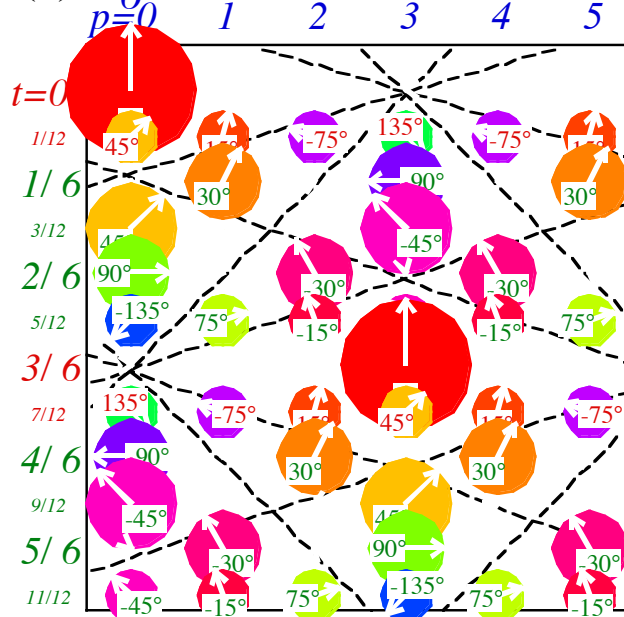


Fig. 9.4.3  $C_5$  and  $C_6$  eigenstates and revivals.

(a) and (b)  $C_5$  and  $C_6$  eigenstate characters.

(c) and (d)  $C_5$  and  $C_6$  revival space time patterns.

The  $N=6$  space-time wave patterns of Fig. 9.4.3d match phasor-for-peak with the revival intensity structure of the  $1/12$ ths,  $1/6$ th's,  $1/4$ th's,  $1/3$ rd's, and  $1/2$  revivals in Fig. 9.4.5 a or b if Fig. 9.4.3 tables are rescaled to the same size and overlapped with their edges centered in Fig. 9.4.5 a or b. Also, each table gives exactly the correct amplitude and phase of each revival peak that belongs to it as well as showing where the zeros reside. Similar character-revival tables of  $C_5$  (Fig. 9.4.3c),  $C_7$ ,  $C_9$ ,... will account for finer odd-fractional revivals occurring at stroboscopic odd-time fractions like the  $1/5$ th's,  $1/7$ th's,  $1/9$ th's,...and so on. (Recall  $1/8$ th's are

revivals for  $C_4$  shown in Fig. 9.4.2d. They will be copied by a  $C_8$  revival table in between its (new)  $1/16th$ 's.) The medium resolution wave plot of Fig. 9.4.5b displays  $N=2, 3, 4, \dots, 8$  structure more clearly than high- $\Delta m$  Fig. 9.4.5a by suppressing or defocusing the even finer revivals and prolonging fewer but more robust peaks or zeros of the more fundamental revivals. But, all zero-centered excitations ( $\bar{m}=0$ ) for larger- $\Delta m$  such as shown in Fig. 9.4.5a-b have the same fundamental X of a ( $0 \leftrightarrow 1$ )  $C_2$  beat in Fig. 9.4.5c, that is, they show a half-time revival that peaks around the center of the largest X.

### Cyclic subgroup hierarchies

$$\dots C_n \subset C_{pn} \subset C_{p^2n} \subset C_{p^3n} \subset \dots$$

are here being used to organize quantum fractal revival dynamics. Schrodinger's approach to quantum theory, which eschewed the *gruppenpest* in favor of differential equations, is not set up to explain the origins of such discrete fractal structure. This is because each successive integer  $N$  starts a new hierarchical group family. If the integer is prime the family is entirely new. But, if it is not prime, then older smaller families belonging to each of  $N$ 's factors are copied and embedded in the new family. In contrast, Schrodinger's wave equation treats every value of its independent variables as just another dumb  $x$  or  $t$ , and rational structure is glossed over.

Each new odd integer  $N=2m+1$  will have  $N$  new revival peaks at time fractions  $t/\tau=v/N=1/N, \dots, q/N$  .. but only for fractions  $q/N$  that are irreducible. Reducible fractions  $q/N$  that reduce to  $q/N = q_R/r$  (by dividing out a highest common factor  $f=N/r=q/q_R$ ) just recreate the "old"  $r=N/f$ -peak revivals already seen for a lesser or reduced integer  $N_R = r=N/f$ . Similarly, for even  $N=2m$  the only new revivals are at found irreducible time fractions  $t/\tau=v/2N=1/2N, \dots, q/2N$  ... . All the rest belong to subgroups  $C_{N_R}$  (if any) of  $C_N$  including  $C_m$  and  $C_2$ . A formula for new revival phasors based on sum (9.4.5) is given in Appendix 3.A. Now we consider a quasi-classical way to understand revival dynamics.

Odd- $N$  revivals clearly display the prime factors and their multiples of the integer  $N$ . If  $N$  is a prime number as it is for  $N=3$  in Fig. 9.4.2c and for  $N=5$  in Fig. 9.4.3c then all reviving kaleidoscopes except the initial one consist of uniform distributions of  $N$  phasors of probability  $1/N$ . However, for a composite odd integer such as  $N=15$ , the phasor distributions are not uniform as shown in Fig. 9.4.4. There are nodes at the  $p=\pm 1$  points for all revivals that correspond to factors of the integer  $N=15$ , namely at the revivals numbered  $1, 3, 6, 9, 12$ , and  $1, 5, 10$ , and  $15$ . The latter are copies of  $C_3$  revivals seen in Fig. 9.4.2c and the former are copies of  $C_5$  revivals seen in Fig. 9.4.3c. Their presence is simply a result of  $C_3$  and  $C_5$  being subgroups of  $C_{15}$ .

By definition,  $1$  is a factor of all  $N$  and  $C_1$  is a subgroup of all  $C_N$ . This is manifest by the first row of each revival table. The only even prime integer is  $N=2$ . This helps to account for the unique status of the  $C_2$  revival table in Fig. 9.4.1b and the extra significance of the  $C_2$  parity of each integer  $N$ , that is, the distinction between odd and even integers.

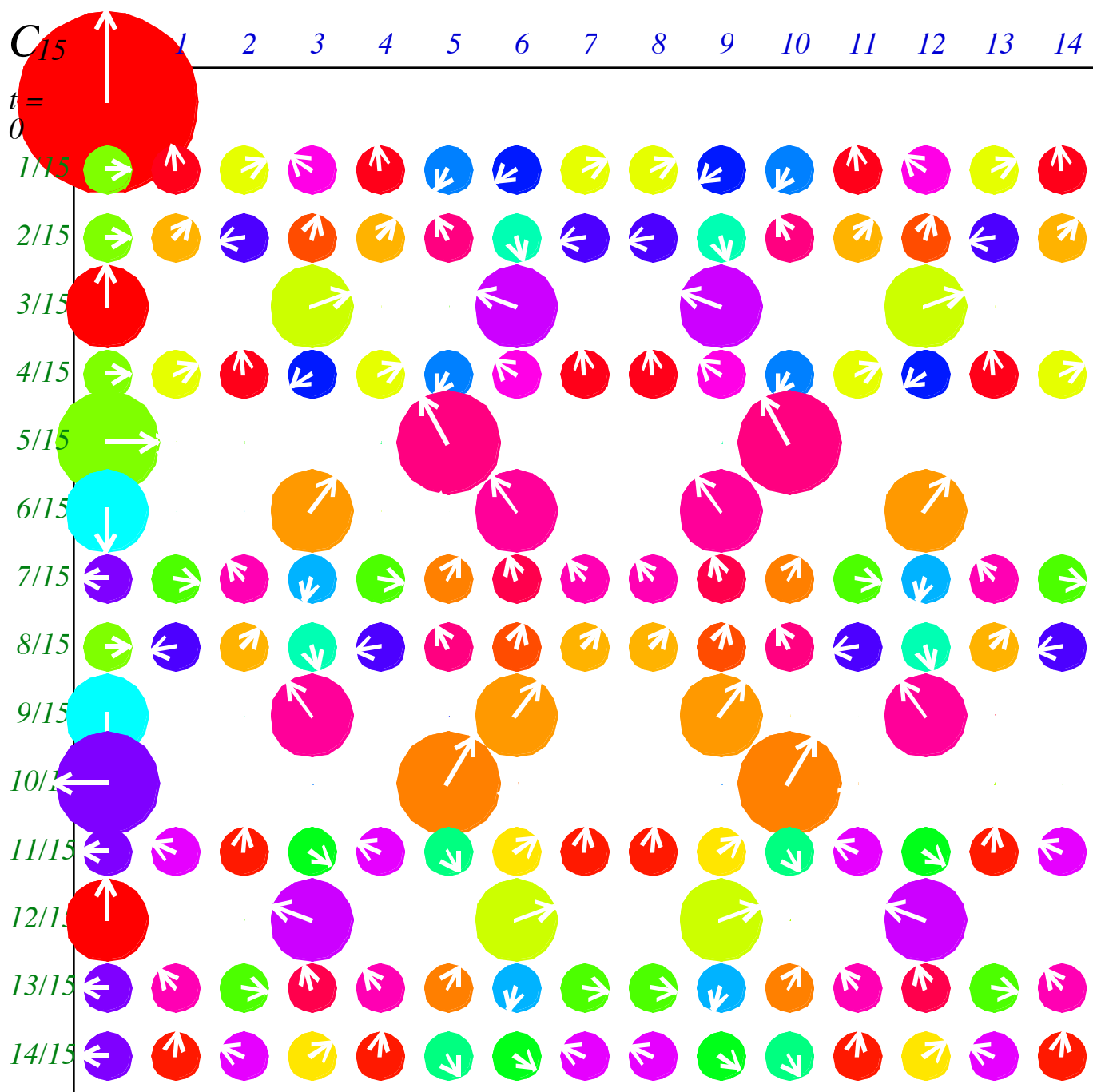


Fig. 9.4.4 Bohr space-time revival pattern for  $C_{15}$  Bohr system.

*Bohr vs. Bloch dispersion*

The value of the  $C_N$  models increases when the purely quantum effects, particularly those of a *single*  $C_N$ , are to be isolated. One imagines having a discrete Bohr ring like those sketched Fig. 9.4.5 composed of  $N$  atoms, quantum dots, optical fibers, or Josephson circuits homo-cyclically coupled in such a way that the usual quadratic Bohr dispersion spectrum  $\omega_m = m^2\omega_1$  is obtained with a finite number  $N$  of states per band. As a first approximation, such a ring has a *Bloch* dispersion spectrum  $\omega_m = (H_0 - 2H_1 \cos am)$  where  $H_1$  is the nearest neighbor coupling amplitude. Such a Bloch spectrum only approximates a Bohr spectrum for low  $m$ -values, and so high- $\Delta m$  revivals would decay eventually. However, by inserting cross-connecting coupling paths  $H_2, H_3, H_4, \dots, H_{N/2}$ , as shown in Fig. 9.4.5, it is possible to achieve any spectrum, including  $m^2$ , by adjusting coefficients  $H_k$  in a Fourier series.

$$\omega_m = H_0 - 2H_1 \cos am - 2H_2 \cos 2am - 2H_3 \cos 3am \dots - H_{N/2} \cos Nam/2 .$$

A quadratic spectrum ( $E_m = \hbar\omega m^2$ ) is achieved for general  $N$  by setting Hamiltonian parameters as follows.

$$\hbar\omega m^2 = \sum_{p=0}^{N-1} H_p e^{-i p m \frac{2\pi}{N}}, \text{ where: } H_p = \frac{\hbar\omega}{N} \sum_{\{m\}} m^2 e^{i p m \frac{2\pi}{N}} \quad (9.4.6)$$

For example, a 4-level  $N=6$  quadratic spectrum  $\{E_0=0, E_{\pm 1}=1^2, E_{\pm 2}=2^2, E_3=3^2\}$  involves six eigenstates:  $|m\rangle_6 = |(0)_6\rangle, |(\pm 1)_6\rangle, |(\pm 2)_6\rangle$ , and  $|(3)_6\rangle$ , using the following coupling amplitudes as given in the  $N=6$  row of Table 9.1.

$$H_0=3.16, H_1=-2.0=H_5^*, H_2=0.67=H_4^*, H_3=-0.5, \quad (9.4.7)$$

With the adjustments in Table 9.1. of  $H_k$  coupling, pure  $C_N$  revivals like those in Fig. 9.4.2-3 would repeat at frequency  $\nu = \hbar^{-1}$  until the coupling is turned off. Such a device would be an  $N$ -ary counter as implied before. By incorporating the  $N$ -ring as the cross-section of a coaxial  $N$ -fiber cable, it would be possible for the revival evolution to occur as an  $N$ -phase wave propagated down the cable. The possibility of storing, processing, and transporting quantum or classical  $N$ -ary data for  $N \gg 2$  using just one kind of basic hardware may yet warm the heart (and portfolio) of a future cyber-entrepreneur.

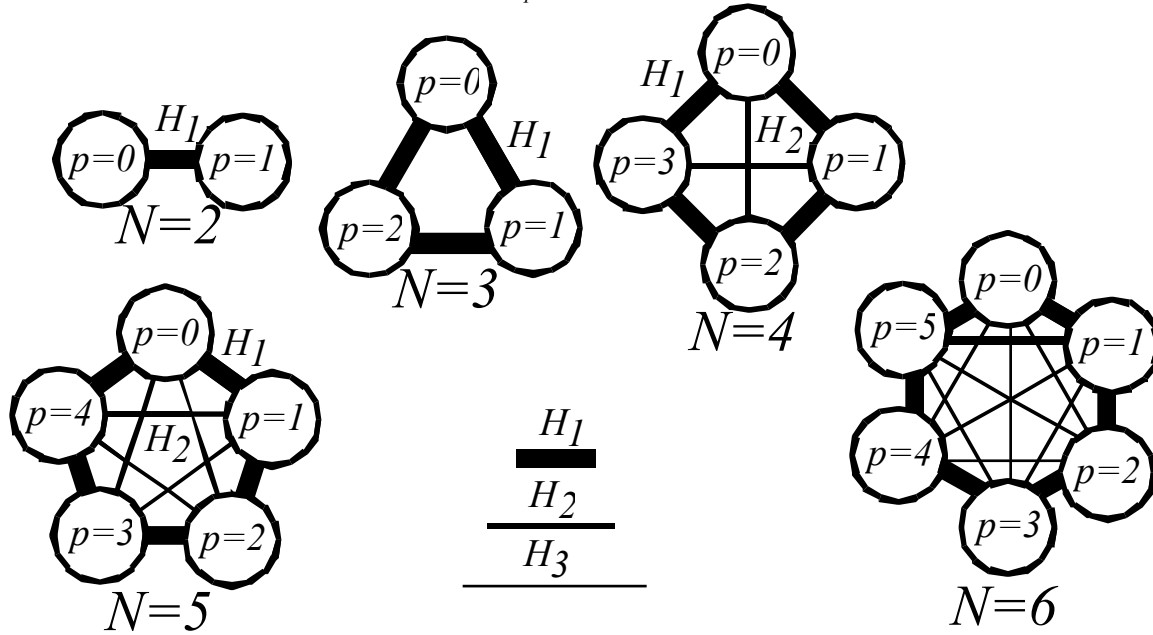


Fig. 9.4.5 Quantum dot or co-axial cable structures with arbitrary dispersion

Table 9.1. *N*-Discrete *m*<sup>2</sup>-Hamiltonian Coupling Amplitudes. All devices have a unit revival rate:  $\hbar\omega=1$ .

	$H_0$	$H_1$	$H_2$	$H_3$	$H_4$	$H_5$	$H_6$	$H_7$	$H_8$	$H_9$
$N=2$	1/2	-1/2								
$N=3$	2/3	-1/3								
$N=4$	3/2	-1	1/2							
$N=5$	2	-1.1708	0.1708							
$N=6$	19/6	-2	2/3	-1/2						
$N=7$	4	-2.393	0.51	-0.1171						
$N=8$	11/2	-3.4142	1	-0.5858	1/2					
$N=9$	20/3	-4.0165	0.9270	-1/3	0.0895					
$N=10$	17/2	-5.2361	1.4472	-0.7639	0.5528	-1/2				
$N=11$	10	-6.0442	1.4391	-0.5733	0.2510	-0.0726				
$N=12$	73/6	-7.4641	2	-1	2/3	-0.5359	1/2			
$N=13$	14	-8.4766	2.0500	-0.8511	0.4194	-0.2028	0.06116			
$N=14$	33/2	-10.098	2.6560	-1.2862	0.8180	-0.6160	0.5260	-1/2		
$N=15$	57/3	-11.314	2.7611	-1.1708	0.6058	-1/3	0.1708	-0.0528		
$N=16$	43/2	-13.137	3.4142	-1.6199	1	-0.7232	0.5858	-0.5198	1/2	
$N=17$	24	-14.557	3.5728	-1.5340	0.81413	-0.4732	0.2781	-0.1479	0.0465	

## Problems for Chapter 9.

*Evolution* (A 2000 Qualifying exam problem)

9.1.1. A two-state quantum system evolves as follows in 5 sec. (First: Is the evolution unitary?)

$$\text{State } |1\rangle \text{ becomes state } |1'\rangle = -\sqrt{3}/2 |1\rangle - i/2 |2\rangle$$

$$\text{State } |2\rangle \text{ becomes state } |2'\rangle = -i/2|1\rangle -\sqrt{3}/2|2\rangle$$

(a) Derive a complete set of states as combinations of  $|1\rangle$  and  $|2\rangle$  so that each combination would stay the same (except for a possible overall phase) at all times.

(b) Compute the energy level splitting  $\Delta E = E_2 - E_1$  for this system assuming  $\Delta E$  is the lowest possible to achieve the 5 sec. evolution given in part (a).

(c) Derive an expression for any state at any time  $t$  and give  $|1(t)\rangle$  and  $|2(t)\rangle$  numerically at  $t=1$  sec.

(d) Does this evolution correspond to a Hamiltonian  $\mathbf{H}$ ? If so, what  $\mathbf{H}$ ?

*Revolution*

9.1.2. A two-state quantum system evolves as follows in  $t$  sec. (First: Is the evolution unitary?)

$$\text{State } |1\rangle \text{ becomes state } |1'\rangle = \cos \omega t |1\rangle - \sin \omega t |2\rangle$$

$$\text{State } |2\rangle \text{ becomes state } |2'\rangle = \sin \omega t |1\rangle + \cos \omega t |2\rangle$$

(a) Does this time evolution correspond to a Hamiltonian  $\mathbf{H}$ ? If so, what  $\mathbf{H}$ ? Is it Hermitian?

*Hexapairs*

9.3.1 The hexagonal  $C_6$  eigenstates  $|0_6\rangle$  and  $|3_6\rangle$  are standing waves while  $[|+1_6\rangle, |-1_6\rangle]$  and  $[|+2_6\rangle, |-2_6\rangle]$  are right and left moving wave pairs.

(a) Do  $[|+3_6\rangle, |-3_6\rangle]$  a moving wave pair make? Explain why or why not?

(b) Can the  $[|+1_6\rangle, |-1_6\rangle]$  pair make a pair of standing waves? If so make them and plot the phasors. If not, explain.

(c) Can the  $[|+2_6\rangle, |-2_6\rangle]$  pair make a pair of standing waves? If so make them and plot the phasors. If not, explain.

(d) What values, if any, for tunneling parameters  $|S|$ ,  $\sigma$ ,  $|\Gamma|$ ,  $\tau$ , and  $U$  allow standing-wave-pair eigenstates. Must they always be degenerate?

*Octapairs*

9.3.2 Consider an octagonal  $C_8$  system of 8 quantum dots.

(a) Write the general form of its Hamiltonian.

(b) Display its eigenkets and write a formula for its energy eigenvalues.

*Back to Roots...again*

9.3.3. Eigensolutions of  $C_2$  and  $C_3$  symmetric  $\mathbf{H}$  can be turned into quadratic and cubic root formulas.

(a) Eigenvalues of  $\mathbf{H} = \begin{pmatrix} A & B \\ B & A \end{pmatrix}$ , namely  $\lambda = A \pm B$  give solutions to  $\lambda^2 - 2A\lambda + A^2 - B^2 = 0$ . Use this to derive the familiar quadratic

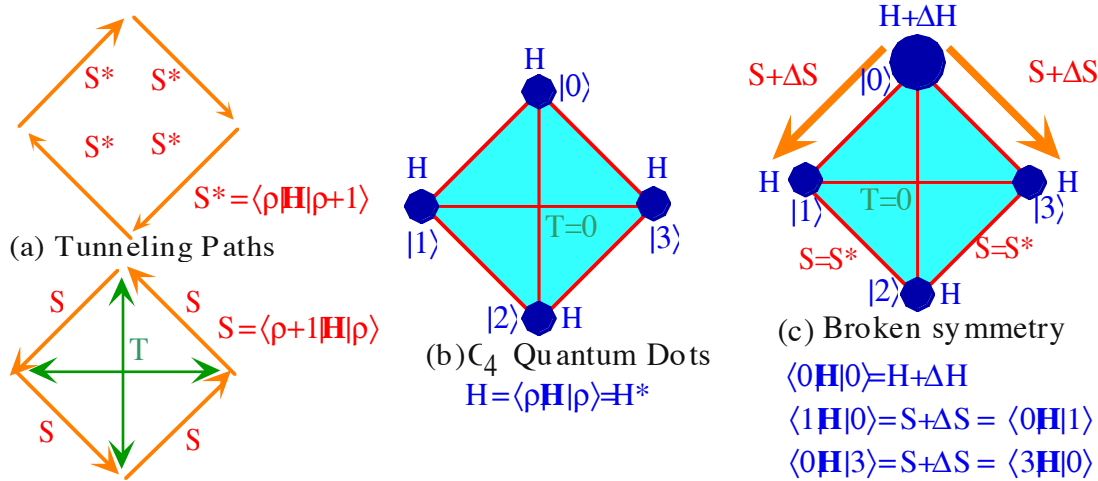
formula for roots of  $a\lambda^2 + b\lambda + c = 0$ .

(b) Use the above and  $C_3$ -derived eigenvalues of  $\mathbf{H} = \begin{pmatrix} A & C & B \\ B & A & C \\ C & B & A \end{pmatrix}$  to derive the less familiar formula for roots to general cubic

equation  $a\lambda^3 + b\lambda^2 + c\lambda + d = 0$ . (Hint: First consider  $\lambda^3 + p\lambda + q = 0$ .)

Quantum baseball

9.3.3 Suppose the Asumma Tummy Quantum Computer Co. has taken over the world and you are the only one in your country that still knows the difference between an amplitude and a phase. Your assignment is to design, make or experiment with some quantum dot computer elements diagrammed below having charge carrier matter-waves that tunnel along edges and diagonals of squares as indicated below.



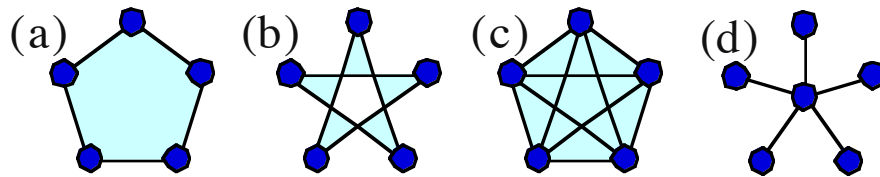
Suppose edge tunneling amplitudes are equal and real ( $S = -1.0$ ) while diagonal tunneling amplitudes are zero ( $T = 0$ ) to give  $C_4$  symmetry as shown in Fig. (b). Suppose at time  $t=0$  the charge carrier amplitude is 100% on "home" base state  $|0\rangle$ . ( $\langle 0 | \Psi(t=0) \rangle = 1$ ).

- (a) Derive eigenlevels and calculate the time dependence of the home-base amplitude  $\langle 0 | \Psi(t) \rangle = ?$  Find the period  $\tau_{\text{rebound}}$  of time it takes home-base to rebound to a maximum again after initially decreasing. Does it rebound to 100% the first time? ever?
- (b) Sketch phasors for each of the four bases  $|0\rangle, |1\rangle, |2\rangle,$  and  $|3\rangle$  at  $1/4 \cdot \tau_{\text{rebound}}$  time intervals and indicate by arrows between phasors the direction of instantaneous charge flow from one to the other. (Tell how you determine this just by looking at the phasors.) Does first, second, or third base ever hold 100% of the charge?
- (c.) Suppose all edge tunneling amplitudes are equal but (possibly) complex ( $S = -e^{i\sigma}$ ) while diagonal tunneling amplitudes are zero ( $T=0$ ).
  - (a) Adjust the tunneling phase angle  $\sigma$  so as to make four equally spaced energy eigenlevels with quantum numbers  $m=(0)_4, (-1)_4, (1)_4,$  and  $(2)_4$ , in that order.
  - Is the order  $(0)_4, (1)_4, (2)_4,$  and  $(3)_4 = (-1)_4$  also possible using this adjustment? If not, can some other kind of adjustment achieve it without changing the form of the eigenstates? Discuss.

Janitor's revenge

9.3.4. Suppose a janitor hits the home-base dot-0 with his broom handle and accidentally resets some  $\mathbf{H}$ -matrix elements shown in Fig. (c) by small amounts: the first diagonal by  $\Delta H = A$  and the first off-diagonal by  $\Delta S = \Delta S^* = B$ . All other matrix elements remain the same as in Problem 9.3.3. Let the new "broken" Hamiltonian be a sum  $\mathbf{H}' = \mathbf{H} + \mathbf{V}(A, B)$ .

- (a) Derive a matrix representation of the janitor's perturbation  $\mathbf{V}(A, B)$  in the original  $|0\rangle$  to  $|3\rangle$  basis, in the moving-wave basis  $| (0)_4 \rangle, | (-1)_4 \rangle, | (1)_4 \rangle,$  and  $| (2)_4 \rangle$ , and in the standing-wave cosine and sine basis  $| (0)_4 \rangle, | (c)_4 \rangle, | (s)_4 \rangle,$  and  $| (2)_4 \rangle$ , where:  $| (c)_4 \rangle = (| (-1)_4 \rangle + | (1)_4 \rangle) / \sqrt{2}$ , and:  $| (s)_4 \rangle = (| (-1)_4 \rangle - | (1)_4 \rangle) / i\sqrt{2}$ .
- (b) Use (a) and perturbation theory to estimate (to 2nd order  $|A|^2 = |\Delta S|^2$  or  $|B|^2 = |\Delta H|^2$ ) the effect of the  $\mathbf{V}(A=0.1, B=0.2)$  on energy eigenlevels  $\epsilon(0)_4, \epsilon(\pm 1)_4,$  and  $\epsilon(2)_4$  as  $\epsilon(m)_4$  turn into eigenlevels of the "broken" Hamiltonian  $\mathbf{H}'$ . Which representation from (a) should be used and why? Show your work.
- (c.) Discuss the effect, if any, on the original eigenstates  $| (0)_4 \rangle, | (-1)_4 \rangle, | (1)_4 \rangle,$  and  $| (2)_4 \rangle$ , and sketch their phasor diagrams next to the corresponding eigenlevels. Are moving-wave eigenstates still possible after the janitor does his or her work?



*Beware the pentagram*

9.3.5. Suppose a *pentagonal*  $C_5$  device in prob. 9.3.3(a).

(a) Could it ever rebound to 100%? Discuss devices (a), (b), and (c).

(b) Discuss the possibility (or impossibility) of constructing such a device that would give a "runner-going-around-the-bases" effect with 100% probability occurring briefly but consecutively on first base, then second base, then third base, and finally home base. If such a device could be made would it also be capable of running in the opposite direction without modifying the H-matrix?

*Quantum dot.com*

9.3.6 The  $C_N$  quantum dots in Fig. 9.4.5 are supposed to belong to an infinite family of structures whose  $\omega_m$ -spectrum is quadratic in quantum number  $m_N$ . This assumes a sequence of tunneling paths or connecting couplers described by (9.4.6). The  $N=2$  example seems an exception having only a single  $H_I = S$  connector on each dot. Is this right? Should the

Hamiltonian be  $\mathbf{H} = \begin{pmatrix} H & S \\ S & H \end{pmatrix}$  or should it be  $\mathbf{H} = \begin{pmatrix} H & 2S \\ 2S & H \end{pmatrix}$  to conform with the rest? Discuss. Compare the  $N=2$

case with, say, that of  $N=4$ .

*Quantum dot.com again*

9.3.7 The  $C_N$  quantum dots in Fig. 9.4.5 might be made to have other spectral band functions such as

(Q) Quadratic spectrum:  $\omega(m) = \varepsilon(m)/\hbar = m^2 = 1, 0, 1, 4, 9, \dots$  for  $(m)_N = -1, 0, 1, \text{ and } \pm 2, \pm 3, \dots$

(L) Linear spectrum:  $\omega(m) = \varepsilon(m)/\hbar = |m| = 1, 0, 1, 2, 3, \dots$  for  $(m)_N = -1, 0, 1, \pm 2, \pm 3, \dots$

(SL) Super-linear spectrum:  $\omega(m) = \varepsilon(m)/\hbar = m = -1, 0, 1, \pm 2, \pm 3, \dots$  for  $(m)_N = -1, 0, 1, \pm 2, \pm 3, \dots$

(a) Derive  $N=8$  coupling parameters for each of these spectra.

## Review Topics & Formulas for Unit 3

*Fourier Series Coefficients*

$$\langle k_m | \Psi \rangle = \int_{-L/2}^{L/2} dx \langle k_m | x \rangle \langle x | \Psi \rangle$$

$$\langle k_m | x \rangle = \frac{e^{-ik_m x}}{\sqrt{L}} = \langle x | k_m \rangle^*$$

*Fourier Integral Transform*

$$\langle k | \Psi \rangle = \int_{-\infty}^{\infty} dx \langle k | x \rangle \langle x | \Psi \rangle$$

$$\text{Kernal: } \langle k | x \rangle = \frac{e^{-ikx}}{\sqrt{2\pi}} = \langle x | k \rangle^*$$

*Fourier  $C_N$  Transformation*

$$\langle k_m | \Psi \rangle = \sum_{p=0}^{p=N-1} \langle k_m | x_p \rangle \langle x_p | \Psi \rangle$$

$$\langle k_m | x_p \rangle = \frac{e^{-ik_m x_p}}{\sqrt{N}} = \langle x_p | k_m \rangle^*$$

*x-Wavefunction  $\Psi(x) =$*

$$\langle x | \Psi \rangle = \sum_{m=-\infty}^{m=\infty} \langle x | k_m \rangle \langle k_m | \Psi \rangle$$

*Ortho – Completeness*

$$\sum_{m=0}^{m=\infty} \langle x | k_m \rangle \langle k_m | x' \rangle = \delta(x - x')$$

$$\int_{-L/2}^{L/2} dx \langle k_m | x \rangle \langle x | k_{m'} \rangle = \delta_{m,m'}$$

*Discrete momentum  $m$*

*Continuous position  $x$*

*x-Wavefunction  $\Psi(x) =$*

$$\langle x | \Psi \rangle = \int_{-\infty}^{\infty} dk \langle x | k \rangle \langle k | \Psi \rangle$$

*Ortho – Completeness*

$$\int_{-\infty}^{\infty} dk \langle x | k \rangle \langle k | x' \rangle = \delta(x - x')$$

$$\int_{-\infty}^{\infty} dx \langle k | x \rangle \langle x | k' \rangle = \delta(k - k')$$

*Continuous momentum  $k$*

*Continuous position  $x$*

*x-Wavefunction  $\Psi(x) =$*

$$\langle x_p | \Psi \rangle = \sum_{m=0}^{m=N-1} \langle x_p | k_m \rangle \langle k_m | \Psi \rangle$$

*Ortho – Completeness*

$$\sum_{m=0}^{m=N-1} \langle x_p | k_m \rangle \langle k_m | x_{p'} \rangle = \delta_{p,p'}$$

$$\sum_{p=0}^{p=N-1} \langle k_m | x_p \rangle \langle x_p | k_{m'} \rangle = \delta_{m,m'}$$

*Discrete momentum  $m$*

*Discrete position  $x_p$*

*Time Evolution Operator  $\mathbf{U}$*

$$|\Psi(t)\rangle = \mathbf{U}(t,0) |\Psi(0)\rangle$$

*Hamiltonian Generator  $\mathbf{H}$*

$$i\hbar \frac{\partial}{\partial t} \mathbf{U}(t,0) = \mathbf{H} \mathbf{U}(t,0)$$

*Time Evolution Operator  $\mathbf{U}$*

$$\mathbf{U}(t,0) = e^{-i t \mathbf{H} / \hbar}$$

*Schrodinger  $t$  – Equation*

$$i\hbar \frac{\partial}{\partial t} |\Psi(t)\rangle = \mathbf{H} |\Psi(t)\rangle$$

$\mathbf{U}$  must be Unitary

$$\mathbf{U}^\dagger(t) = \mathbf{U}^{-1}(t) = \mathbf{U}(-t)$$

$$(e^{-i\mathbf{H}t/\hbar})^\dagger = e^{i\mathbf{H}^\dagger t/\hbar} = e^{i\mathbf{H}t/\hbar}$$

so  $\mathbf{H}$  is Hermitian  $\mathbf{H}^\dagger = \mathbf{H}$

*Schrodinger time-independent energy eigen equation.*

$$\mathbf{H} | \omega_m \rangle = \hbar \omega_m | \omega_m \rangle = \varepsilon_m | \omega_m \rangle \quad (9.3.1a)$$

$\mathbf{H}$ -eigenvalues use  $\mathbf{r}$ -expansion (9.2.6) of  $\mathbf{H}$  and  $C_6$  symmetry  $\mathbf{r}^p$ -eigenvalues from (8.2.9).

$$\langle k_m | \mathbf{r}^p | k_m \rangle = e^{-ipk_m a} = e^{-ipm2\pi/N} \quad \text{where: } k_m = m(2\pi/Na)$$

$$\begin{aligned} \langle k_m | \mathbf{H} | k_m \rangle &= H \langle k_m | \mathbf{1} | k_m \rangle + S \langle k_m | \mathbf{r} | k_m \rangle + T \langle k_m | \mathbf{r}^2 | k_m \rangle + U \langle k_m | \mathbf{r}^3 | k_m \rangle + T^* \langle k_m | \mathbf{r}^4 | k_m \rangle + S^* \langle k_m | \mathbf{r}^5 | k_m \rangle \\ &= H + S e^{-ik_m a} + T e^{-i2k_m a} + U e^{-i3k_m a} + T^* e^{i2k_m a} + S^* e^{ik_m a} \end{aligned} \quad (9.3.5a)$$

*Bloch dispersion relation.* And Bohr limit ( $k \ll \pi/a$ ) approximation. *Band group velocity  $V_{group}$ .*

$$\hbar \omega_m = E_m = H - 2|S| \cos(k_m a) = H - 2|S| + |S| (k_m a)^2 + \dots \quad (9.3.8)$$

$$V_{group} = \frac{d\omega_m}{dk_m} = 2 \frac{|S|}{\hbar} a \sin(k_m a) \left( \cong 2 \frac{|S|}{\hbar} k_m a^2, \text{ for: } k_m \ll \pi/a \right) \quad (9.3.10)$$

*Effective mass  $M_{eff}$  inversely proportional to  $S$ .*  $M_{eff}(0) = \hbar^2 / (2|S| a^2)$  (9.3.11a)

Fourier transform of a Gaussian  $e^{-(m/\Delta m)^2}$  momentum distribution is a Gaussian  $e^{-(\phi/\Delta\phi)^2}$  in coordinate  $\phi$ .

$$\langle m | \Psi \rangle = e^{-(m/\Delta m)^2} \quad \text{implies:} \quad \langle \phi | \Psi \rangle = e^{-(\phi/\Delta\phi)^2} \quad (9.3.14)$$

The relation between momentum uncertainty  $\Delta m$  and coordinate uncertainty  $\Delta\phi$  is a *Heisenberg relation*.

$$\Delta m / 2 = 1 / \Delta\phi, \text{ or:} \quad \Delta m \Delta\phi = 2 \quad (9.3.15)$$

*Bohr wave quantum speed limits*

$$V_{group}^{Bohr}(m \leftrightarrow n) = \frac{\omega_m - \omega_n}{k_m - k_n} = \frac{(m^2 - n^2)h\nu_1}{(m - n)h/L} = (m + n)\frac{L}{\tau_1} = (m + n)V_1 \quad (9.3.16)$$

Predicting fractional revivals: *Farey Sum*  $\oplus_F$  of the rational fractions  $n_1/d_1$  and  $n_2/d_2$

$$t_{12\text{-intersection}} = \frac{n_2 + n_1}{d_2 + d_1} = \frac{n_2}{d_2} \oplus_F \frac{n_1}{d_1} \quad (9.3.18)$$

### Appendix 9.A. Relative phase of peaks in a revival lattice

The first derivation here of revival amplitudes at stroboscopic time fractions  $t_v = \tau(v/N)$  and kaleidescopic angular positions  $\phi_\rho = 2\pi(\rho/N)$  assumes  $N$  is odd. At times when fraction  $(v/N)$  is reduced, all  $N$  revival peak sites hop up with identical magnitude and with particular arrangement of phases that clearly distinguishes each  $v/N$  from all others. First we derive formulas for these phases as a function of site index  $\rho$  and revival time index  $v$ . (If time fraction  $v/N$  reduces to  $v_R/N_R$ , then use  $(v_R, N_R)$  in place of  $(v, N)$  to find  $N_R$  peak phases of subgroup  $C_{N_R}$  revivals.) The first step is to complete the square of exponent in sum.

$$\begin{aligned} \psi_0(\phi_\rho, t_v) &= \frac{1}{N} \sum_{m=0}^{N-1} e^{i\left(m\rho - m^2 v\right) \frac{2\pi}{N}} = \frac{1}{N} \sum_{m=0}^{N-1} e^{-i\left(m^2 v - m\rho + \frac{\rho^2}{4v}\right) \frac{2\pi}{N}} e^{i \frac{\rho^2}{4v} \frac{2\pi}{N}} \\ &= \frac{1}{N} \sum_{m=0}^{N-1} e^{-i\left(mv - \frac{\rho}{2}\right) \left(m - \frac{\rho}{2v}\right) \frac{2\pi}{N}} e^{i \frac{\rho^2}{4v} \frac{2\pi}{N}} \\ &= \frac{1}{N} \sum_{m=0}^{N-1} e^{-i(2mv - \rho)^2 \frac{2\pi}{4vN}} e^{i \frac{\rho^2}{4v} \frac{2\pi}{N}} \end{aligned} \quad (\text{A.1})$$

The integer square  $(2mv - \rho)^2$  in the exponent is to be treated as an integer-modulo- $4vN$  since the phase factor repeats after that value. However, as summation index  $m$  runs through the integers  $m = 0, 1, 2, \dots, N-1$  it exhausts all the possible values of  $(2mv - \rho)^2 \pmod{4vN}$  for a given  $v$  and  $\rho$ , and the values are the same no matter what we take for the range of  $m$ . For example, consider tables of phase index  $(2mv - \rho)^2 \pmod{4vN}$  for select times of  $v=1$  and  $v=2$  for an  $N=5$  level excitation.

$(2mv - \rho)^2 \pmod{4vN}$ for $N=5$							$(2mv - \rho)^2_{4vN}$ for $N=5$												
$v=1$	$m=0$	1	2	3	4	5	6	$v=2$	$m=0$	1	2	3	4	5	6	7	8	9	10...
$\rho=0$	$\bar{0}$	4	16	16	4	0	4	$\rho=0$	$\bar{0}$	16	24	24	16	0	16	24	24	16	0
1	1	1	9	<u>5</u>	9	1	1	1	1	9	9	1	<u>25</u>	1	9	9	1	25	1
2	4	<u>0</u>	4	16	16	4	0	2	4	4	36	<u>20</u>	36	4	4	36	20		
3	9	1	1	9	<u>5</u>	9	1	3	9	1	<u>25</u>	1	9	9	1				
4	16	4	<u>0</u>	4	16	16	4	4	16	<u>0</u>	16	24	24	16					

Note that  $N$  consecutive values for  $m$  give the same sum no matter whether the sum starts at  $m=0$  or at a *sum-shift* value  $m=\mu$ . The idea is to shift the summation index  $m$  to  $m-\mu$  so that a  $(2mv - \rho)^2 \pmod{4vN}$  binomials in row- $\rho$  can be replaced by a simple square  $(2mv)^2 \pmod{4vN}$  monomial found in the  $\rho=0$  row. This will reduce the exponent to a term independent of site-index  $\rho$  plus a  $\Delta$ -term independent of summation-index  $m$ .

It would be nice if the  $\Delta$ -term were also independent of  $\rho$  but the tables show that is asking too much! So,  $\Delta = \Delta(\rho, v)$  and, each of the rows  $\rho = 1, \dots, N-1$  differ from the  $\rho=0$  row by a single *modular difference*  $\Delta(\rho, v)$  in phase index which is overlined in the table and is the *single unpaired* number in each row. For example, subtracting  $\Delta(1, 1) = 5 \pmod{20} = (5)_{20}$  from the  $(\rho=1)$  row of the  $(v=1)$  table and shifting forward by  $\mu_1=2$  gives the  $(\rho=0)$  row  $(\pmod{20})$ . The shifts needed to line up rows  $\rho=1, 2, 3,$  and  $4$  are  $\mu_1=2, \mu_2=4, \mu_3=6,$  and  $\mu_4=8$  respectively, that is  $\mu_\rho = \mu_1 \rho$ . These observations are summarized by a modular equation.

$$\left(2(m - \mu_\rho)v - \rho\right)^2 \pmod{4vN} \equiv \left(2(m - \mu_\rho)v - \rho\right)^2_{4vN} = (2mv)^2_{4vN} - \Delta(\rho, v) \quad (\text{A.3a})$$

This is supposedly valid for all values of  $m$  so for  $m=0$  the equation reads

$$\left(-2\mu_\rho v - \rho\right)_{4vN}^2 = 0 - \Delta(\rho, v) , \quad (\text{A.3b})$$

where

$$\mu_\rho = \mu_1 \rho . \quad (\text{A.3c})$$

Subtracting equation (A.3b) from (A.3a) gives the following, again valid for all  $m$ .

$$\begin{aligned} & \left(2(m - \mu_\rho)v - \rho\right)_{4vN}^2 - \left(-2\mu_\rho v - \rho\right)_{4vN}^2 = (2mv)_{4vN}^2 \\ & \left(4mv(-2\mu_\rho v - \rho)\right)_{4vN} = (0)_{4vN} = \kappa 4vN = 0, 4vN, 8vN, \dots, 4vN(N-1) \end{aligned}$$

Next, set  $m=1$ , and solve for the  $m$ -sum-shift  $\mu_\rho$  of row  $\rho$ .

$$\begin{aligned} -8\mu_\rho v^2 - 4v\rho &= -\kappa 4vN = 0, -4vN, -8vN, \dots, -4vN(N-1) \\ 2\mu_\rho v + \rho &= \kappa N = 0, N, 2N, \dots, N(N-1) \text{ or: } \mu_\rho = \frac{\kappa N - \rho}{2v} = (\text{integer})_N \end{aligned} \quad (\text{A.4a})$$

A value  $\kappa=0, 1, 2, \dots, N-1$  is selected so that  $m$ -sum-shift  $\mu_\rho$  is an integer  $\mu_\rho=0, 1, 2, \dots, N-1$ , too. Substituting the resulting  $\mu_\rho$  value in (A.3a) gives the phase modular difference  $\Delta$  first defined there and in (A.3b).

$$\Delta(\rho, v) = -\left(2v\mu_\rho + \rho\right)_{4vN}^2 = -\left(2v\left(\frac{\kappa N - \rho}{2v}\right) + \rho\right)_{4vN}^2 = -(\kappa N)_{4vN}^2 , \quad (\text{A.4b})$$

where

$$\kappa = \frac{2v\mu_\rho + \rho}{N} . \quad (\text{A.4c})$$

Putting (A.3a) into the revival wavefunction sum (A.1) gives

$$\begin{aligned} \Psi_0(\phi_\rho, t_v) &= \frac{1}{N} \sum_{m=0}^{N-1} e^{-i(2mv-\rho)\frac{2\pi}{4vN}} e^{i\frac{\rho^2}{4v}\frac{2\pi}{N}} \\ &= \frac{1}{N} \sum_{m=0}^{N-1} e^{-i\left[(2mv)^2 - \Delta(\rho, v)\right]\frac{2\pi}{4vN}} e^{i\frac{\rho^2}{4v}\frac{2\pi}{N}} \quad [\text{using:(A.3a)}] \\ &= \frac{1}{N} \sum_{m=0}^{N-1} e^{-i\left[(2mv)^2 + (\kappa N)^2 - \rho^2\right]\frac{2\pi}{4vN}} \quad [\text{using:(A.4b)}] \\ &= \frac{1}{N} \sum_{m=0}^{N-1} e^{-i\left[(2mv)^2 + 4\mu_\rho^2 v^2 + 4\mu_\rho v\rho\right]\frac{2\pi}{4vN}} \quad [\text{using:(A.4c)}] \\ &= P(v)e^{\frac{-i\left[\mu_\rho^2 v + \mu_\rho \rho\right]2\pi}{N}} = P(v)e^{\frac{-i\left[\mu_1^2 v + \mu_1\right]\rho^2 2\pi}{N}} \quad [\text{using:(A.3c)}] \quad (\text{A.5a}) \end{aligned}$$

The overall phase and amplitude prefactor  $P(v)$  is a Gaussian sum discussed in Appendix 9B.

$$P(v) = \frac{1}{N} \sum_{m=0}^{N-1} e^{-i(2mv)^2 \frac{2\pi}{4vN}} = \frac{1}{N} \sum_{m=0}^{N-1} e^{-ivm^2 \frac{2\pi}{N}} \quad (\text{A.5b})$$

Finally, the ( $\rho=1$ )  $m$ -sum-shift  $\mu_1$  is the first fraction  $(N-1)/2v, (2N-1)/2v, (3N-1)/2v, \dots$ , or  $(N^2-1)/2v$ , to yield an integer according to (A.4a). Recall that it was assumed that  $N$  and  $v$  are relatively prime, that is, have no common factors. It seems evident that the integer arithmetic behind base- $N$  counter revivals is not trivial, even for the case of odd- $N$ . To complete this particular  $N=5$  example we find the sum-shift  $\mu_1$  at each revival time  $v=1-4$ .

$$\begin{array}{c|ccccc}
\mu_1 = \frac{\kappa N - 1}{2\nu} & \kappa N - 1 = & 4 & 9 & 14 & 19 & 24 \\
\hline
2\nu = 2 & & \bar{2} & . & 7 & . & 12 \\
2\nu = 4 & & \bar{1} & . & . & . & 6 \\
2\nu = 6 & & . & . & . & . & \bar{4} \\
2\nu = 8 & & . & . & . & . & \bar{3}
\end{array} \quad (\text{A.6})$$

From the discussion of Appendix 9B come the overall prefactors  $P(\nu=1)=1/\sqrt{5}$ ,  $P(2)=-1/\sqrt{5}$ ,  $P(3)=-1/\sqrt{5}$ , and  $P(\nu=4)=1/\sqrt{5}$ , which are needed to complete the following  $N=5$  revival table using (A.5).

$$\begin{array}{c|ccccc}
\psi(\rho, \nu) & \rho=0 & \rho=1 & \rho=2 & \rho=3 & \rho=4 \\
\hline
\nu=0 & 1 & 0 & 0 & 0 & 0 \\
\nu=1 & 1/\sqrt{5} & e_1^* & e_1 & e_1 & e_1^* \\
\nu=2 & -1/\sqrt{5} & -e_2 & -e_2^* & -e_2^* & -e_2 \\
\nu=3 & -1/\sqrt{5} & -e_2^* & -e_2 & -e_2 & -e_2^* \\
\nu=4 & 1/\sqrt{5} & e_1 & e_1^* & e_1^* & e_1
\end{array} \quad \text{where:} \quad (\text{A.7})$$

$$e_1 = e^{i2\pi/5} / \sqrt{5}$$

$$e_2 = e^{2i2\pi/5} / \sqrt{5}$$

A phasor gauge plot of the  $N=5$  revivals (A.7) is shown in Fig. 9.4.3c.

The summation (A.1) for *even-N* is mostly the same as the above. Time index  $\nu$  is replaced by  $\nu/2$ .

$$\begin{aligned}
\psi_0(\phi_\rho, t_\nu) &= \frac{1}{N} \sum_{m=0}^{N-1} e^{-i(m\nu-\rho)^2 \frac{2\pi}{2\nu N}} e^{i\frac{\rho^2}{2\nu} \frac{2\pi}{N}}, \text{ where; } t_\nu = \nu \frac{2\pi}{2N}, \text{ for } N\text{-even.} \\
&= P(\nu) e^{\frac{-i[\mu_\rho^2 \nu + 2\mu_\rho \rho] 2\pi}{2N}} = P(\nu) e^{\frac{-i[\mu_1^2 \nu + 2\mu_1] \rho^2 2\pi}{2N}}
\end{aligned} \quad (\text{A.8a})$$

where

$$\mu_1 = \frac{\kappa N - 1}{\nu} = \text{first integer in } \frac{N-1}{\nu}, \frac{2N-1}{\nu}, \frac{3N-1}{\nu}, \dots \quad (\text{A.8b})$$

Again the overall phase and amplitude prefactor  $P(\nu)$  is a Gaussian sum discussed in Appendix B.

$$P(\nu) = \frac{1}{N} \sum_{m=0}^{N-1} e^{-i(m\nu)^2 \frac{2\pi}{2\nu N}} = \frac{1}{N} \sum_{m=0}^{N-1} e^{-i\nu m^2 \frac{2\pi}{2N}} \quad (\text{A.8c})$$

This works for odd-numerator time fractions  $1/2N, 3/2N, 5/2N, \dots = \nu/2N$ . For the even numerator ones, we take advantage of the revival sequence  $\nu/N = 1/N, 2/N, 3/N, \dots$  for  $N$  cut in half and shifted by  $\pi$ . If  $N/2$  is odd then (A.5) is used. If  $N/2$  is even then (A.8) is used again, but with  $N$  cut in half to  $N/2$ . Note that fractions with singly-even denominators have zeros at  $\phi=0$  and peaks at  $\phi=\pm\pi$ . Fractions with odd denominators have peaks at  $\phi=0$  and zeros at  $\phi=\pm\pi$ . Fractions with doubly-even denominators have zeros at  $\phi=0$  and  $\phi=\pm\pi$ .

*Appendix 9.B. Overall phase of peaks in a revival lattice*

The evaluation of the  $N$ -term integral Gaussian sum

$$G(v) = \sum_{m=0}^{N-1} e^{-ivm^2 \frac{2\pi}{N}} = NP(v) \tag{B.1}$$

in the prefactor  $P(v)=G(v)/N$  given by (A.5b) is, perhaps, the least trivial part of the revival formulation. The development involves complex Gaussian integer analysis, a subject which occupied Gauss for more than the first decade of his most productive years. Here we will be content with giving a list of the results for the first few integer combinations that would be relevant for the revivals shown previously.

$N =$	2	3	4	5	6	7	8	9	10	11	12
$\sum_{m=0}^{N-1} e^{-im^2 \frac{2\pi}{N}} =$	0	$-i\sqrt{3}$	$(1-i)\sqrt{4}$	$\sqrt{5}$	0	$-i\sqrt{7}$	$(1-i)\sqrt{8}$	$\sqrt{9}$	0	$-i\sqrt{11}$	$(1-i)\sqrt{12}$
$\sum_{m=0}^{N-1} e^{-i2m^2 \frac{2\pi}{N}} =$	2	$i\sqrt{3}$	0	$-\sqrt{5}$	$-i\sqrt{12}$	$-i\sqrt{7}$	$(1-i)4$	$\sqrt{9}$	$\sqrt{20}$	$i\sqrt{11}$	0
$\sum_{m=0}^{N-1} e^{-i3m^2 \frac{2\pi}{N}} =$	0	3	$(1+i)\sqrt{4}$	$-\sqrt{5}$	0	$i\sqrt{7}$	$-(1+i)\sqrt{8}$	$-i\sqrt{27}$	0	$-i\sqrt{11}$	$(1-i)6$
$\sum_{m=0}^{N-1} e^{-i4m^2 \frac{2\pi}{N}} =$	2	$-i\sqrt{3}$	4	$\sqrt{5}$	$i\sqrt{12}$	$-i\sqrt{7}$	0	$\sqrt{9}$	$-\sqrt{20}$	$-i\sqrt{11}$	$-i\sqrt{48}$
$\sum_{m=0}^{N-1} e^{-i5m^2 \frac{2\pi}{N}} =$	0	$i\sqrt{3}$	$(1-i)\sqrt{4}$	5	0	$i\sqrt{7}$	$-(1-i)\sqrt{8}$	$\sqrt{9}$	0	$-i\sqrt{11}$	$-(1-i)\sqrt{12}$
$\sum_{m=0}^{N-1} e^{-i6m^2 \frac{2\pi}{N}} =$	2	3	0	$\sqrt{5}$	6	$i\sqrt{7}$	$(1+i)4$	$i\sqrt{27}$	$-\sqrt{20}$	$i\sqrt{11}$	0
$\sum_{m=0}^{N-1} e^{-i7m^2 \frac{2\pi}{N}} =$	0	$-i\sqrt{3}$	$(1+i)\sqrt{4}$	$-\sqrt{5}$	0	7	$(1+i)\sqrt{8}$	$\sqrt{9}$	0	$i\sqrt{11}$	$-(1+i)\sqrt{12}$

(B.2)

Particularly simple general results are had for the case of doubly-even integer.

$$\begin{array}{cccccc} N = 2n & 4 = 2 \cdot 2 & 8 = 2 \cdot 4 & 12 = 2 \cdot 6 & 16 = 2 \cdot 8 & 20 = 2 \cdot 10 \\ \hline \sum_{m=0}^{N-1} e^{-im^2 \frac{2\pi}{N}} = & (1-i) & (1-i)\sqrt{2} & (1-i)\sqrt{3} & (1-i)\sqrt{4} & (1-i)\sqrt{5} \end{array} \tag{B.3}$$

A complex vector diagram of the first few  $G(u)$  sums is shown below in Fig. 9B.1.

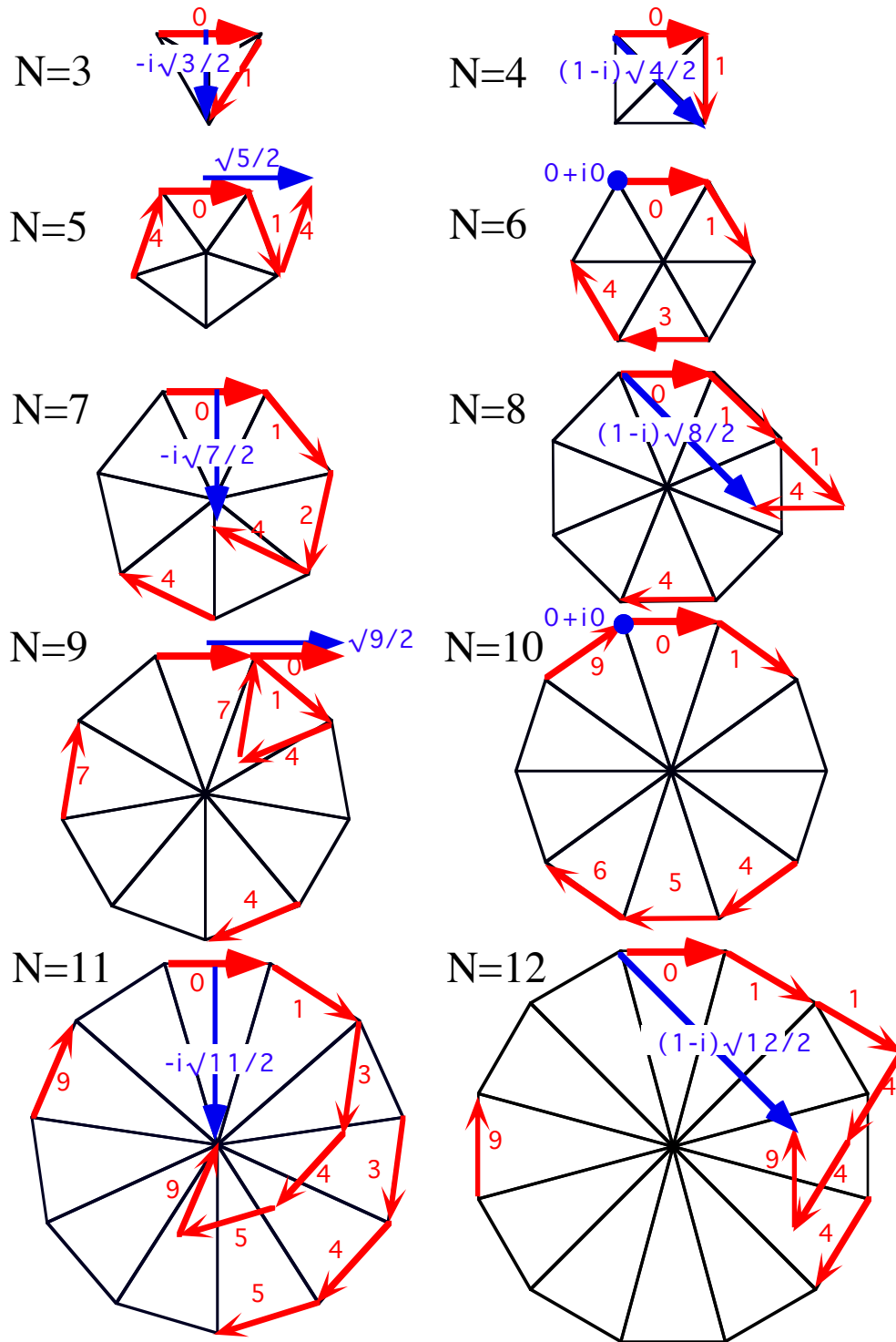


Fig. 9B.1 Sums of modular squares  $(m^2)_N = m^2 \bmod N$  ( $N = 3-12$ ).

